# Neurogenetics of active sensing in *Caenorhabditis elegans* interneurons

**Marie-Hélène Ouellette**

Biology

McGill University

Montreal, Québec, Canada

First Published on December 2023

A thesis submitted to McGill University in partial fulfillment of the requirements of the degree of Doctor of Philosophy

**TABLE OF CONTENT**

## LIST OF FIGURES AND TABLES

Table

## LIST OF ABBREVIATIONS

| | |
|---|---|
| Ach | Acetylcholine |
| CNS | Central Nervous System |
| HD | Head Direction Cells |
| IAA | Isoamyl Alcohol |
| mAchR | Muscarinic Acetylcholine Receptor |
| $mCa^{2+}$ | Motor Calcium Events in RIA (occuring in nRV and nRD) |
| nAchR | Nicotinic Acetylcholine Receptor |
| NGM | Nematode Growth Medium |
| nrD | Nerve Ring Dorsal (motor compartment of the RIA) |
| nrV | Nerve Ring Ventral (motor compartment of the RIA) |
| $sCa^{2+}$ | Sensory evoked Calcium Events in RIA |
| SMD | Head Motor Neurons |
| SMDD | Dorsal Head Motor Neuron |
| SMDV | Ventral Head Motor Neuron |
| Tc | Cultivation Temperature |
| TeTX | Tetanus toxin |
| UV | UltraViolet |

**ABSTRACT**

In its broad definition, active sensing consists of the integration of all sensorimotor inputs that lead to a specific behavior. Classic examples of it are echolocation used by bats and dolphins to optimally navigate their environment and eye movements in that pair with visual perception in mammals. In the central nervous system, one of the main neurotransmitters, acetylcholine (Ach), acts through nicotinic and muscarinic receptors (mAchRs) to regulate cortical signaling. This Ach-mediated signaling contributes to many cognitive processes and is critical to sensorimotor control. In the nematode *Caenorhabditis elegans*, we identified a small circuit that integrates both sensory and motor inputs, sharing similarities with mammalian central cholinergic signaling. It involves a glutamatergic interneuron, RIA, which receives cholinergic feedback from head motor neurons (SMDs) via muscarinic acetylcholine receptors (mAchRs). This input, which is mediated through mAChR GAR-3 in motor compartments (nrV and nrD), occurs in phase with head movement during locomotion, leading to compartmentalized local calcium events and gait regulation.

The main goal of this work was to identify cellular mechanisms linking muscarinic activation to glutamate release in response to this cholinergic modulation, and explore novel components involved in this process.

First, this study has shown that sensory input is integrated and processed in the loop region, the sensory compartment of the RIA, following a gate-and-switch model. It has been demonstrated that the positioning of the head gates sensory responses to mediate

directional head withdrawal away from repulsive stimuli when needed, and when the head is mostly bent to one side or the other.

Secondly, the study has shown that motor compartment dynamics in RIA impact muscle activity at the head level and, when this function is disrupted, lead to an abnormal novel phenotype we call head lifting. Using this new phenotype as a correlate to screen for genes involved in RIA circuit dynamics has proven successful in identifying candidates that specifically impact calcium activity in RIA motor compartments. Through calcium imaging in RIA, those specific defects have also been characterized in candidate strains while assessing the relevant mode of action in the neuron.

As a whole, this work sheds light on the mechanisms at play in the RIA circuit dynamics, and its implications in head orientation behavior which is an essential staple of active sensing, at both the physiological and molecular level. Future studies could focus on the gene candidates found here to pinpoint their exact function in the process.

**RÉSUMÉ**

L’intégration de l’ensemble des signaux entrants sensoriels et moteurs menant à une réponse comportementale spécifique peut être défini comme *active sensing*. L’écholocalisation qu'utilisent les chauve-souris et les dauphins pour naviguer dans leur environnement ou les mouvements de l'œil couplés à la détection visuelle chez les mammifères en sont des exemples classiques. Au niveau du système nerveux central, un des principaux neurotransmetteurs, l’Acétylcholine, agit par l’interaction des récepteurs nicotiniques (nAchRs) et muscariniques (mAchRs) afin de réguler les voies de signalisation corticales. Les voies de signalisation médiées par l’Ach contribuent à de nombreux processus cognitifs et jouent un rôle critique dans le contrôle nerveux sensorimoteur. Chez l’animal modèle *Caenorhabditis elegans*, un petit circuit nerveux intégrant les signaux moteurs et sensoriels a été découvert. L'intégration de ces signaux partagent des similarités avec la voie de signalisation principale cholinergique chez les Mammifères. Un des acteurs importants de ce circuit est un interneurone glutamatergique, le RIA, qui reçoit les signaux de la boucle de rétroaction cholinergique des neurones moteur de la tête (SMDs) via les mAchRs. Ces signaux, qui sont transmis par GAR-3, un récepteur muscarinique (mAChR) localisé au niveau des compartiments moteurs du RIA (nRV et nRD), arrivent de façon synchrone avec le mouvement de la tête pendant la locomotion. Cette synchronicité entre l’intégration des signaux par le RIA et le mouvement de la tête a pour conséquence une compartimentalisation des événements calciques locaux dans le RIA et est également impliquée dans la régulation du maintien de la posture de la tête.

L’objectif principal de ce travail de thèse se décline en deux parties: (i) l’identification des mécanismes cellulaires sous jacents menant à la libération du glutamate par les récepteurs muscariniques et régulant la dynamique du calcium en réponse l’intégration du signal cholinergique reçu par le RIA; (ii) l'identification de nouveaux acteurs impliqués dans ce mécanisme.

Dans un premier temps, les résultats de cette étude démontrent que les signaux sensoriels reçus sont intégrés et traités au niveau de la boucle (loop) du RIA (suivant un modèle “gate-and-switch”). Ils mettent en avant également que le positionnement de la tête déclenche périodiquement des réponses sensorielles afin de réguler son retrait de façon directionnelle en réponse à un stimuli répulsif lorsque celle-ci est principalement tournée dans un sens. Dans un second temps, afin d’identifier de potentiels modulateurs de la dynamique du calcium déclenchée par l'activité des mAChRs, des phénotypes comportementaux et physiologiques corrélant avec une fonction altérée du RIA furent investigués. Cette étude a démontré que les compartiments moteurs du RIA jouent un rôle dans la régulation de l’activité musculaire au niveau de la tête. Une altération de l’intégration au sein de ces compartiments moteurs génère un nouveau phénotype spécifique que nous avons nommé: *head lifting.* Ce phénotype fut utilisé avec succès pour identifier un groupe de gènes candidats qui impacte la dynamique du calcium dans les compartiments moteurs (nRV et nRD) du RIA. En utilisant de l’imagerie calcique cellule-spécifique au niveau du RIA, ces défauts spécifiques furent caractérisés pour chacune des souches candidates tout en mettant en avant leur rôle potentiel au sein du mécanisme d’action du RIA.

Dans son ensemble, ce travail met en lumière de nouveaux mécanismes impliqués dans la dynamique du RIA ainsi que son implication dans l'orientation de la tête du ver qui est un comportement essentiel au active sensing, au niveau physiologique mais également au niveau moléculaire. Comprendre l’exacte fonction de ces gènes candidats dans ce processus pourrait être le point focal d’études ultérieures.

**ACKNOWLEDGEMENTS**

Doing a PhD is a process that requires a lot of personal commitment on all levels, so I would like to take a moment to properly thank the people who supported me on this journey.

First off, a big thank you to my supervisor, Dr. Michael Hendricks, for the opportunity, the trust, and all the great conversations that helped me become a better scientist and researcher. It's been an absolute pleasure evolving in his laboratory, and being able to benefit from his knowledge.

Second, I would like to extend my gratitude to the members of my Supervisory Committee Prof Donald van Meyel and Prof Joseph Dent. Their inputs have been insightful throughout, and it has been a joy to be able to discuss with them about my project.

Third, to all my labmates and close friends who have been there every step of the way to help me navigate the good as well as more challenging times. Your unwavering support means the world. You made the whole path worth it ten times over.

Last but not least, I would like to thank my parents for always believing in me and my capabilities. They've always been nothing but uplifting, and their unfaltering faith and support has been heartwarming.

To all of you, thank you from the bottom of my heart for having made this journey fun and fulfilling.

## CONTRIBUTION TO ORIGINAL WORK

Chapter 1: This chapter is an introduction to the work presented in this thesis. It encompasses a literature review.

Chapter 2: Material and Methods used in this work.

Chapter 3 (from 3.1 to 3.1.5) : Previous work showed that RIA motor compartments show a compartmentalized calcium activity as *C. elegans* crawl on its side while the loop compartment integrates sensory stimuli. Data shown in Figures 3.1 to 3.6 were reported in (Ouellette et al. 2018).

Original findings in this chapter are:

1. RIA overviews and is required for control of head orientation
2. Responses to odor removal is dependent on posture
3. RIA mediates directional head withdrawal
4. Head orientation gates sensory responses
5. Temporal features of sensory responses in RIA axonal compartments
6. RIA compartments act as a gate and switch to drive head orientation behaviors

Chapter 3 (from 3.2 to 3.2.6): The second half of this chapter identifies potential key genes involved in RIA motor compartments calcium dynamics. Data shown in Figures 3.7 to 3.14 and Table 3.1 are part of a manuscript that is ready to be submitted.

Original findings identified in this chapter are:

1. RIA motor compartments function impact muscle activity at the head level in both restrained as well as freely moving animals
2. RIA impaired function leads to head lifting (new phenotype)

3. Head lifting can be used as a correlate to screen for genes involved in RIA/head orientation circuit dynamic
4. Head lifting screen led to identifying candidates that specifically impact calcium activity in RIA motor compartments
5. Candidate genes found through the head lifting screen also show behavioral impairments performing active sensing tasks such as isothermal tracking

Chapter 4: This chapter is a discussion on findings from this work as well as offers potential explanations on drawbacks experienced throughout the project, and future directions that could be explored to build on new knowledge that emerged from this project.

## CONTRIBUTION OF AUTHORS

Ioana Ghia and I together acquired data for Figure 3.1 F-G and Figure 3.14

Sarah Zhao and I together performed the experiments for Figure 3.8 A-B and Figure 3.9 A-C.

Ryan Ramos adapted the FluoroSNNAPP code in MatLab R2016b to make it work for analysis on RIA.

All other experiments and analyses were performed by me.

Dr. Michael Hendricks helped with designing all the experiments, analyzing the data, making figures, writing the paper and providing feedback on this thesis.

CHAPTER 1

# INTRODUCTION

## 1.1 Navigation and Orientation Strategies

Animals devise successful navigation strategies by assessing their surroundings through the integration of multiple environmental cues, deriving sensorimotor information from them. In this way, animals can become adapted to their surroundings and thrive. It is through goal-directed navigation or probabilistic locomotion leading to navigation that every species decides where it wants to go at any given point in time be it to track food, to seek shelter or to find a mate (Bartumeus et al. 2005; Lohmann et al. 2008). For example, it has been shown that various bird species tend to migrate toward areas where food is more easily available and environments for breeding are better suited to them during the winter. Besides, whimbrels move from Canada to the Caribbean each year to spend the colder months along the shore, in the same spot each year (Watts et al. 2021).

Throughout the animal kingdom, navigation essentially depends on the starting point, the destination and how to get from the former to the latter. To achieve this, animals use all kinds of techniques. As such, European starlings, pigeons, honey bees, penguins and butterflies use the sun as a compass and are able to keep track of time throughout the day (Milius 2004), while birds that migrate during the night are dependent on star patterns (Emlen 1967; Sauer 1958). It has even been demonstrated that birds become disoriented when stars become dimmer or if their patterning/localisation are artificially changed (Wiltschko and Wiltschko 2003). Interestingly, monarch butterflies use a very precise system of polarized light to reach their destination. The part of their visual system that is devoted to polarized light detection is enriched with UV photoreceptors

linked to circadian clocks, allowing the integration of geographical and temporal information (Sauman et al. 2005). The same sort of locomotory tactics have been studied in mammals, where specific circuits have evolved to provide effective navigation adapted to the wide arrays of habitats they live in—from the skies to the ocean all the way to deserts and forests. Using these different strategies can make it possible for them to evade predators, feed themselves, and is key to their survival (Hills et al. 2015). It also allows some, like deers or wolves, to be able to return to their preferred area after traveling away from their natural environment (Glazener; Henshaw and Stephenson 1974; Putman et al. 2014).

Within this wide range of navigation methods, some species such as bats and dolphins use particular techniques such as echolocation to orient themselves (Ulanovsky and Moss 2008; Au 1993). Other mammals such as shrews and oilbirds also use echolocation even if this behavior is less studied in these species. Tree mice have been the most recent species shown to perform echolocation (Jones 2021). Echolocation works in such a way that the animal emits a specific soundwave pulse and analyzes its echo when it comes back to them after rebounding from something within the environment (Figure 1.1 A). That way, an echolocating animal is able to create a mental representation of their environment and the distance separating them from objects present in it, allowing them to successfully navigate (Thomas et al. 2004; Verfuß et al. 2009; Benoit-Bird and Au 2009). Notably, echolocation is of particular interest here because it is a classic example of **active sensing**, a larger category of navigation behavior.

## 1.2 Active Sensing

In the central nervous system (CNS), a given sensory perception and its associated motor response are closely connected. While stimuli come from all around in the environment, they also occur in response to our own behaviors, causing what is known as **reafferent sensory stimulation** (Brooks and Cullen 2019). It is then imperative that each type of stimulus, whether from the environment or the individual themself, be integrated and processed differently in order to efficiently create an accurate map of one's surroundings and react in accordance to it (Straka et al. 2018). To account for reafferent sensory stimulation, our own actions are continuously monitored by our sensory systems through a type of input called **corollary discharge,** which originates from motor regions (Crapse and Sommer 2008). This system exists to predict the outcomes of our actions and compensate when needed.

Sensorimotor integration that leads to a specific behavior is commonly called **active sensing**. It is to note that active sensing is also adaptive to the changing sensory cues and behavior in the environment. Active sensing links an animal to its environment as the former engages in exploratory behavior in order to understand its surroundings. In this way, the animal receives sensory information from the environment, and this is integrated with information produced by the animal's own motor cues (corollary discharge) (Figure 1.1 B) (Straka et al. 2018). Active sensing arises from the production of specific motor events that lead the animal to then better gain and analyze sensory information coming at them (Bajcsy 1988; König and Luksch 1998).

Electric fishes, *Eigenmannia virescens,* use their body movement to create electric ripples in the water that makes it possible to orient themselves with enhanced sensory feedback (Stamper et al. 2012; Babineau et al. 2007). In this case, the electricity the fish emits through body movements act as a corollary discharge to then gather sensory information from the environment when those ripples encounter an object.

Vision for humans and primates depends on eye movements, that is the motor control of ocular muscles becomes linked to the transduction of visual information (Ahissar and Arieli 2012, 2001). The act of sniffing leads to olfaction in humans and rats (Wachowiak 2011; Ranade et al. 2013; Kepecs et al. 2006; Smear et al. 2011; Porter et al. 2007). From insects to mammals, touch is also an active sensing mechanism used by species to get as much feedback from their environment as possible (Schütz and Dürr 2011; Catania 2011; Brecht et al. 2011).

Whisking in rodents—where they move their vibrissaes back and forth to come into contact with objects in their environment—is one of the most well-known active sensing mechanisms (Berg and Kleinfeld 2003; Hill et al. 2008). Rats are even able to distinguish textures (Guić-Robles et al. 1989; Prigg et al. 2002; Zuo et al. 2011; Heimendahl et al. 2007) as well as the distance and shape of objects (Harris et al. 1999; Brecht et al. 1997; Phil et al. 2001) using this strategy as they navigate throughout their surroundings.

All in all, those are all key examples of active sensing from across the animal kingdom. While a lot of those navigation behaviors which rely heavily on active sensing are not well understood at the molecular level, some others can be linked to specific circuits.

### 1.3 Neural Networks, Head Orientation and Acetylcholine in Mammals

Modifying one's head orientation in response to sensorimotor cues present in the environment is a key feature in maintaining proper spatial orientation and accurately adapting to one's environment (Taube 2007).

In mammals, the circuit of spatial orientation coding has been linked to cells in the hippocampus, including head direction cells (HD) that have been extensively studied in rodents where they act as an internal compass (Peyrache et al. 2015, 2017; Butler et al. 2017; Winter and Taube 2014). Multiple cell types within the rodent hippocampus are required to execute successful navigation strategies. In addition to HDs, there are space cells that only become active when the animal discovers a specific spot in its environment (O'Keefe and Nadel 1979; Muller et al. 1994; Fenton et al. 2008), boundary cells (including border cells) that fire when a boundary is found (Savelli et al. 2008; Lever et al. 2009; Solstad et al. 2008) and grid cells that, as their name implies, create a grid leading the animals to be able to get more precise coordinates for objects present (Barry et al. 2007; Hafting et al. 2005; Derdikman et al. 2009). These hippocampal cells represent a neural substrate linking the animal to a precise location within its environment.

While the neural circuitry involved in the control of head orientation has been found and documented, much still remains unknown as to how neural networks function to

integrate environmental signals in order to appropriately guide head orientation at the molecular level. In terms of the molecular underpinnings of orientation, one component that has been well documented is acetylcholine (Ach) signaling. Acetylcholine is a primary neuromodulator in the CNS. It acts through either nicotinic (nAchRs) or muscarinic receptors (mAchRs) which are named after their main agonist molecules, respectively nicotine and muscarine (Tiwari et al. 2013). The nAchRs are ionic channels whereas the mAChRs are transmembrane proteins coupled with G-proteins (Tiwari et al. 2013). Through their activation, they trigger a plethora of signaling pathways that contribute to cognitive processes such as arousal, attention, learning and, more importantly here, sensorimotor control (Felder 1995; Role and Berg 1996; Picciotto et al. 2012).

As such, it has been shown that in rodents, olfaction is coupled to respiration via cholinergic input that is in phase with breathing. This cholinergic input functions to enhance odor detection during inhalation (D'Souza and Vijayaraghavan 2014). During whisking, cholinergic input to the barrel cortex desynchronizes local cortical activity and enhances discrimination of mechanosensory input. In each of these cases, an Ach signal correlates with a motor activity, and serves to couple sensory perception to ongoing behavior (Liu et al. 2015; Rothermel et al. 2014) (Figure 1.2).

There is a wealth of electrophysiological and pharmacological data on cholinergic modulation in mammals. However, the understanding of the molecular mechanism by which cholinergic input regulates transmitter release downstream of mAchRs requires additional study.

## 1.4 *Caenorhabditis elegans* as a model to study active sensing at the single neuron level

*Caenorhabditis elegans* is a one millimeter long nematode that has a short three-day life cycle, and is easy to maintain in culture in laboratory conditions (Figure 1.3 A). A plethora of unique characteristics render it a great model to study genetics, cellular processes, and neuronal pathways. Among these characteristics is the fact that *C. elegans* populations are mainly composed of hermaphrodites, meaning that isolated populations consist of the same genome, passed through generations for almost indefinite life cycles (Brenner 1974). While nematodes are predominantly hermaphroditic, there is a small proportion of males, and modifying the genome can therefore be easily achieved by maintaining males from strains of interest and crossing them with the desired hermaphrodites expressing a genetic background of interest.

Furthermore, adult *C. elegans* are transparent, thus permitting easy monitoring of all cellular processes through microscopy. Transgenic proteins can also be integrated into the *C.elegans* genome to visualize their expression and function when fused to fluorescent markers. Accordingly, using imaging techniques that have been optimized for this model, multiple processes can be studied in parallel with a high level of detail (Breimann et al. 2019) (Figure 1.3 C). Finally, of utmost importance for this project, the whole *C. elegans* nervous system, consisting of 302 neurons, has been completely mapped (White et al. 1986) (Figure 1.3 B). Altogether, these characteristics make *C. elegans* a perfect model for the investigation of head orientation, in tandem with the process of active sensing, which requires the integration of both sensory and motor inputs at the single neuron level. As mentioned above, the nematode's small size and

transparency permit simultaneous stimulation and quantification of both neuronal and physical activity, which was required to assess active sensing.

In terms of physical activity, nematode locomotion is easily tracked and quantified. Specifically, *C. elegans* lie on their side and crawl in a sinusoidal motion in the dorsoventral plane (Hart 2006). The main navigation strategy for worms is the biased random walk, which essentially functions on the same basis as bacterial chemotaxis (Berg 1975). The biased random walk consists of forward locomotion with some reorientation events in the form of reversals and turns (Figure 1.4 A-B). Animals integrate all sensory changes they encounter when moving forward to reorient accordingly, based on probability (Pierce-Shimomura et al. 1999; Hart et al. 1995; Faumont et al. 2012).

Isothermal tracking is a good example of sensorimotor integration in a radial temperature gradient for *C. elegans*. During each undulation, the worm assesses its preferred temperature ($T_S$), normally near the one it was raised at, also called the cultivation temperature ($T_C$), and adjusts its trajectory accordingly in order to follow that temperature (called isotherm) moving forward (Figure 1.4 C-F) (Luo et al. 2006). This requires fine tuning of sensory inputs along with motor commands to be able to track (Luo et al. 2014). Interestingly, it happens quite often that worms stop tracking an isotherm and start tracking another shortly after. This can give rise to multiple tracks during the course of an assay.

In a similar fashion, klinotaxis occurs when worms are crawling in a chemoattractant gradient. In this case, *C. elegans* assess sensory changes as the head bends back and

forth, in order to steer towards a favorable direction (towards the chemoattractant) (Kato et al. 2014; Iino and Yoshida 2009). Klinotaxis involves more sensory-guided decision making.

As the worm's head swings back and forth, sensory structures located at the tip of the nose assess any changes and transmit this information downstream for further processing in order to guide locomotory decision making (Hart et al. 1995). So, in addition to the biased random walk described above, which is more probabilistic, worms use other locomotion strategies such as steering, which requires real time integration of sensorimotor inputs to successfully navigate through their surroundings (Kato et al. 2014; Wakabayashi et al. 2015). As defined above, active steering occurs when sensorimotor integration leads to a specific behavior, and as such steering can be considered a form of active sensing in *C. elegans*. As such, steering is a form of active sensing in *C. elegans*.

### 1.5 The RIA circuit

We previously identified a small circuit that consists of a unipolar glutamatergic interneuron, RIA, which integrates both motor and sensory input at the single neuron level (Hendricks et al. 2012). The axonal portion of the RIA projects to the nematode's nerve ring, a brain-like structure. Notably, RIA has well-defined compartments that have been identified through synaptic innervation pattern studies and calcium physiology: the nrV (ventral nerve ring), nrD (dorsal nerve ring) and the loop, the segment that is outside of the nerve ring itself but close to the cell body (Figure 1.5 A) (Hendricks et al. 2012; Hendricks and Zhang 2013).

As mentioned previously, RIA receives both sensory and motor inputs (Figure 1.5 C). These are relayed to its specific compartments as the worm crawls forward, on its side, with its head undulating in the dorsoventral plane. The muscarinic motor inputs from the SMD head motor neurons on the ventral (SMDV) or dorsal (SMDD) side synapse respectively onto RIA nrV and nrD through mAchR GAR-3. This occurs in phase with head movements while also regulating gait amplitude (Figure 1.5 D-E). For their part, sensory events reach the RIA through the loop region of the axon and trigger whole axon responses (Hendricks et al. 2012). This is to say, there appears to be a spatial and functional divide between motor and sensory input, with motor input being relayed to the nrV and nrD while sensory information is received onto the loop region. Furthermore, this circuit shows a noticeable similarity to what is found in mammalian central cholinergic signaling (Figure 1.2).

**1.6 Rationale and objectives**

We hypothesize that the functional homology between the RIA circuit in *C. elegans* and central cholinergic function in mammals share some degree of homology in terms of molecular constituents and functional logic. As such, we hypothesize *C. elegans* can serve as a model system for the genetic analysis of Ach activity in the brain and active sensing. Since the RIA interneuron in *C. elegans* receives feedback from both head motor neurons and convergent sensory input (Figure 1.5 B), and that its calcium dynamics are linked to steering, we chose to use this model to study the molecular events underlying active sensing in a small neural network.

The RIA circuit provides a strong platform for identifying and characterizing the components involved in active sensing at the molecular and cellular level, as well as analyzing physiological events at subcellular resolution *in vivo*. Moreover, seeing as calcium dynamics within the RIA circuit are linked to steering behavior and a new phenotype we named head lifting, there is a quantifiable physical readout for RIA function.

To achieve these goals, we used a multidisciplinary approach uniting genetics, molecular biology, live microscopy, calcium imaging and genetic engineering. This project has been divided into three aims.

*Aim 1 Study RIA function in head orientation behavior.*

This first goal was directed at better comprehending how the RIA interneuron functions to integrate sensory stimuli at its own circuit level, and how RIA is involved in head orientation behaviors during navigation. It led to the findings published in (Ouellette et al. 2018) and detailed in Chapter Three of this thesis under sections 3.1-3.1.4.

*Aim 2 Candidate gene screen for impaired RIA circuit function.*

This second aim was to identify genes implicated in RIA circuit function at the motor compartment level, and assess function by using specific, newly-identified behavioral correlates of compromised RIA function. The results of this aim are grouped into a manuscript that is ready to be submitted. They can be found in Chapter Three of this thesis under sections 3.2-3.2.6.

*Aim 3 Functional analysis and characterization of genes involved in calcium dynamics.*

The candidate genes identified in Aim 2 were submitted to further study to assess their specific impact on the calcium dynamics within RIA motor compartments, as well as on other known active sensing behaviors. The basis for future molecular studies of those candidates, which involve assessment at the single cell level, has also been established. The findings of this last aim are in Chapter Three of this thesis under sections 3.2.5-3.2.6, as well as briefly discussed in Chapter Four.

A

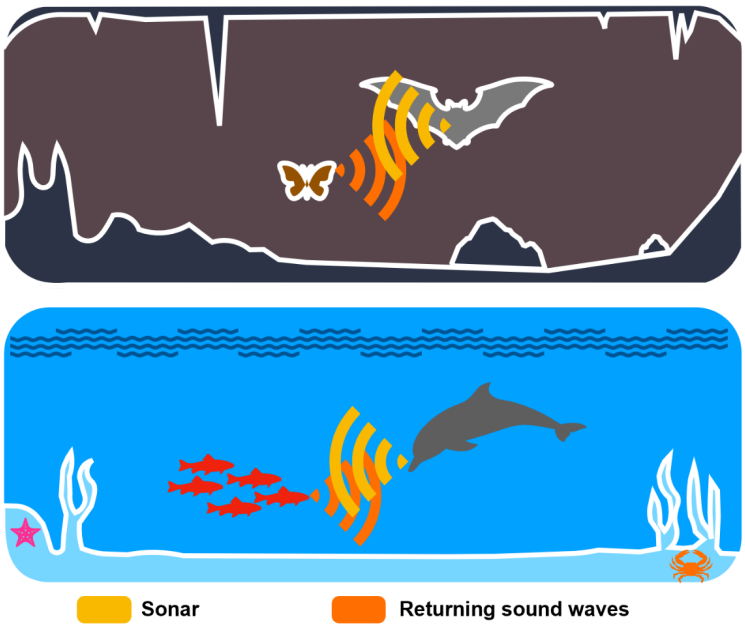
Sonar
Returning sound waves

B

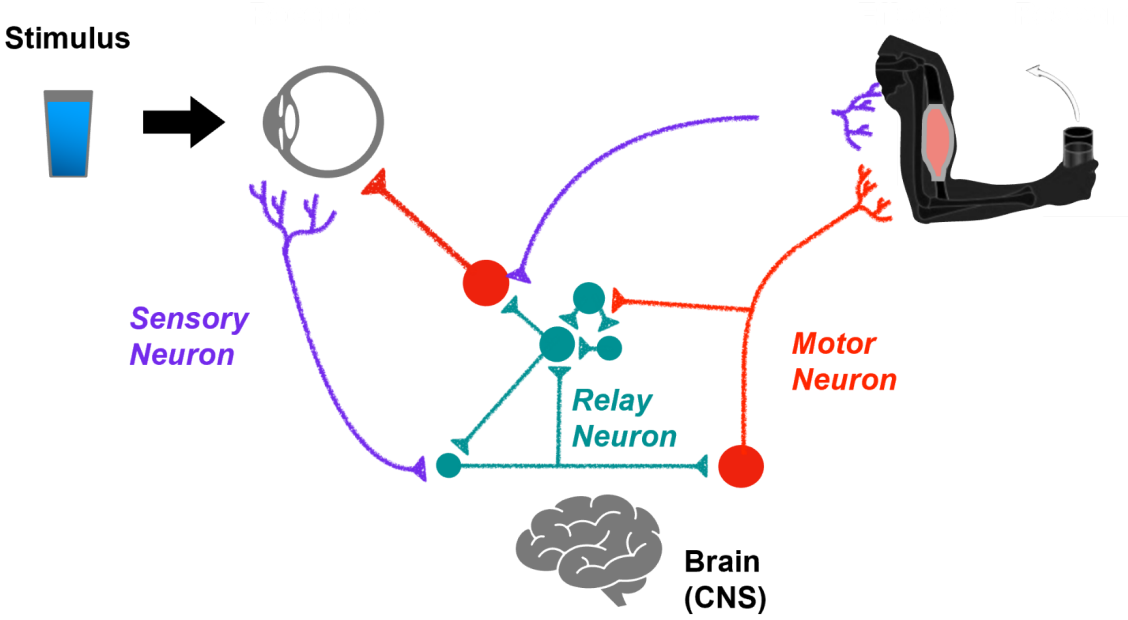
Stimulus
Sensory Neuron
Relay Neuron
Motor Neuron
Brain (CNS)

**Figure 1.1 Echolocation and Active Sensing.** ***A****,* Echolocation schematic showing how bats and dolphins emit specific sound waves in the environment and how those get returned to them when they get into contact with objects so the animals can create a mental map of their surroundings. Inspired and adapted from Elizabeth Hagen. "Echolocation". ASU - Ask A Biologist. 04 November, 2009. Available at https://askabiologist.asu.edu/echolocation. ***B****,* Schematic of an example of mammal active sensing doing a casual task such as picking up a glass of water. Every sensory cue in the environment has to be monitored in real time and the motor response adapted to successfully pick up the glass appropriately.

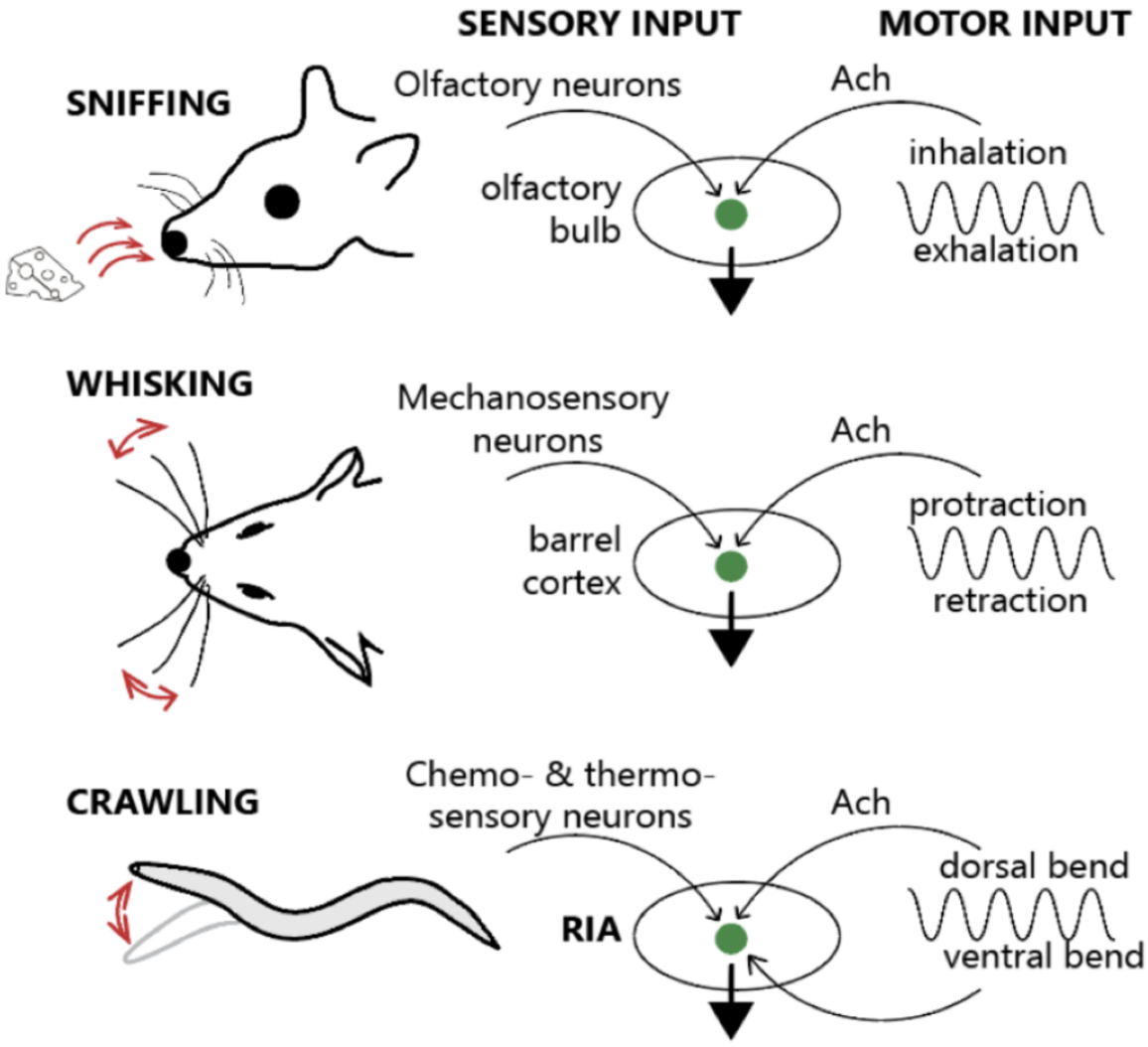
SENSORY INPUT
MOTOR INPUT
SNIFFING
Olfactory neurons
Ach
olfactory bulb
inhalation
exhalation
WHISKING
Mechanosensory neurons
Ach
barrel cortex
protraction
retraction
CRAWLING
Chemo- & thermo-sensory neurons
Ach
RIA
dorsal bend
ventral bend

**Figure 1.2 Active Sensing and cholinergic input in rodents and *C. elegans.*** Cholinergic signaling pairing with inhalation and whisking in rodents behavior. Small RIA circuit that we discovered in *C. elegans* shows striking similarities. Adapted from (Hendricks et al. 2012; Rothermel et al. 2014).

A

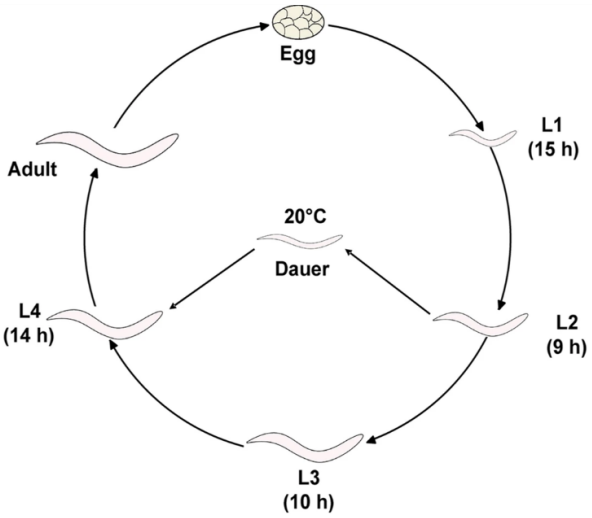
Egg
L1
(15 h)
L2
(9 h)
L3
(10 h)
L4
(14 h)
Adult
20°C
Dauer

B

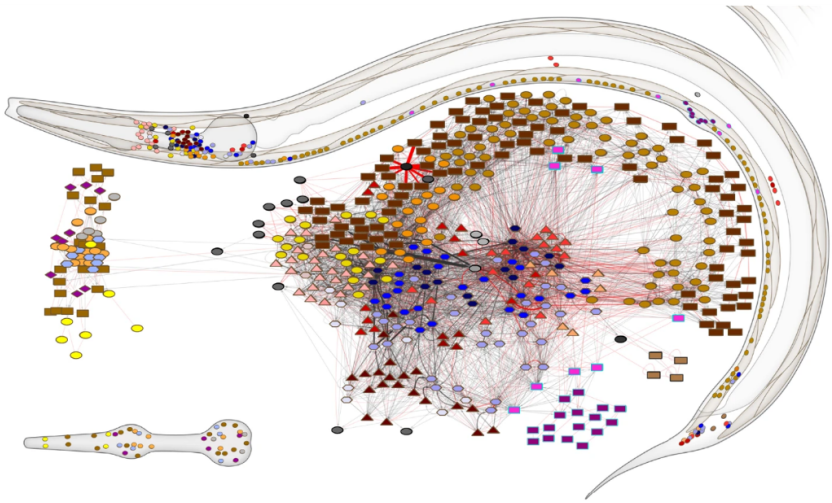

C

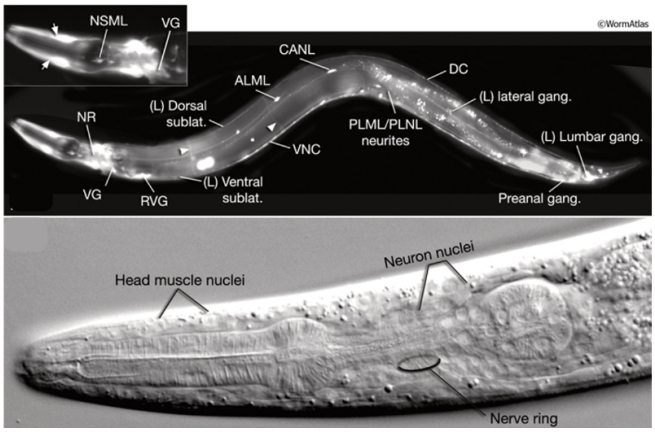
NSML
VG
©WormAtlas
CANL
DC
ALML
(L) lateral gang.
(L) Dorsal sublat.
NR
PLML/PLNL neurites
(L) Lumbar gang.
VNC
VG
RVG
(L) Ventral sublat.
Preanal gang.
Neuron nuclei
Head muscle nuclei
Nerve ring

**Figure 1.3. *C. elegans* as a neuronal circuit model.** ***A***, Life cycle of *C. elegans*. It begins with an egg laid by an adult *C.elegans*. The embryo goes through developmental processes until it hatches as the first larval stage. From hatching, the small worm is going through 4 larval stages (L1-L4) to reach adulthood. ***B***, Schematic of the whole mapped nervous system from a *C. elegans* adult hermaphrodite ***C***, Image of an adult *C. elegans* expressing UNC-119::GFP, a pan-neuronal fluorescent reporter (top). DIC image of the head of a young *C. elegans* adult (bottom). Adapted from (Cook et al. 2019; Ha et al. 2022; Altun and Hall).

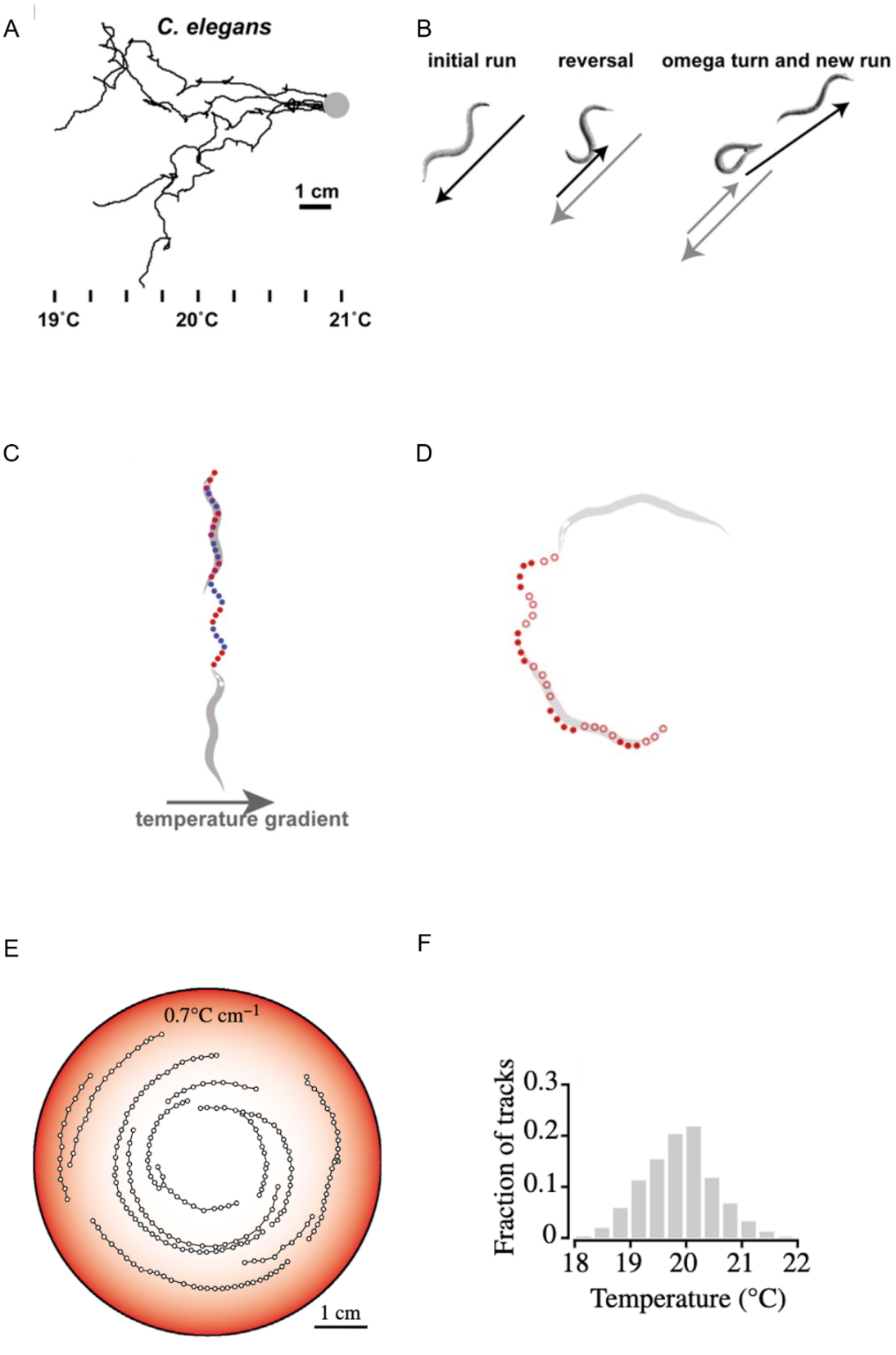
A
C. elegans
1 cm
19˚C
20˚C
21˚C
B
initial run
reversal
omega turn and new run
C
temperature gradient
D
E
0.7°C cm$^{-1}$
1 cm
F
Fraction of tracks
0.3
0.2
0.1
0
18
19
20
21
22
Temperature (°C)

**Figure 1.4 Locomotion strategies in temperature gradients for *C. elegans. A*,** Schematic to illustrate the biased random walk in worms. Four worms were raised at 15°C and placed in a gradient. It is to note that each trajectory is unique. ***B*,** Schematic of moves used by *C. elegans* to navigate toward the preferred destination/temperature. Forward runs are punctuated by reversals and Omega turns. Reversals are often followed by Omega turns which then leads the nematode to begin a new run. Following the gradient it's been put in, the biased random walk, and those reversals and turns, are adapted in order to lead to the preferred temperature. Runs are shorter when going further away from a preferred temperature and lengthened when going toward it. ***C*,** Schematic of how *C. elegans* steers within a temperature gradient near its cultivation temperature ($T_C$) (isothermal tracking). By assessing temperature changes through head sweeps (blue dot for temperatures lower than $T_C$ and red dots for temperatures higher than $T_C$), it adjusts its course to keep crawling within its preferred range, at $T_C$. ***D*,** *C. elegans* can also adjust its trajectory to go away from the temperature stimulation (solid red dots). ***E*,** Isothermal tracks of wild type worms on 9 cm agar plates subjected to a gradient of 18.5°C to 21.5°C when raised at 20°C. Dots are the worm centroid at every 10 seconds while isotracking. ***F*,** Plot rendering of more than 400 isothermal tracks performed by worms raised at 20°C in gradients ranging from 15°C to 25°C. Adapted from (Garrity et al. 2010; Luo et al. 2006)

A

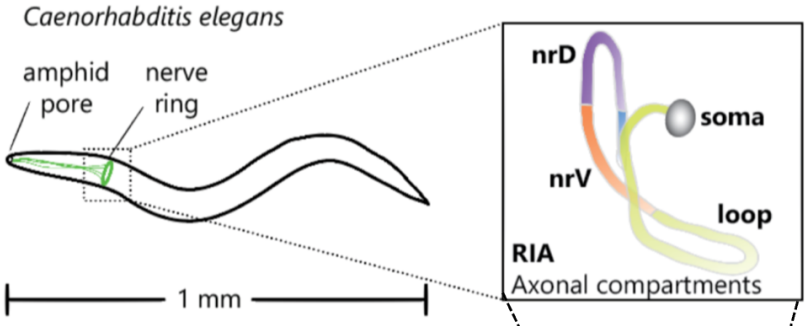
Caenorhabditis elegans
amphid pore
nerve ring
1 mm
nrD
soma
nrV
loop
RIA
Axonal compartments

B

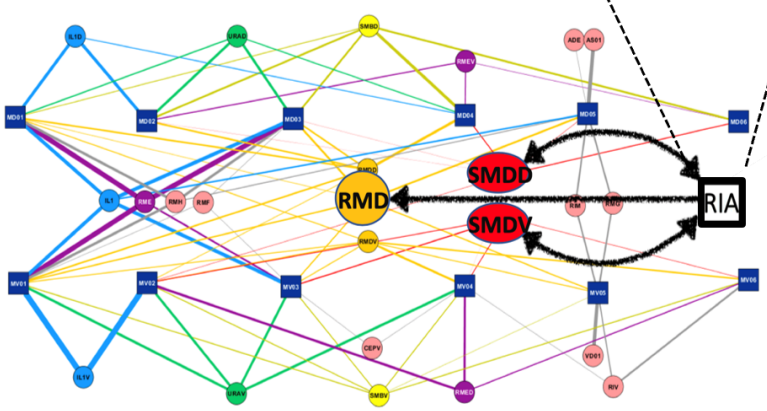
RMD
SMDD
SMDV
RIA

C

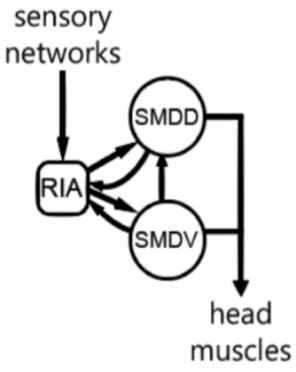
sensory networks
SMDD
RIA
SMDV
head muscles

D

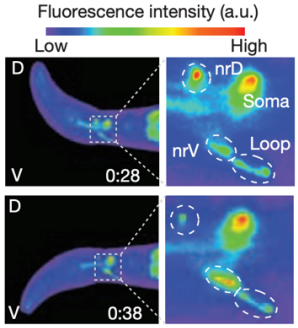
Fluorescence intensity (a.u.)
Low
High
D
V
0:28
nrD
Soma
nrV
Loop
D
V
0:38

E

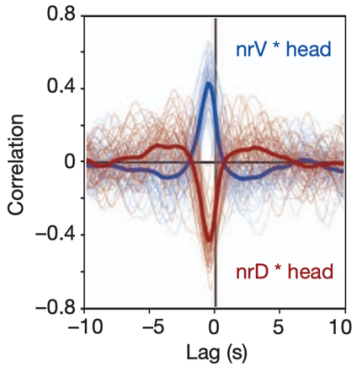
0.8
0.4
0
−0.4
−0.8
Correlation
nrV * head
nrD * head
−10
−5
0
5
10
Lag (s)

**Figure 1.5 The RIA circuit.** ***A****,* Anatomy schematic of the RIA interneuron composed of its two motor compartments (nrV and nrD) and its sensory one (the loop) as well as its localisation in the *C.elegans* head/nerve ring. ***B,*** Schematic of the location of RIA in the head neuron network of *C. elegans* showing its direct connections to head motor neurons. ***C***, Schematic of the RIA circuit as well as its sensory and motor inputs ***D,E*** Images showing the compartmentalized calcium activity during head bending ***D****,* that occurs in phase with head orientation as the cross correlation indicates ***E****,* When the head is bent ventrally, there is specific calcium activity in the nrV, when it is bent dorsally, specific calcium activity in the nrD can be observed. Adapted from (Hendricks et al. 2012; Rothermel et al. 2014).

CHAPTER 2

# MATERIAL AND METHODS

## 2.1 Experimental model and subject details

*Caenorhabditis elegans* were raised on nematode growth medium (NGM) and fed with *E. coli* strain OP50 according to standard methods (Brenner 1974; Stiernagle 2006) Experiments were conducted on young (three day old) adult hermaphrodites. N2; AN87: *sel-12(ty11)* X*;* BA714: *sDF5/spe-4(hc78)* I*;* CB5: *unc-7(e5)* X*;* CB101: *unc-9(e101)* X*;* CB251: *unc-36(e251)* III*;* CB540: *unc-68(e540)* V*;* CF1038: *daf-16(mu86)* I*;* CX12708: *ggr-2(lf62)* X*;* CZ19982: *mcu-1(ju1154)* IV*;* DA702: *eat-16(ad702)* I*;* DA1051: *avr-15(ad1051)* V*;* DA1302: *avr-14(ad1302)* I *;avr-15(ad1051)* V*;* DA1316: *avr-14(ad1305)* I *;avr-15(vu227);glc-1(pk54)* V*;* DA1370: *avr-15(vu277);glc-1(pk54)* V*;* DA1371: *avr-14(ad1302)* I*;* DA1384: *avr-14(ad1302)* I*;glc-1(pk54)* V*;* DA1814: *ser-1(ok345)* X*;* DA2250: *mgl-2(tm355)* I*; mgl-1(tm1811)* X*;* GS1894: *sel-12(ar131)* X*;* GS2447: *hop-1(ar179)* I*;* GS2477: *arIs37* I*; cup-5(ar495)* III*; dpy-20(e1282)* IV*;* GS2527: *arIs37 I; mca-3(ar493); dpy-20(e1282)* IV*;* HBR4: goeIs3 [myo-3p::SL1::GCamP3.35::SL2::unc54 3'UTR + unc-119(+)]; HK30: *unc-68(kh30)* V*;* JD21: *cca-1(ad1650*) X*;* JD217: *gar-3(vu78)* V*;* JT6: *exp-1(sa6)* II*;* KP4: *glr-1(n2461)* III*;* KP2048: *ric-7(nu447)* V*;* LX702: *dop-2(vs105)* V*;* MT6308: *eat-4(ky5)* III*;* MT14680: *lgc-55(n4331)* V*;* NL788: *gpa-14(pk347)* I; PS3818: *unc-68(r1158); him-5(e1490)* V*;* RB888: *casy-1(ok739)* II*;* RB918: *acr-16(ok789)* V*;* RB1137: *rig-4(ok1160)* IV*;* RB1172: *acr-15(ok1214)* V*;* RB1173: *plc-4(ok1215)* IV*;* RB1330: *npr-1(ok1447)* X*;* RB1667: *tax-6(ok2065)* IV*;* RB1672*: sel-12(ok2078)* X*;* RB1690: *ser-2(ok2103)* X*;* RB1808: *glr-2(ok2342)* III*;* RB1915: *ins-3(ok2488)* II*;* RB1990: *flp-7(ok2625)* X*;* RB2185: *glt-4(ok2961)* X*;* RB2544: *ins-4(ok3534)* II*;* TR2170: *unc-68(r1161)* V*;* TR2171: *unc-68(r1162) V;* TQ225: *trp-1(sy690)* III*;* TZ181: *rap-1(pk2082)* IV*;* VC160: *trp-1(ok323)*

III*;* VC271: *end-1 & ric-7(ok558)* V*;* VC350: *glc-2(gk179)* I*;* VC657: *gar-3(gk305)* V*;* VC602*: trp-2(gk298)* III; VC722: *glc-2(ok1047)* I; VC963: *ppk-1(ok1411)/szT1 /* [lon-2(e68)] I; +/szT1 *X;* VC1125: *rig-6(ok1589)* II; VC1408: *magi-1(gk657)* IV; VC1757: *acc-2(ok2216)* IV; VC1801: *cnx-1(ok2234)* III; VC2000: *mca-1(ok2532) IV/nT1* [*qIs51*] (IV;V); VC2623*: nmr-2(ok3324*) V; VC3024: *gcy-2(ok3721)* II; VM487: *nmr-1(ak4)* II; MMH98: [Pglr-3::TeTx::mCherry, Punc-122::GFP]; MMH99: [Pglr-3a::GCaMP3.3, Punc-122::DsRed]; MMH100: [Pglr-3a::GCaMP3.3; Pglr-3a::TeTx]; MMH113: *ric-7(nu447) V;* [Pglr-3a::GCaMP3.3, Punc-122::DsRed] ; MMH114: [myo-3p::SL1::GCamP3.35::SL2::unc54 3'UTR + unc-119(+); Pglr-3::TeTx::mCherry]; MMH116: [*gar-3(gk305)* V; myo-3p::SL1::GCamP3.35::SL2::unc54 3'UTR + unc-119(+)]; MMH117: *gar-3(gk305)* V*;* [Pglr-3a::GCaMP3.3, Punc-122::DsRed]; MMH120: *sel-12(ok2078)* X*;* [Pglr-3a::GCaMP3.3, Punc-122::DsRed]; MMH121: *mca-3(ar493)* IV; [Pglr-3a::GCaMP3.3, Punc-122::DsRed].

Some strains were provided by the *Caenorhabditis* Genetics Center (CGC), which is funded by NIH Office of Research Infrastructure Programs (P40 OD010440).

### 2.2 Method Details

#### 2.2.1 Isolation of strains carrying mutant alleles and transgenes

MMH113: *ric-7(nu447) V;* [Pglr-3a::GCaMP3.3, Punc-122::DsRed] ; MMH114: [myo-3p::SL1::GCamP3.35::SL2::unc54 3'UTR + unc-119(+); Pglr-3::TeTx::mCherry]; MMH116: [*gar-3(gk305)* V; myo-3p::SL1::GCamP3.35::SL2::unc54 3'UTR + unc-119(+)]; MMH117: *gar-3(gk305)* V*;* [Pglr-3a::GCaMP3.3, Punc-122::DsRed]; MMH120:

*sel-12(ok2078)* X*;* [Pglr-3a::GCaMP3.3, Punc-122::DsRed] and MMH121: *mca-3(ar493)* IV; [Pglr-3a::GCaMP3.3, Punc-122::DsRed] were obtained by crossing either *gar-3(gk305) V*, *mca-3(ar493) IV, sel-12(ok2078) X* , *ric-7 (nu447*) V or MMH98: [Pglr-3::TeTx::mCherry, Punc-122::GFP] hermaphrodites with MMH99: [Pglr-3a::GCaMP3.3, Punc-122::DsRed] males. Double homozygotes were isolated from the F2 progenies as animals segregating only fluorescent progeny (from transgene) and mutant alleles were identified in genomic DNA using PCR and sequencing when required (Table 2.1).

### 2.2.2 Head lifting assays

Worms were raised under standard conditions. Reproducible assay consisted of young adults that were individually picked and placed on a non-seeded NGM plate for a few body bends, in order to clear off residual bacteria, then picked again and placed on a second non-seeded plate. They were then left to crawl freely for 30 minutes before head lifts were scored by eye during a one-minute trial. The minute-long trial period was initiated by tail-poking, administered by a worm pick by tapping the tail once, which triggers worms to initiate a forward run. Other conditions were tested and detailed in (Figure 3.10).

### 2.2.3 Microfluidic device fabrication

Standard soft lithography methods were used to fabricate photoresist (SU8) masters for microfluidic devices (San-Miguel and Lu 24AD). Devices were replica mastered in a two part epoxy resin (Smooth Cast 310, Sculpture Supply Canada #796220) according to the manufacturer's instructions for long term use. Polydimethylsiloxane (PDMS) (Dow

Corning Sylgard 184, Ellsworth Adhesives #4019862) was mixed at 10:1, degassed, poured over masters, degassed again, and cured at 60°C for at least 3 hours. Inlet holes made with a Milltex 1 mm biopsy punch (Fisher). Chips were cleaned and then bonded to glass coverslips using air plasma generated by a handheld corona treater (Electro-Technic Products, Chicago, IL). Coupling to fluid reservoirs was done by directly inserting PTFE microbore tubing (Cole-Parmer #EW-06417-21) into inlet holes.

### 2.2.4 Calcium imaging

GCaMP3.3 fluorescence, on animals semi-restrained in a microfluidic channel (Chronis et al. 2007) that were exposed to alternate streams of NGM buffer or a 1:10000 dilution of IAA in NGM buffer every 10 seconds during 1 minute, was acquired at 5 frame per second rate with 100ms exposure time. Fluid flow was controlled with a ValveBank (AutoMate Scientific). The timelapse acquisitions were performed on an Olympus IX83 inverted microscope (Olympus Life Science) using an 40X/1.25 N.A. silicon-immersion objective. During calcium imaging, animals were free to move the anterior portion of their head, and these movements were captured as well. Both head position and GCaMP3.3 fluorescence intensity (Tian et al. 2009) from axonal compartments were measured using our custom FluoroSNNAP MatLab code (The MathWorks, R2016b).

### 2.2.5 Muscle imaging in semi-restrained animals and head orientation assays

Microfluidic chips were based on a design by (Tian et al. 2009; McCormick et al. 2011) with minor adjustments to allow stimulus switching. Animals were exposed to streams of NGM buffer and 100 $\mu$M IAA (BioShop ISO900) from alternate directions, so animals experienced the olfactory stimulus from either side of their head. Worms were loaded

individually into the chip and, once in place, their movements were recorded for 2 minutes, with a switch between buffer and IAA occuring every 10 seconds, for a total of 2 minutes. Fluorescence intensity and head position were analyzed in MatLab (FluoroSNNAP) as mentioned previously.

### 2.2.6 Muscle imaging in freely moving animals

Animals were submitted to the same conditions as the reproducible head lifting assay. After 30 minutes on the second unseeded plate, each animal was recorded for one minute while freely crawling using an Olympus MVX10 upright microscope (Olympus Life Science). Usable consecutive frames were used for further processing and analysis (at least 30 seconds per animal). Fluorescence intensity of GCaMP3.35, showing muscle activity on both sides, was measured using image analysis software Fiji.

### 2.2.7 Head orientation measurements

In both calcium imaging and head orientation devices, head bending was measured at each time point as the angle between the tip of the animal's nose and the midline of its body at the most anterior restrained point using Matlab.

### 2.2.8 Isothermal Tracking Assays

Glacial acetic acid vial was put in the middle of a chemotaxis agar plate to create gradients ranging from 16°C in the middle (under the vial) and 23°C on the outside borders (temperature reading performed with infrared thermometer). Once the gradient had been established for 15 minutes, worms were placed on the plate after being washed in NGM buffer and behavior was recorded for 20 minutes.

The percentage of total worms per strain that tracked isotherms during the assay was assessed and duration of each track is then assessed by eye on the recording. Average duration for every strain was plotted. Percentage of worms in each time category (0-30s, 30-60s or more than 60s) was also defined.

### 2.2.9 Normalization and cross-correlation analysis

For each experiment of calcium imaging and muscle fluorescence in semi-restrained or freely moving worms, the fluorescence intensity in each compartment (dorsal or ventral) was scaled from 0 to 1 using a custom macro with the formula (F-Fmin)/(Fmax-Fmin) in JMP software for each individual.

Those time series data of fluorescence intensities were derived based on time constant. Taking also into account the head position cross-correlations were performed using JMP Pro 16 (SAS) with +/- 25 time lags. The average value of peak +/- 5 lags of each cross-correlation were compared. Bilateral t-tests, taking into account the difference between sample variance, were performed to assess the significance between comparison.

### 2.2.10 Statistical analysis

Statistical tests were performed using JMP Pro 13 (SAS) and MatLab. Wherever possible complete distributions of all data points are shown. All error bars are standard errors of the mean. Statistical tests, including sample size, test statistics, and resulting p-values are reported in figure legends.

| Genotype | Primer Sequences (5’ —> 3’) |
|---|---|
| *gar-3* | **F:** CCG TTG CGT ACG AGC CTC<br>**R:** GTA CTG CCC GGA CAT TTT CTG |
| *mca-3* | **F:** TTG AGC AAC TCT TCA GTT GGC<br>**R:** CAT GAC CGC CAT CGC TGT C |
| *ric-7* | **F:** CAA TCA GGA CTT TCT CGT GG<br>**R:** CTG TAT CGA GTA TTC AAA TTA TTC |
| *sel-12* | **F:** CGG TAC AAA TCT GAT AAC AAA TCG<br>**R:** GAA TGG CCA CAT AAC AAG CGA T |

**Table 2.1. Primers used for genotyping.** List of genotypes and sequences of primers used for PCR to screen for their respective mutant alleles.

CHAPTER 3

# RESULTS

## 3.1 A Gate-and-Switch model for head orientation behaviors in *Caenorhabditis elegans*

We first showed that RIA is required to bias head movement in response to asymmetrically presented stimuli and that the loop compartment acts in a gate and switch mechanism to lead to correct steering response (Ouellette et al. 2018).

### 3.1.1 *RIA function in head orientation behavior*

As stated previously, *C. elegans* undulates on its side in the dorso-ventral plane. When the worms crawl, local compartmentalized calcium activity in the ventral and dorsal compartments of RIA (nrV and nrD) can be detected. These local motor-evoked calcium events ($mCa^{2+}$) are triggered by muscarinic input from head motor neurons onto nrV and nrD compartments. Input from head motor neurons is processed via muscarinic acetylcholine receptors (mAchRs), specifically GAR-3 (Hendricks et al. 2012) (Figure 3.1 A-B). By contrast, sensory input is received from upstream sensory neurons and is integrated within the loop region of RIA to lead to whole axon sensory calcium events ($sCa^{2+}$). While presenting an attractive stimulus results in a whole axon calcium reduction, the removal of that attractant—thereby becoming repulsive—resulting in whole axon calcium increase (Hendricks et al. 2012) (Figure 3.1 C). Moreover, if a stimulus is presented symmetrically to both sides of the worm, the inhibitory RIA output to SMDs is also symmetric. In the case where stimulus presentation is asymmetric, though, RIA interneuron output in turn also becomes asymmetric presumably in order to drive steering behavior (Hendricks and Zhang 2013). This sensory integration at the RIA

level then leads to head withdrawal away from the repulsive stimulus (Hendricks et al. 2012) (Figure 3.1 D-E).

To address the hypothesis that RIA was involved to bias head movement when presented with asymmetric olfactory stimuli, we used microfluidic devices called *river chips*, where worms are semi-restrained but can freely move their heads as two laminar streams flow on either side of the worm (McCormick et al. 2011) (Figure 3.1 F). This allows the animals to demonstrate a preference for either stream by biasing head movement towards one side or the other throughout the trials. Each worm was recorded for two minutes, switching the attractive odor (in this case isoamyl alcohol—IAA) (Chalasani et al. 2007) and buffer streams every 10 seconds after one minute to control for any intrinsic bias in head bending direction.

In wild type animals, a clear preference for the stream containing the odor was observed. Transgenic RIA::TeTx animals were used to examine the effect of blocking RIA synaptic output. In RIA::TeTx animals, no preference between buffer and an attractive stimulus was present. The same absence of affinity could be observed when worms were treated with scopolamine, a known muscarinic acetylcholine receptor antagonist (Broadley and Kelly 2001), mimicking the effects of a lack of function *gar-3* mutant, as both conditions result in a lack of motor input to nrV and nrD (Figure 3.1 G). These results suggest that RIA is required to correctly respond to asymmetrically presented stimuli, and to generate a correct steering response.

### 3.1.2 *RIA mediates directional head withdrawal*

From there, we focused on the loop compartment of RIA more closely in order to understand what was happening as the sensory inputs reached the interneuron. Calcium imaging microfluidic chips were used to simultaneously track head movement and calcium activity in all RIA compartments at odor (IAA) ON or OFF. This device allowed us to control the temporal presentation of olfactory stimuli in such a way that we could evaluate the effect of stimulus withdrawal at specific points of the head bending cycle. To fully visualize the phasic properties of head bending during calcium imaging, we used a 2D position-velocity plot to associate velocity values with the head position. Thus, positive and negative values reflect a head bending or a head withdrawal, respectively (Figure 3.2 A,B).

When analyzing head movement directly following odor removal at each phase of the cycle (Figure 3.2 B and D), we observed that strong ventral movements were correlated with odor removal occurring during a dorsal head bend and clear dorsal movements were correlated with odor removal taking place during a ventral head bend (Figure 3.2 C).

During normal locomotion, head withdrawal (return toward the worm's midline) is set to happen after each head bend. Knowing this we hypothesized that presenting or removing a stimulus should change this normal oscillation.

We sought to examine stimulus-induced active head withdrawal as well as the head movements that occur during the normal oscillatory cycle or crawling. As such, we tracked head movements before and after odor removal or presentation, as well as

head movements not associated with any stimulus delivery. Since responses should be a mirror image along the dorsoventral axis, head movement on either side was labeled as positive. Positive velocities were used to describe head bending and negative ones were linked to head withdrawal (Figure 3.3 A).

As expected, head bending as a general rule is indeed followed by head withdrawal (Figure 3.3 B), but we found out that only odor removal leads to a rapid head movement. This head withdrawal away from the repulsive stimulus was only observed to happen when the head is bent (Figure 3.3 C-D).

Furthermore, since $mCa^{2+}$ events are dependent on synaptic inputs from SMDs through GAR-3 (Hendricks et al. 2012), we performed the same head bending analysis in *gar-3* mutants, a muscarinic acetylcholine receptor (mAchR) loss of function mutant which lacks cholinergic inputs from SMDs unto RIA motor compartments, and RIA::TeTx animals, in which the synaptic release from RIA is blocked by cleaving synaptobrevin (Schiavo et al. 1992), to address the possibility that those $mCa^{2+}$ events might play a role in modulating head movements made in response to sensory stimuli.

Both *gar-3* mutants or RIA::TeTx animals displayed no stimulus-dependent head withdrawals. Expressing *gar-3* cDNA specifically in RIA led to a partial rescue of this behavior but it was not significantly different from *gar-3* mutant responses (Figure 3.3 D).

### 3.1.3 *RIA sensory responses through the loop compartment are gated according to head position*

We next went on to analyze the link between head movements, $mCa^{2+}$ and $sCa^{2+}$. While we observed that the motor compartments (nrV and nrD) show asynchronous compartmentalized activity throughout head bending, the loop doesn't have a clear relationship with head movement (Figure 3.4 A-B).

Knowing that head movements occur very frequently while odor switches are set to happen at discrete time points, we hypothesized that maybe the spontaneous $sCa^{2+}$ events might hide a link between head movement and the stimulus-evoked events.

As such, we assessed whether loop $sCa^{2+}$ events were dependent on head phase using heatmap for data visualization. After odor removal, a higher magnitude of calcium can be observed (dark green regions) when the head is bent towards the dorsal or ventral side, with no clear activity if the head is parallel to the midline of the worm (Figure 3.4 C-D). This strongly suggests that the loop only responds to stimulus removal and only when the head is bent is one side or the other.

Following these findings, we concluded that there is clear evidence of a sensory gating mechanism present at the RIA level which makes the loop compartment of the interneuron respond to sensory cues in accordance to the worm's head position. This gating ensures that large $sCa^{2+}$ events occur when the motor "switch" downstream in nrV and nrD is engaged either dorsally or ventrally due to asymmetric $mCa^{2+}$ events.

To investigate whether the sensory gating mechanism is dependent on motor feedback, we pursued the same analysis in *gar-3* mutants. As shown previously (Hendricks et al. 2012), the $mCa^{2+}$ events in this mutant are non-existent while $sCa^{2+}$ are intact. In our case, *gar-3* mutants showed normal sensory gating (Figure 3.4 E). This suggests that the gating mechanism we observed is not motor compartment dependent and is located at the interneuronal level within the RIA loop. Whether the loop alone is sufficient for gating or whether it relies on upstream interneurons is unknown. Maybe this mechanism could also be linked to a yet unidentified proprioceptive pathway linked to mechanoreceptor neurons located in the head.

### 3.1.4 *RIA axonal compartments have temporal features of sensory responses*

To gain a better understanding of RIA function as a whole in this process, we analyzed the motor compartments (nrV and nrD) individual responses during $sCa^{2+}$ events. This allowed us to dig further into how both sensory and motor signals can pair to influence synaptic output. As previously stated (Hendricks et al. 2012), sCa2+ and mCa2+ are additive. When quantifying motor compartment responses during head bending, we observed a significant lag of peak responses that appeared to be dependent on head orientation (Figure 3.5 A-B). That is to say, the motor compartment that was located in the direction of the head bending showed a stronger calcium signal during bending, as well as a shorter latency time to reach peak calcium level.

Head movement always precedes the $mCa^{2+}$ response, possibly due to the fact that muscle contractions are dependent on nicotinic acetylcholine receptors which are faster to respond than the muscarinic receptors (Greenwood et al. 2009) found on nrV and

nrD. Since the lag time is negligible, we considered that $mCa^{2+}$ responses in RIA are indicative of ongoing head movements (Figure 3.5 C).

Cross correlation analyses were performed on head velocity and calcium activity during odor removal to study the timing of events and how it could lead to the shift we observed in peak calcium activity. Positive peaks near the *y*-axis indicate a calcium event that coincides in phase with head motion while peaks shifted to the left represent events that are delayed relative to head motion.

During odor removal, we observed that when the head is bent ventrally, the peak calcium activity in nrV is in sync with head withdrawal in the dorsal direction as nrD calcium lags. The opposite is also true; during dorsal head bends, the peak calcium activity in nrD syncs with withdrawal in the ventral direction while nrV calcium lags. When the head is at midline position (not bent), this relationship between motor compartment responses and head position is lost due to the lack of $sCa^{2+}$ events (Figure 3.5 D).

Once again, we performed the same analysis on *gar-3* mutants to observe the impact of motor input ablation. As expected, we observed a desynchronization of motor compartment responses and head position in gar-3 mutant animals. Reexpression of *gar-3* specifically in RIA rescued some of this desynchronization phenotype, but this was insufficient to fully rescue normal nrV and nrD dynamics (Figure 3.5 C-D). This was also reminiscent of the failure to completely rescue the head withdrawal phenotype shown previously (Figure 3.4 D).

This could indicate that GAR-3 is playing a role outside of the RIA circuit to mediate head withdrawal. Alternatively, the re-expressed construct may lead to insufficient expression or could be mislocalized, leading to an inability to rescue GAR-3 function to wild type a level in RIA.

All of this indicates that $mCa^{2+}$ and $sCa^{2+}$ have additive properties that decouple the events' timing following odor removal. This suggests that, while $mCa^{2+}$ responses lag slightly relative to head movements, these responses function additively with $sCa^{2+}$ to decrease latency, leading to quicker neurotransmitter (glutamate) release toward head motor neurons, and on one side vs the other, leading to head withdrawal.

### 3.1.5 *Gate and Switch Model for Head Orientation*

These results led us to propose a gate and switch system for the integration of sensory stimuli at the RIA level. Essentially, when the head is situated in the middle of an oscillation, the gate (the loop compartment) is closed and doesn't respond to sensory stimuli. But when the head is bent towards one side or the other—either ventrally or dorsally—the gate is open, allowing sensory input to signal to motor compartments, which ultimately leads to head withdrawal away from the repulsive stimulus (Figure 3.6).

## 3.2 Head lifting as a novel phenotype to screen *Caenorhabditis elegans* Interneurons for the molecular underpinnings of head orientation

### 3.2.1 *Candidate Gene Screen for Impaired RIA Function*

Knowing that the loop integrates sensory stimuli using the aforementioned gate and switch mechanism, and that $sCa^{2+}$ events are linked to head orientation, we next wanted

to assess what is happening on a molecular level within the motor compartments (nrV and nrD) in regards to behavior and $mCa^{2+}$ calcium activity.

As stated previously, *C.elegans* normally undulates on its side in the dorso-ventral plane. However, we noticed that when RIA function is impaired, animals exhibit an abnormal phenotype where they display head bending in the left-right plane, which can be observed as the worm actively lifts its head from the agar substrate (Figure 3.7). What is happening at the RIA circuit level during this head lifting behavior is still unknown.

### 3.2.2 *RIA is required for proper muscle activity at the head level in semi-restrained animals*

Since RIA signals to head motor neurons (SMDs), we sought to investigate the role of RIA signaling in SMD function. To achieve this, we quantified muscle activity using a strain expressing the calcium reporter GCaMP3 in body wall muscles [*myo-3p::GCaMp3.35*], in order to visualize muscle activity during head bending. This strain was crossed into an N2 background, *gar-3(gk305)* background, and in animals expressing the tetanus toxin light chain (TeTx) under the RIA-specific promoter, *glr-3p*.

To quantify calcium levels relative to head bending angle, worms were placed in a river chip, as described previously (McCormick et al. 2011). Animals were exposed to alternating streams of NGM buffer and IAA, so as to experience the olfactory stimulus from either side of their head to stimulate head bending. Head position as they moved was determined using pixel density and muscle activity at the head level was assessed

by measuring the calcium intensity on both the ventral and dorsal side of the animals (Figure 3.8 A-B).

Similarities between values were analyzed by plotting cross correlations to visualize whether there was a correlation between two distinct parameters (perfect correlation = 1). Muscle activity on either side (ventral or dorsal) and head position were first compared and showed a significant correlation difference for both RIA impaired strains vs wild type (Figure 3.8 C). This suggests that the RIA is involved in the control of muscle activity during head bending.

Therefore, we looked at the cross correlation of only muscle calcium activity on both sides (ventral and dorsal). We found out that activity is mostly localized on one side at a time in wild type (negative correlation) and significantly less so when RIA motor output (*glr-3p*::TeTx) or inputs (*gar-3(gk305*)) are blocked (Figure 3.8 D). This suggests that muscle activity is less compartmentalized when RIA function is impaired, leading to aberrant muscle activity in the nrV and nrD. This observed lack of asynchrony could give rise to overactivation and/or inhibition of both dorsal and ventral muscles, leading to incorrect gait.

### 3.2.3 *RIA is required for proper muscle activity at the head level in freely-moving animals*

Due to the physical constraints associated with the PDMS microfluidic chip described in the previous section (chip depth: 30um), semi-restrained worms were unable to perform the head lifting behavior that was observed in freely-crawling worms. However, the possibility remained that worms were capable of the intent to perform head lifting, even

if they were unable to correctly perform the motion. In order to address this possibility, we chose to analyze calcium muscle activity while worms are freely moving.

We recorded freely moving worms on non-seeded NGM plates and measured the calcium intensity for both ventral and dorsal muscles as they crawled (Figure 3.9 A-B). Head lifts were observed in *gar-3(gk305)* and RIA::TeTx backgrounds throughout the trials. Bouts of crawling behavior, with and without head lifting, were recorded and analyzed in order to get a better sense of the complete head bending strategy at the head muscle level.

A negative correlation between dorsal and ventral muscle activity was obtained for wild type animals once again, with the asynchrony even more striking than was observed in semi-restrained worms (Figure 3.9 C). Moreover, blocking the cholinergic input (*gar-3(gk305)*) or the glutamate output (RIA::TeTx) of RIA reduced that negative correlation significantly. This corroborated that, even in a more natural environment in which animals can freely crawl and head lift, muscle activity is impaired and less compartmentalized when RIA dynamics are impaired.

### 3.2.4 *Head lifting as a correlate to identify genes implicated in RIA dynamics*

Through the observation of crawling behavior and testing different conditions (as described in Figure 3.10 A-E), three different types of head lifts, differing by magnitude of the lift, were found to occur. These head lift variants formed three categories: types 1-3, varying from very shallow (type 1) to highest lift (type 3) (Figure 3.11 B-E). Following that, a reproducible assay was optimized to reduce variability and obtain more consistent results (see Materials and Methods 2.2.2). More than sixty different genes all

involved in calcium signaling or coding for GPCRs or subunits of glutamate receptors were submitted to the assay (Table 3.1).

Each candidate strain was submitted to this assay, although only type 2 and 3 head lifts were scored because these tended to vary the most strongly by strain and therefore allowed for better distinction between wild type and RIA-impaired strains. For example, *gar-3(gk305)* almost exclusively showed type 2 and 3 head lifts. It is also important to note that type 1 head lifts were excluded due to the variability and difficulty involved in scoring low-magnitude (shallow) head lifts. In addition, all strains engage in consistent type 1 head lifting and therefore monitoring this particular behavior did not add to our analysis.

Head lifting was then manually scored for candidate strains (Figure 3.11 F). This screen identified some promising candidates and several genes of interest were retained for further investigation (Figure 3.11 F, blue boxes). They were curated from the top ten highest head lifters (plus one that was head lifting significantly less). Amongst these candidates, we observed an increase in overall head lifting frequency in strains already known to have impaired RIA function, as is the case for the aforementioned *gar-3(gk305)* and RIA::TeTX. The following strains were noted as interesting candidates due to their frequent head lifting, which was observed to be significantly different than wild type and often on par with known candidates. These strains are presented below according to their potential involvement in the RIA circuit.

The *mca-3(ar493)* mutant strain had the most striking phenotype and displayed only type 3 head lifts throughout the trials. *mca-3* encodes a plasma membrane calcium ATPase (PMCA). PMCAs actively pump calcium from the cytosol into the extracellular

space, and as such play a prominent role in regulating calcium signaling (Di Leva et al. 2008; Carafoli et al. 2001).

Another retained candidate identified by the screen is *ric-7*, which has been shown to be localized in mitochondria and at the synapse. While *ric-7* is a nematode-only gene, it is involved in neuropeptide secretion from dense core vesicles (DCVs) (Rawson et al. 2014) and is essential for correct localization of mitochondria in axons (Rawson et al. 2014; Hao et al. 2012). A recent study linked those two events together by showing that DCVs release is impaired when there is an incorrect distribution of mitochondria in axons (Zhao et al. 2018).

Furthermore, mitochondria can interface with and uptake $Ca^{2+}$ from the endoplasmic reticulum (ER), which is a major source of calcium in cells (de Brito and Scorrano 2008, 2010). Again, further studies could focus on RIC-7 involvement in RIA, in order to elucidate the role of mitochondrial function, specifically as it relates to calcium dynamics. Further study of RIC-7 could provide some insight as to how calcium enters the RIA neuron, where it comes from, and how calcium is regulated within RIA motor compartments.

In addition to *ric-7*, other genes involved in mitochondrial calcium dynamics were submitted to the screen and one stood out as a high head lifter. Three genes belonging to the *C. elegans* presenilin (PSEN) family, namely *spe-4, sel-12* and *hop-1,* along with the mitochondrial calcium uniporter, *mcu-1*, were tested. PSEN are transmembrane proteins that are expressed in the ER and have been shown to be enriched in ER compartments that are in contact with mitochondria; accordingly, it has been suggested that PSEN proteins might play a role in calcium exchange between the two (Sarasija

and Norman 2015). Out of the three PSEN family members, *sel-12* was retained for screening because of its direct involvement in mediating calcium release from the ER, as well as the role it plays in maintaining the mitochondrial structure and function (Sarasija and Norman 2015; Sarasija et al. 2018). Upon screening, the *sel-12* strain was categorized as a top tier head lifter and retained for further analysis (Figure 3.11 F).

### 3.2.5 *Top head lifters show impaired calcium dynamics within RIA motor compartments*

To confirm whether our retained chosen candidates play a role in RIA function, calcium imaging was performed and a custom MatLab script, FluoroSNNAP (Figure 3.12 A-F), was used to analyze results. Every candidate strain was submitted to imaging in a *glr-3p::GCaMP3* background, which expresses the calcium indicator GCaMP3 specifically in RIA neurons.

As described previously, cross correlations were plotted, this time for calcium activity (in either nrV or nrD motor compartments) and head bending (tracking the head position through time) (Figure 3.13 C). Interestingly, while *mca-3(ar493)* and *gar-3(gk305)* mutants, as well as RIA::TeTx, all showed significantly decreased compartmentalization, *sel-12(ok2078)* and *ric-7(nu447)* seem to demonstrate more complex calcium dynamics. While the correlation between head bending and calcium activity is significantly different from wild type on the ventral side, *sel-12* mutants showed no significant difference on the dorsal side. A slight shift to the left can also be observed on the ventral side, hinting at a potential lag in response. This suggests that *sel-12* may control motor compartment dynamics in a temporal manner, though differently in both compartments.

When looking at the cross correlation of compartments only (nrV and nrD) (Figure 3.13 D), we found out that activity is synchronous in both compartments and significantly different than wild type animals in *mca-3(ar493)*, *ric-7(nu447)*, *sel-12(ok2078)* or *gar-3(gk305)* background (shown by a higher correlation value) (Figure 3.13 B and D). A lower correlation value, observed in wild type worms, is indicative of normal compartmentalized $Ca^{2+}$ activity (Figure 3.13 A and D). These results suggest and further confirm that high head lifting genes identified from the candidate screen do appear to play a role in RIA motor compartments, and are essential for normal calcium dynamics in the interneuron.

It is important to note that *ric-7*, while being a high head lifter, showed no significant difference from WT in calcium activity relative to head position. However, *ric-7* was significantly different from WT in terms of the compartments themselves, which showed abnormal synchronous calcium activity. Knowing that *ric-7* has been shown to regulate the correct localization of mitochondria along axons in *C. elegans* (Rawson et al. 2014), whole axon calcium responses could occur in *ric-7* mutants due to spatially dysregulated mitochondria. The fact that it has also been involved in the correct release of neuropeptides (Hao et al. 2012) could be a clue that it can potentially act at the level of the output the motor compartments have.

Moreover, the same analysis was performed with a strain that was a low head lifter, *unc-68(kh30)*. This strain showed a significant difference when looking at calcium activity compartmentalization, as well as abnormal calcium activity in the dorsal motor compartment during head movement. These deficits could suggest that *unc-68* plays a role in synaptic partners downstream of RIA. This hypothesis could be plausible as

*unc-68* codes for a ryanodine receptor that has been shown to be involved in body wall muscle contractions (Maryon et al. 1996; Umanskaya et al. 2014; Forrester 2018). Since RIA outputs to head motor neurons that, in turn, signal to head muscles, *unc-68* could link both.

### 3.2.6 *Top head lifters show impaired isothermal tracking behavior*

Since isothermal tracking is an efficient way to gauge the correct pairing of sensory inputs of the environment to motor commands, we tested it with chosen candidate gene strains. We optimized a protocol based on (Mori and Ohshima 1995) and the defined period of time they track each isotherm is identified as an individual forward track. A forward track was defined as a single motion track during which the worms do not reverse or change orientation. Duration of each forward track was assessed and showed that the ability of worms to track isotherms is impaired in candidate strains vs wild type (Figure 3.14 A-B). The average length of tracks is significantly different than wild type for all and the percentage of worms that follow isotherm during the course of the assay is also significantly diminished (Figure 3.14 C-E). These results show that, when RIA function is unbalanced, sensory-motor coupling is compromised. This further suggests that RIA has a direct role to play in active sensing.

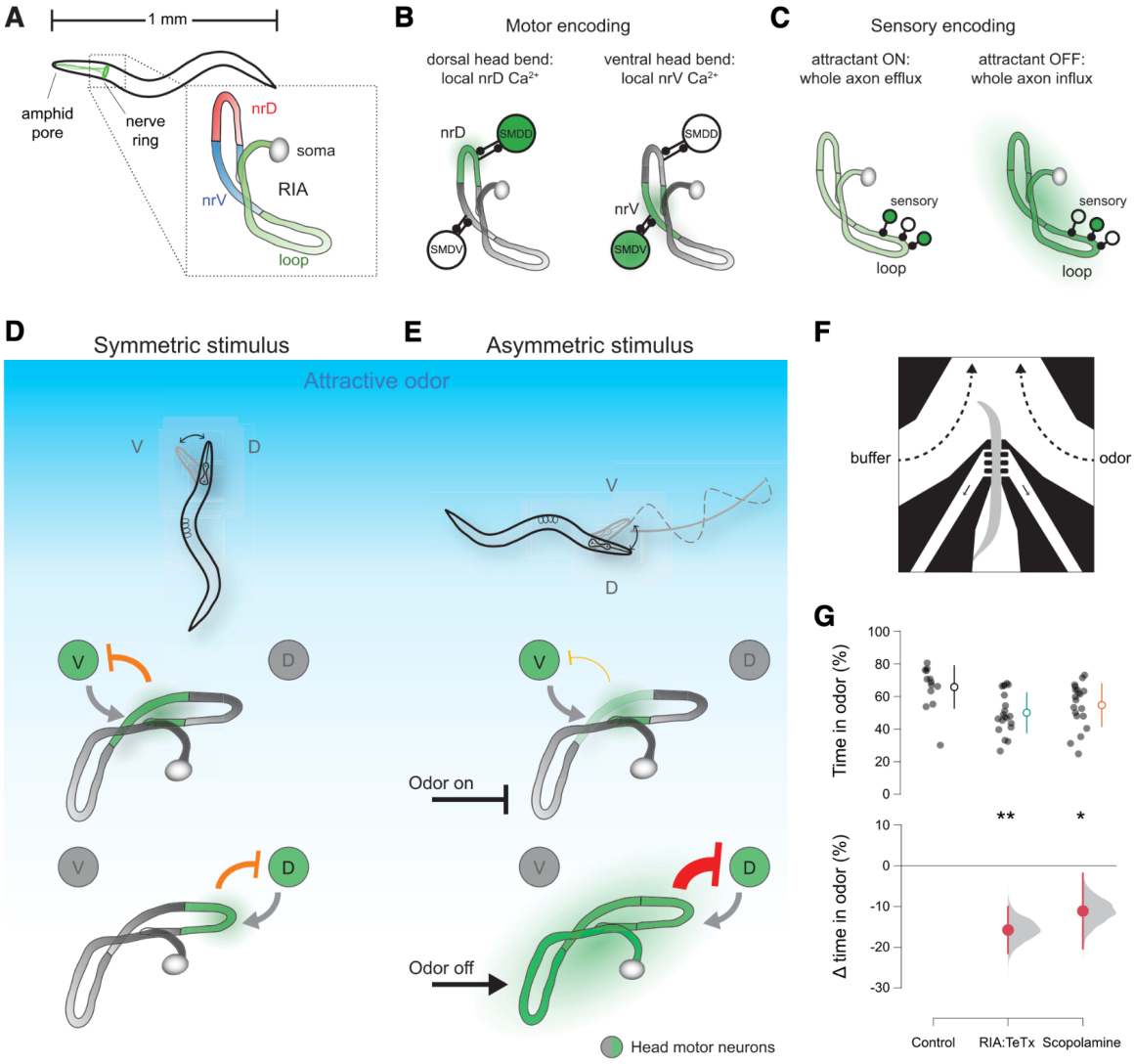
A
1 mm
amphid pore
nerve ring
nrD
soma
RIA
nrV
loop
B
Motor encoding
dorsal head bend: local nrD Ca2+
ventral head bend: local nrV Ca2+
nrD
SMDD
SMDV
nrV
C
Sensory encoding
attractant ON: whole axon efflux
attractant OFF: whole axon influx
sensory
loop
D
Symmetric stimulus
Attractive odor
V
D
E
Asymmetric stimulus
Odor on
Odor off
Head motor neurons
F
buffer
odor
G
Time in odor (%)
Δ time in odor (%)
**
*
Control
RIA:TeTx
Scopolamine

**Figure 3.1 RIA overview and requirement for control of head orientation.** ***A***, RIA is a unipolar interneuron whose axon extends into the ventral nerve cord and throughout the nerve ring. There are two RIAs, left and right, one is shown. ***B***, Two axonal compartments within the nerve ring, nrV and nrD, encode head movements via local calcium signals ($mCa^{2+}$) triggered by muscarinic input from SMD head motor neurons. ***C***, Sensory pathways synapse on the loop domain of the RIA axon in the ventral nerve cord. Attractive stimuli lead to whole-axon reduction in calcium, while attractant removal causes whole axon calcium increases ($sCa^{2+}$) ***D***, Model for RIA function in steering behaviors. Where stimuli are symmetric across head bends, inhibitory output from RIA to motor neurons is symmetric. ***E***, If the stimulus changes across head sweeps, RIA output to motor neurons become asymmetric, driving steering behavior. ***F***, Schematic of head orientation measurement in response to a unilaterally presented stimulus. ***G***, Estimation plot of difference between wild-type preference for odor as measured by percentage of the assay time (120 s) with their head within the odor stream and RIA::TeTx animals or animals treated with scopolamine. ANOVA $F(2,50) = 5.7771$, $p = 0.0055$, $*p < 0.05$, $**p < 0.01$ *post hoc* Student's *t* test, $n = 13$, $n = 20$, $n = 20$. V, ventral; D, Dorsal. Open circles and lines are mean +/- SD (top). Closed circles and lines are mean differences from control +/- 95% confidence interval, shown with distribution of estimated means. (Ouellette et al. 2018)

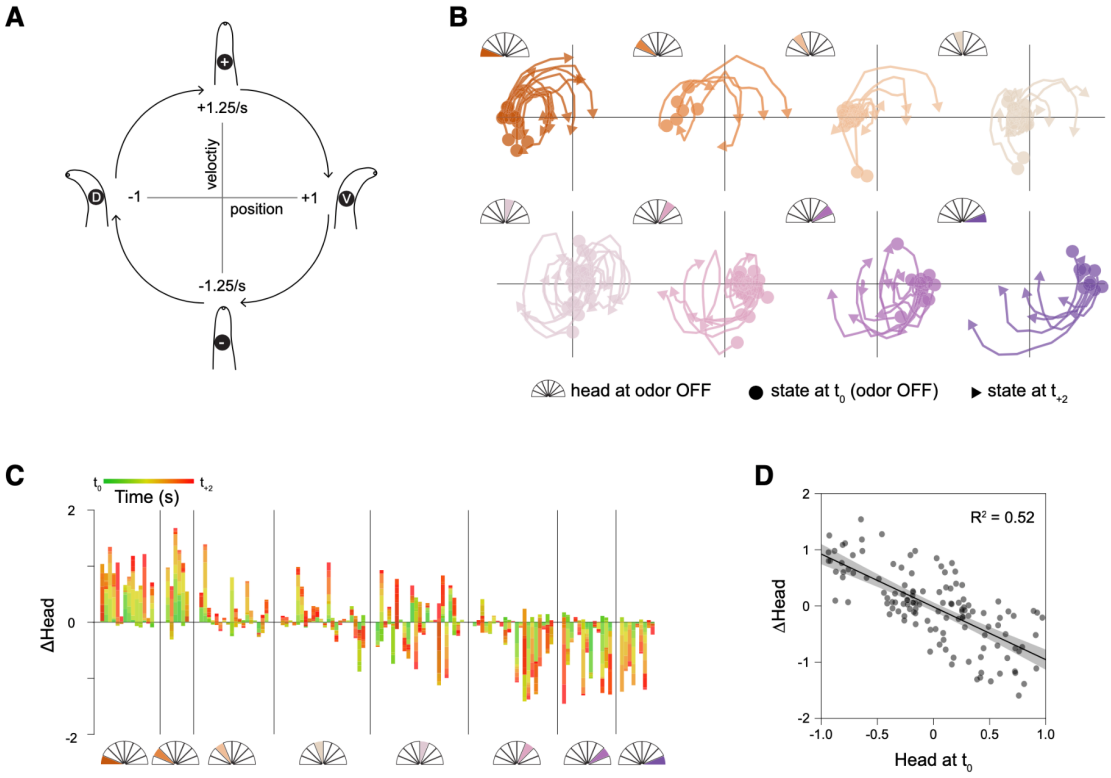
A
+1.25/s
velocity
-1
+1
position
-1.25/s
D
V
B
head at odor OFF
state at t0 (odor OFF)
state at t+2
C
t0
t+2
Time (s)
ΔHead
2
0
-2
D
R² = 0.52
ΔHead
2
1
0
-1
-2
-1.0
-0.5
0
0.5
1.0
Head at t0

**Figure 3.2 Responses to odor removal depend on posture.** ***A***, Schematic of position-velocity plots to illustrate oscillatory head movements. ***B***, Position-velocity trajectories from odor removal (circles) to 2 s after (arrowheads). ***C***, Head displacement in the 2 s immediately following odor removal, with the start position normalized to head orientation at the odor switch. ***D***, Relationship between head position at odor removal and the change in head position 2 s later. Linear regression $F(1,124) = 132.3145$, $p < 0.0001$; $n = 126$.

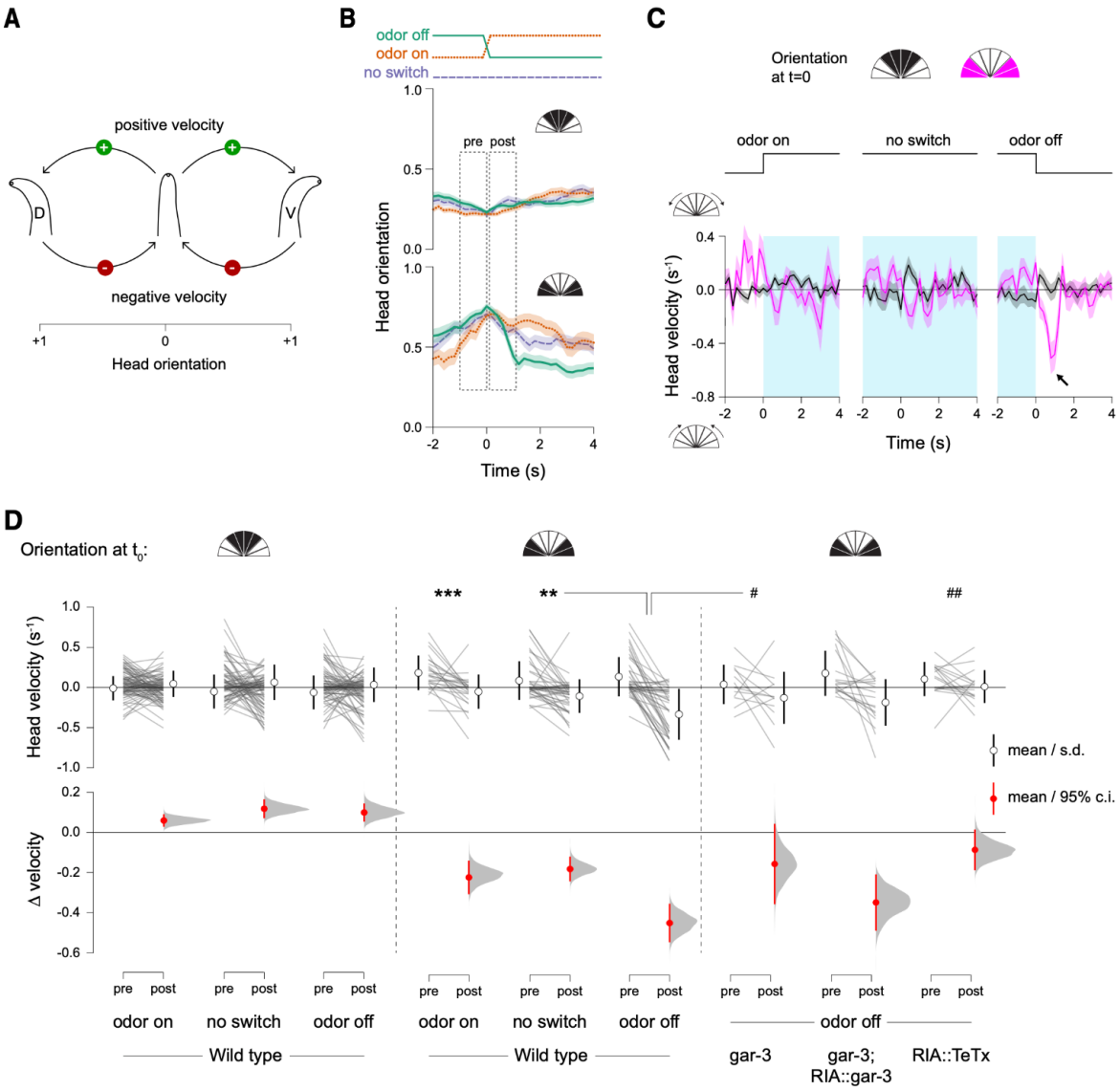
A
positive velocity
D
V
negative velocity
+1
0
+1
Head orientation
B
odor off
odor on
no switch
pre post
Head orientation
Time (s)
C
Orientation at t=0
odor on
no switch
odor off
Head velocity (s-1)
Time (s)
D
Orientation at t0:
***
**
#
##
Head velocity (s-1)
Δ velocity
mean / s.d.
mean / 95% c.i.
pre post
odor on
no switch
odor off
Wild type
gar-3
gar-3; RIA::gar-3
RIA::TeTx

**Figure 3.3 RIA mediates directional head withdrawal.** ***A***, To analyze head withdrawal behaviors, which are mirror-symmetric across the dorsoventral axis, head deflection in either the dorsal (D) or ventral (V) direction is defined as positive. Positive velocities correspond to bending away from the body axis and negative velocities indicate head withdrawal. ***B***, Mean plots of peristimulus head orientation at odor off, odor on, or in constant odor (no switch), binned according to whether the head is unbent (top) or bent in either direction (bottom) at the time of stimulus change ($t$ = 0). Dashed "pre" and "post" boxes indicate time windows used for quantitation in ***D***. ***C***, Comparison of head velocity in response to stimulus changes (or no switch) when the head is bent or unbent. Arrow indicates characteristic head withdrawal in response to odor removal when the head is bent. ***D***, Paired mean pre- and post-switch head velocities (upper panels, open circles and lines are mean +/- SD) and estimations of the size of the head velocity change (lower panel, closed circles and lines are mean difference +/- 95% confidence interval, along with probability distribution of means, see Materials and Methods). Odor switch (on, off, or constant odor) has no effect on head movements when the head is not bent (left panel, repeated measures ANOVA $F(2,263) = 0.9386$, $p = 0.3925$, $n = 100$, $n = 82$, $n = 84$). Sharp decreases in velocity are seen when odor removal occurs when the head is bent, but not for odor presentation or constant odor (middle panel, repeated measures ANOVA, $F(2,109) = 7.7932$, $p = 0.0007$, $n = 26$, $n = 44$, $n = 42$). In *gar-3* mutants and animals expressing tetanus toxin in RIA these sharp decreases in head velocity are absent (right panel, repeated measures ANOVA $F(3,85) = 4.4105$, $p = 0.0062$, $n = 42$, $n = 12$, $n = 18$, $n = 17$); ***$p < 0.001$, **$p < 0.01$ *post hoc* Student's $t$ test between odor conditions (on, off, no switch) for wild-type animals; ##$p <$

0.01, #$p < 0.05$ *post hoc* Student's *t* test between genetic manipulation (wild type, *gar-3*, *gar-3* rescue, RIA::TeTx) for odor off responses during head bending.

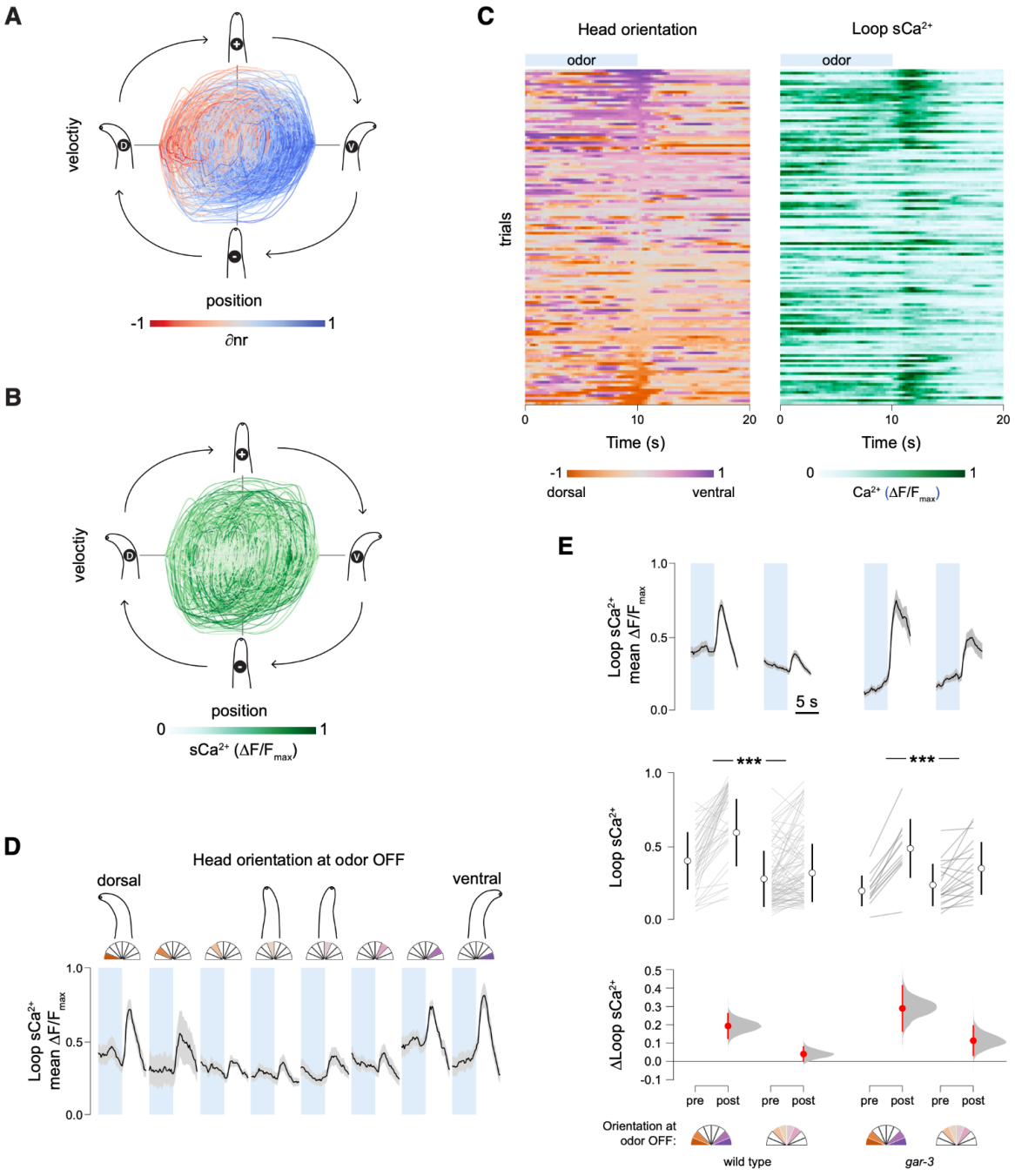
A
velocity
position
-1
1
∂nr
B
velocity
position
0
1
sCa²⁺ (ΔF/F_max)
C
Head orientation
Loop sCa²⁺
odor
odor
trials
0
10
20
Time (s)
0
10
20
Time (s)
-1
1
dorsal
ventral
0
1
Ca²⁺ (ΔF/F_max)
D
Head orientation at odor OFF
dorsal
ventral
Loop sCa²⁺ mean ΔF/F_max
1.0
0.5
0.0
E
Loop sCa²⁺ mean ΔF/F_max
1.0
0.5
0.0
5 s
***
***
Loop sCa²⁺
1.0
0.5
0.0
ΔLoop sCa²⁺
0.5
0.4
0.3
0.2
0.1
0.0
-0.1
pre
post
pre
post
pre
post
pre
post
Orientation at odor OFF:
wild type
gar-3

**Figure 3.4 Head orientation gates sensory responses.** ***A***, Head position-velocity trajectories color-coded by dnr (= nrV – nrD), a measure of normalized $mCa^{2+}$ asymmetry in nrV and nrD. ***B***, Head position-velocity trajectories color-coded by loop calcium signal, *n* = 126, 40 s each. ***C***, Spontaneous head movements (left) and $sCa^{2+}$ signals in the loop region of the RIA axon (right). Rows are matched and sorted according to head orientation at odor off (*t* = 10 s). A linear regression of loop response magnitudes and head deflection in either direction was significant ($F(1,124) = 29.98$, $p < 0.0001$, $n = 126$). ***D***, Mean traces of loop calcium responses 5 s before and after odor removal binned by head orientation at the odor off time point. Shading is SEM. Left to right, *n* = 14, *n* = 6, *n* = 18, *n* = 22, *n* = 23, *n* = 21, *n* = 13, *n* = 9. ***E***, Comparison of the magnitude of loop calcium responses to odor removal when the head is bent (head orientation > 0.5 or < – 0.5) or unbent (head orientation between – 0.5 and 0.5). Pre- and post-measurements are mean loop $Ca^{2+}$ levels in 1s windows just before odor OFF and centered on the peak of the mean response, respectively, shown as paired responses (lines) and mean +/- SD (open circles and lines). Estimations of the mean changes are shown below as mean difference +/- 95% confidence interval (closed circles and lines) along with probability distributions of the means (see Materials and Methods). In both wild-type ($n = 84$, $n = 42$) and *gar-3* ($n = 20$, $n = 12$) animals, the loop response magnitude is larger when the head is bent (repeated measures ANOVA $F(1,154) = 41.4529$, $p < 0.0001$, $^{***}p < 0.001$ *post hoc* Student's *t* test). *gar-3* mutants have larger responses under both head orientation conditions, but there is no significant interaction between loop $Ca^{2+}$ responses, head position at odor off, and genotype (repeated measures ANOVA $F(1,154) = 0.2145$, $p = 0.6439$).

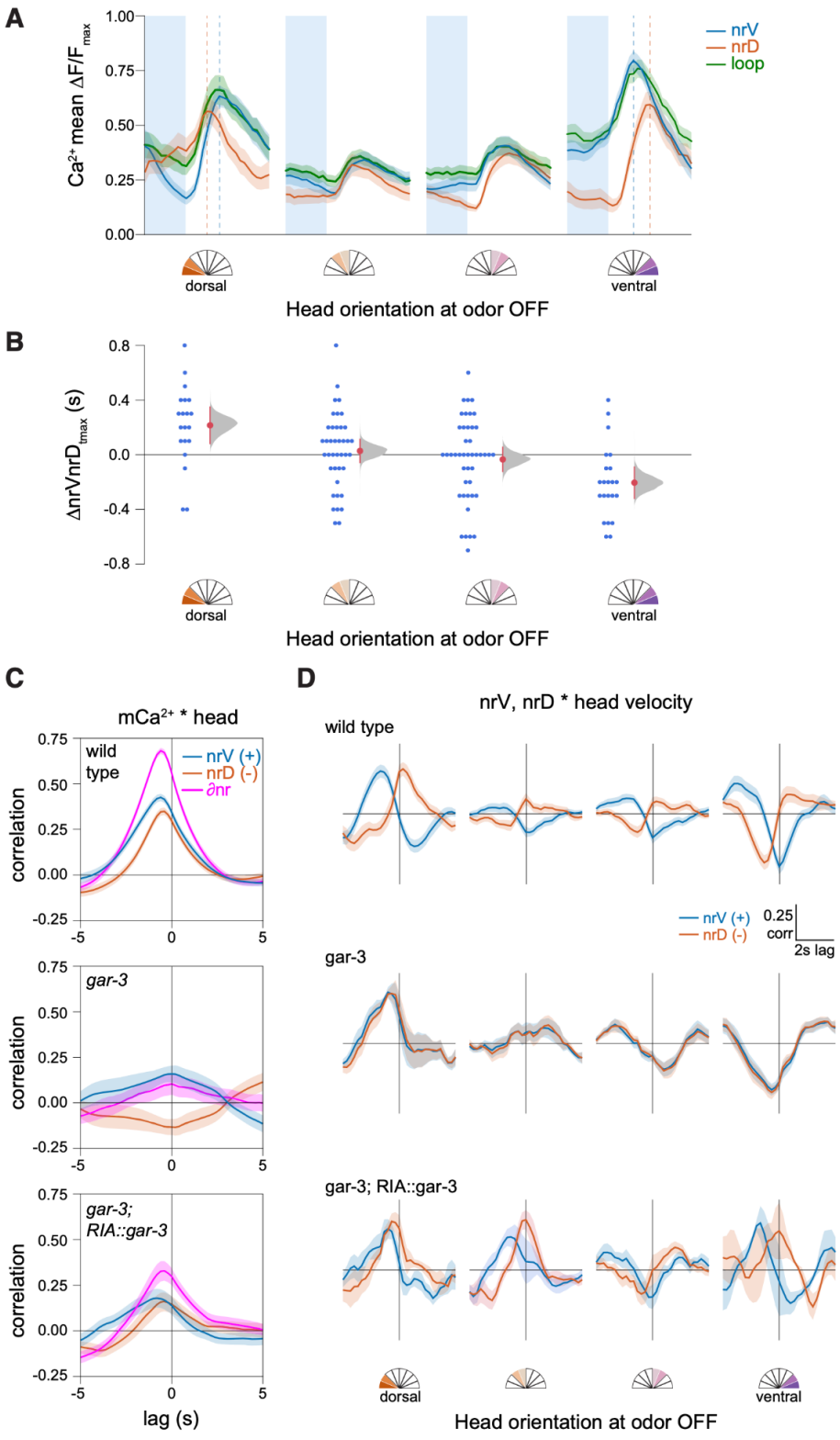
A
Ca2+ mean ΔF/Fmax
1.00
0.75
0.50
0.25
0.00
nrV
nrD
loop
dorsal
ventral
Head orientation at odor OFF
B
ΔnrVnrDtmax (s)
0.8
0.4
0.0
-0.4
-0.8
dorsal
ventral
Head orientation at odor OFF
C
mCa2+ * head
wild type
nrV (+)
nrD (-)
∂nr
gar-3
gar-3; RIA::gar-3
correlation
0.75
0.50
0.25
0.00
-0.25
-5
0
5
lag (s)
D
nrV, nrD * head velocity
wild type
nrV (+)
nrD (-)
0.25
corr
2s lag
gar-3
gar-3; RIA::gar-3
dorsal
ventral
Head orientation at odor OFF

**Figure 3.5 Temporal features of sensory responses in RIA axonal compartments.** ***A***, Mean nrV, nrD, and loop responses on odor removal. Shading is SEM, dashed lines indicate position of nrV and nrD mean peaks. ***B***, Head orientation predicts the mean lag between nrV and nrD peaks post-odor removal. ANOVA $F(1,124) = 13.47$, $p = 0.0004$. ***C***, Cross-correlation of nrV, nrD, and $mCa^{2+}$ asymmetry (dnr) and head orientation, showing $mCa^{2+}$ lag with head movements. *gar-3* mutants lack $mCa^{2+}$ and do not show head correlations. Re-expression of *gar-3* cDNA in RIA partially rescues this relationship. ***D***, nrV and nrD cross-correlations with head velocity for wild-type, *gar-3*, and RIA-specific *gar-3* rescue in a 6-s time window comprising 2-s pre-odor removal and 4-s post-odor removal in relation to head orientation at odor off. When the head was bent, we observed no lag between head withdrawal and peak calcium responses in the nerve ring compartment ipsilateral to the direction of bending. *gar-3* mutants show no distinction between nerve ring compartments. Expression of *gar-3* cDNA in RIA in *gar-3* mutants does not rescue the temporal features of sensory responses in the nerve ring. Analysis groups are the same as Figure 4.

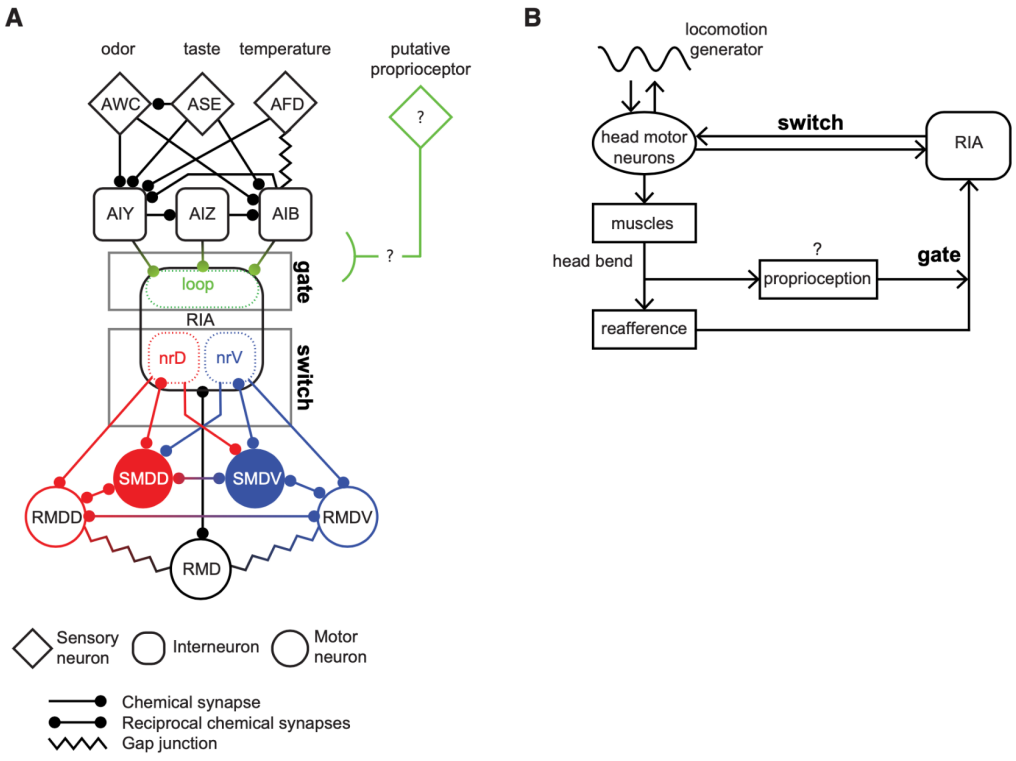
A
odor
taste
temperature
putative proprioceptor
AWC
ASE
AFD
?
AIY
AIZ
AIB
?
loop
gate
RIA
nrD
nrV
switch
SMDD
SMDV
RMDD
RMDV
RMD
Sensory neuron
Interneuron
Motor neuron
Chemical synapse
Reciprocal chemical synapses
Gap junction
B
locomotion generator
head motor neurons
switch
RIA
muscles
head bend
?
proprioception
gate
reafference

**Figure 3.6 Gate and switch model for RIA function in head orientation behaviors.** ***A***, RIA circuit diagram, with major upstream sensory pathways and head motor connections. Gating of sensory inputs to the loop domain and the nerve ring connections that constitute the dorsal-ventral switch. ***B***, Ethological model in which head movements simultaneously produce proprioception-gated reafference and efference copies that converge on RIA. RIA output to motor neurons biases the undulatory gait dorsally or ventrally when reafferent stimuli are asymmetric across head sweeps.

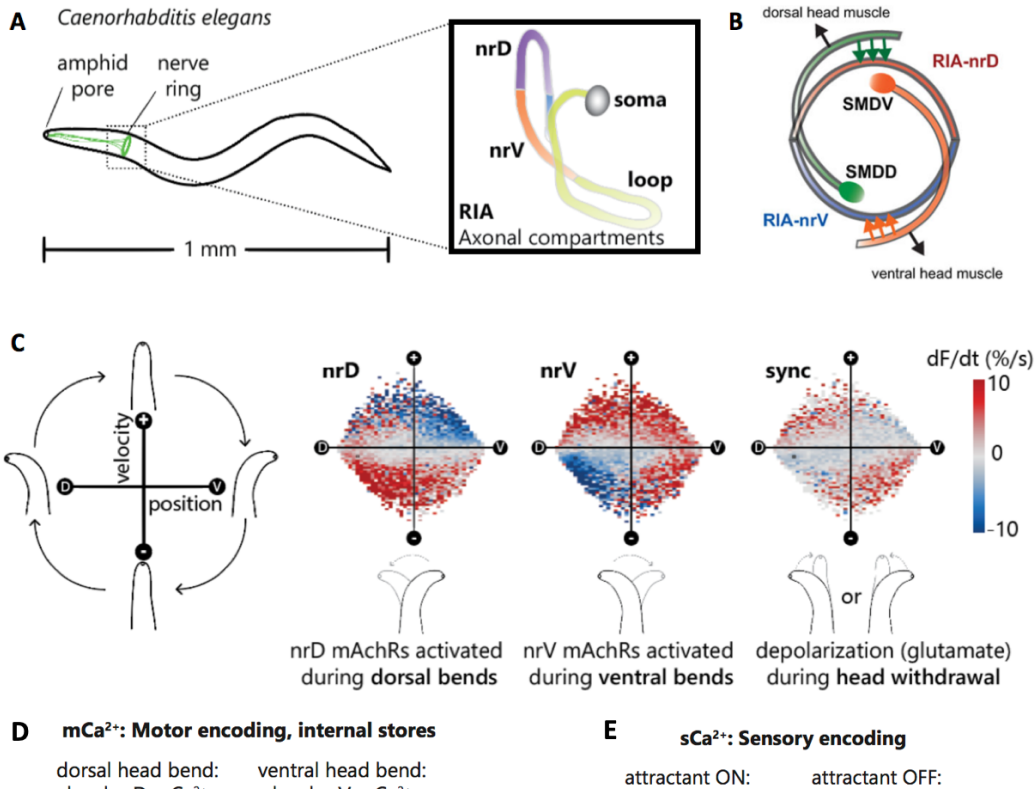
A
Caenorhabditis elegans
amphid pore
nerve ring
1 mm
nrD
soma
nrV
loop
RIA
Axonal compartments
B
dorsal head muscle
RIA-nrD
SMDV
SMDD
RIA-nrV
ventral head muscle
C
velocity
position
nrD
nrV
sync
dF/dt (%/s)
10
0
-10
or
nrD mAchRs activated during dorsal bends
nrV mAchRs activated during ventral bends
depolarization (glutamate) during head withdrawal
D
mCa2+: Motor encoding, internal stores
dorsal head bend: local nrD mCa2+
ventral head bend: local nrV mCa2+
SMDD
nrD
nrV
SMDV
loop
nrD
nrV
E
sCa2+: Sensory encoding
attractant ON: sCa2+efflux
attractant OFF: sCa2+influx
sensory
loop
F
CRAWLING
HEAD LIFTING
Head lifts / min
20
15
10
5
gar-3(gk305)
RIA::TeTX
wild type

**Figure 3.7 RIA interneuron dynamics in *C. elegans*. *A*,** RIA schematic showing its localization and compartments (nRV and nRD) along its single axon ***B*** RIA compartmentalized and reciprocal interactions with head motor neurons. ***C*,** Cross-correlation analysis showing compartmentalized response of GAR-3 in both nRV or nRD in sync with head movement as well as a complete depolarization during head withdrawal. ***D*,** Schematics showing local $Ca^{2+}$ responses to head bends in the RIA (motor inputs) as well as synchronous influx or efflux when worms are faced with different kinds of stimulus (sensory inputs) ***E***. ***F*,** Worms with impaired RIA function show head lifting phenotype (schematic on left) up to 20 times per minute. Adapted in parts from (Hendricks et al. 2012; Hendricks and Zhang 2013).

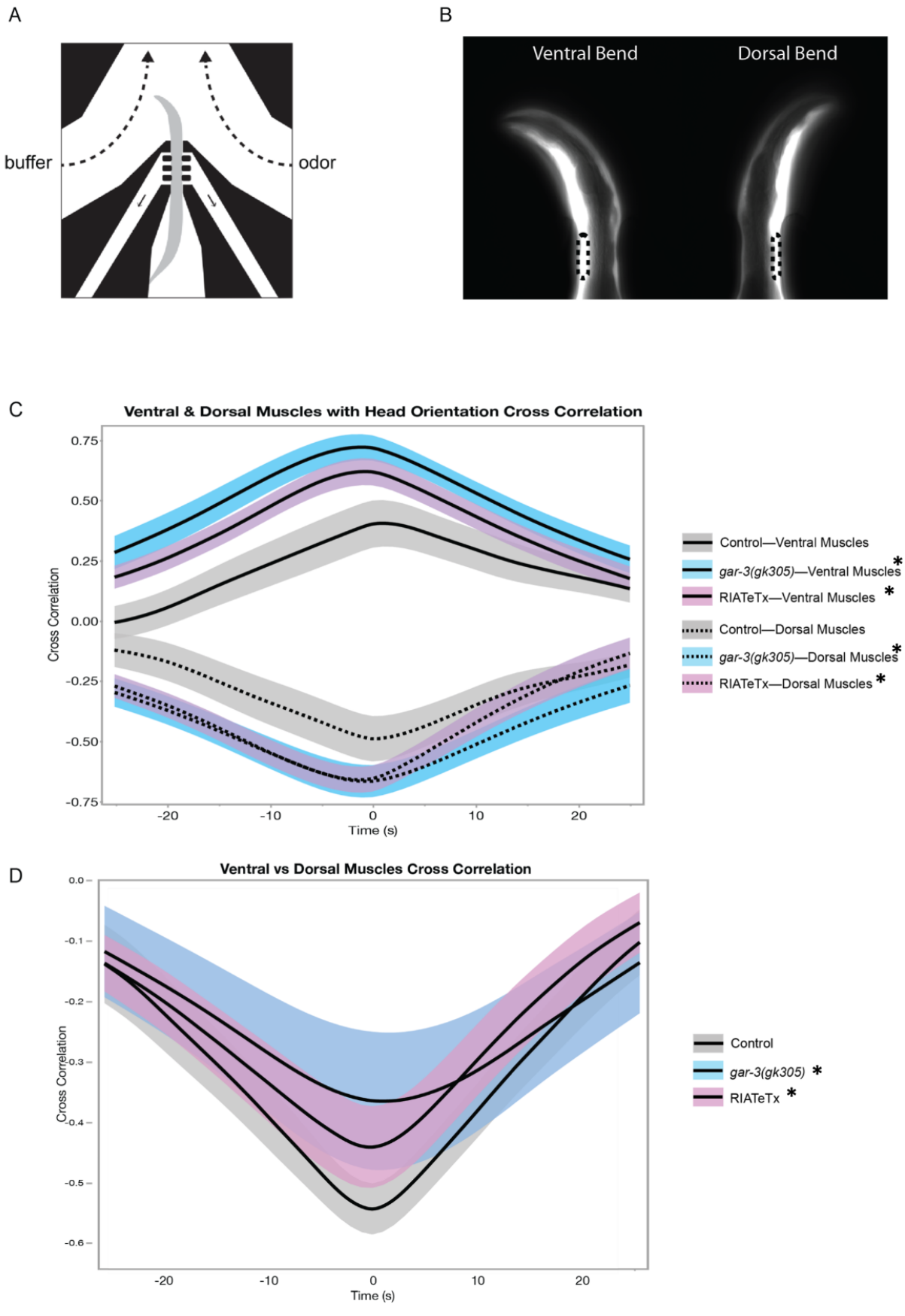
A
buffer
odor
B
Ventral Bend
Dorsal Bend
C
Ventral & Dorsal Muscles with Head Orientation Cross Correlation
Cross Correlation
Time (s)
Control—Ventral Muscles
gar-3(gk305)—Ventral Muscles *
RIATeTx—Ventral Muscles *
Control—Dorsal Muscles
gar-3(gk305)—Dorsal Muscles *
RIATeTx—Dorsal Muscles *
D
Ventral vs Dorsal Muscles Cross Correlation
Cross Correlation
Time (s)
Control
gar-3(gk305) *
RIATeTx *

**Figure 3.8 RIA is required for proper muscle activity at the head level in semi-restrained animals.** ***A****,* Sample acquisition of pmyo-3::GCaMP3.35 worms in a microfluidic river chip (shown on left). Dotted area used for calcium intensity measurements. ***B****,* Cross correlation of ventral muscle calcium activity (positive values, top) or dorsal muscle calcium activity (negative values, bottom) in regards to head position showing a significant difference between strains (t-test *p value* < 0.001). ***C****,* Cross correlation of both muscle calcium activity showing no correlation in wild type but an even greater non-correlation when RIA function is impaired (RIA::TeTX and *gar-3* mutants) t-test *p-value* < 0.001. Suggesting that muscle activity is less compartmentalized when RIA function is impaired. Bold lines are mean. n ≥ 20. Scale Bar: 50 μm

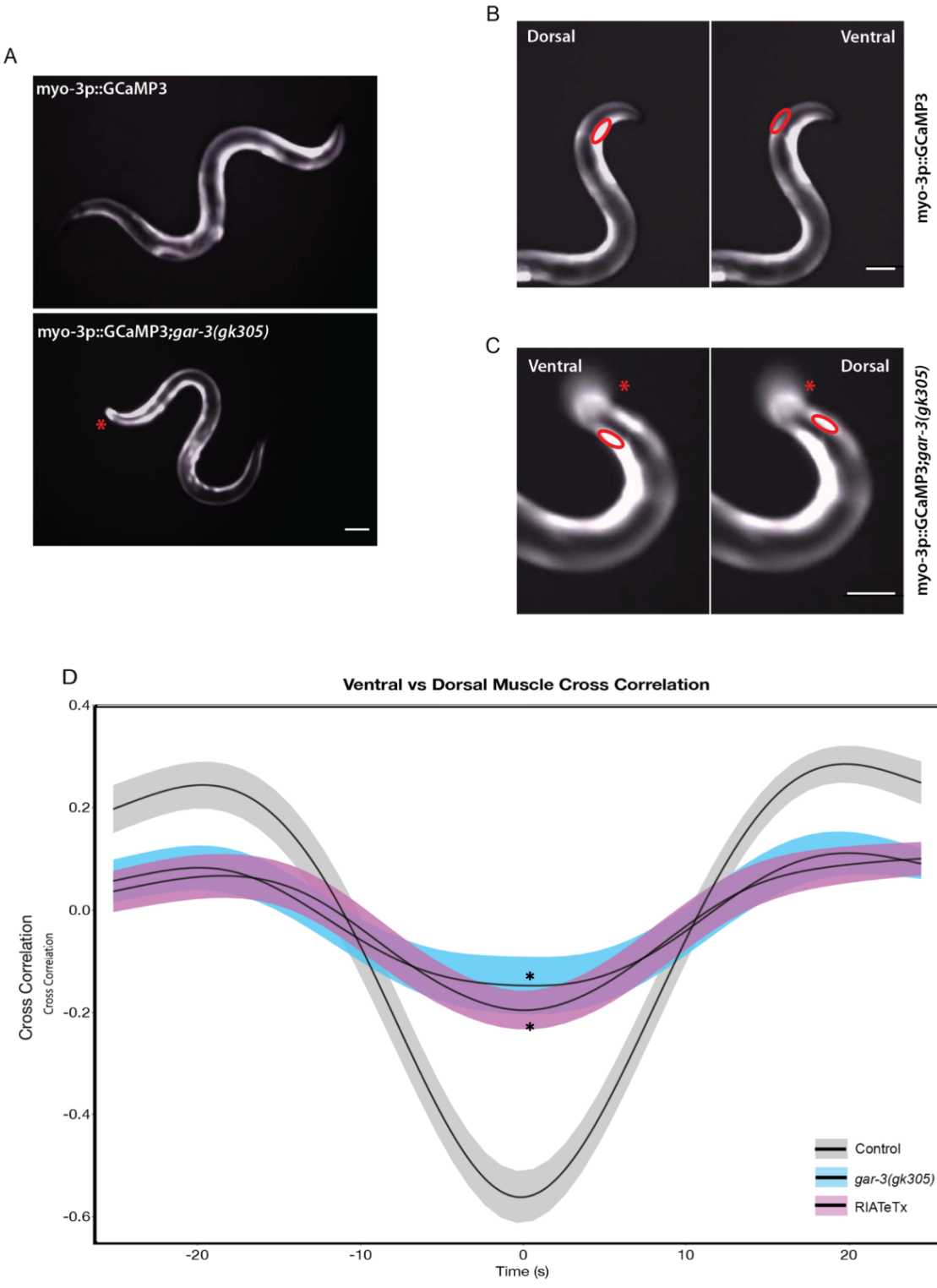
A
myo-3p::GCaMP3
myo-3p::GCaMP3;gar-3(gk305)
B
Dorsal
Ventral
myo-3p::GCaMP3
C
Ventral
Dorsal
myo-3p::GCaMP3;gar-3(gk305)
D
Ventral vs Dorsal Muscle Cross Correlation
Cross Correlation
Cross Correlation
0.4
0.2
0.0
-0.2
-0.4
-0.6
-20
-10
0
10
20
Time (s)
Control
gar-3(gk305)
RIATeTx

**Figure 3.9 RIA is required for proper muscle activity at the head level in freely-moving animals.** ***A****,* Sample acquisition of freely moving myo-3p::GCaMP3.35 (top) and myo-3p::GCaMP3.35;*gar-3(gk305)* (bottom) worms on agar surface. ***B****,****C*** Close-ups of sample acquisitions from myo-3p::GCaMP3.35 (top-***B***) and myo3p::GCaMP3.35;*gar-3(gk305*) (bottom-***C***) worms. Red ellipse shows the area used for calcium intensity measurements. Red asterisk identifies ongoing head lifting. ***D****,* Cross correlation of both ventral and dorsal muscle calcium activity showing no correlation in wild type but an even greater non-correlation when RIA function is impaired (in RIA::TeTX and *gar-3* mutants) *correlation peaks range t-test *p value* <0.0001. Bold line is the mean of all trials. n ≥ 15 runs. Scale Bar: 50 μm.

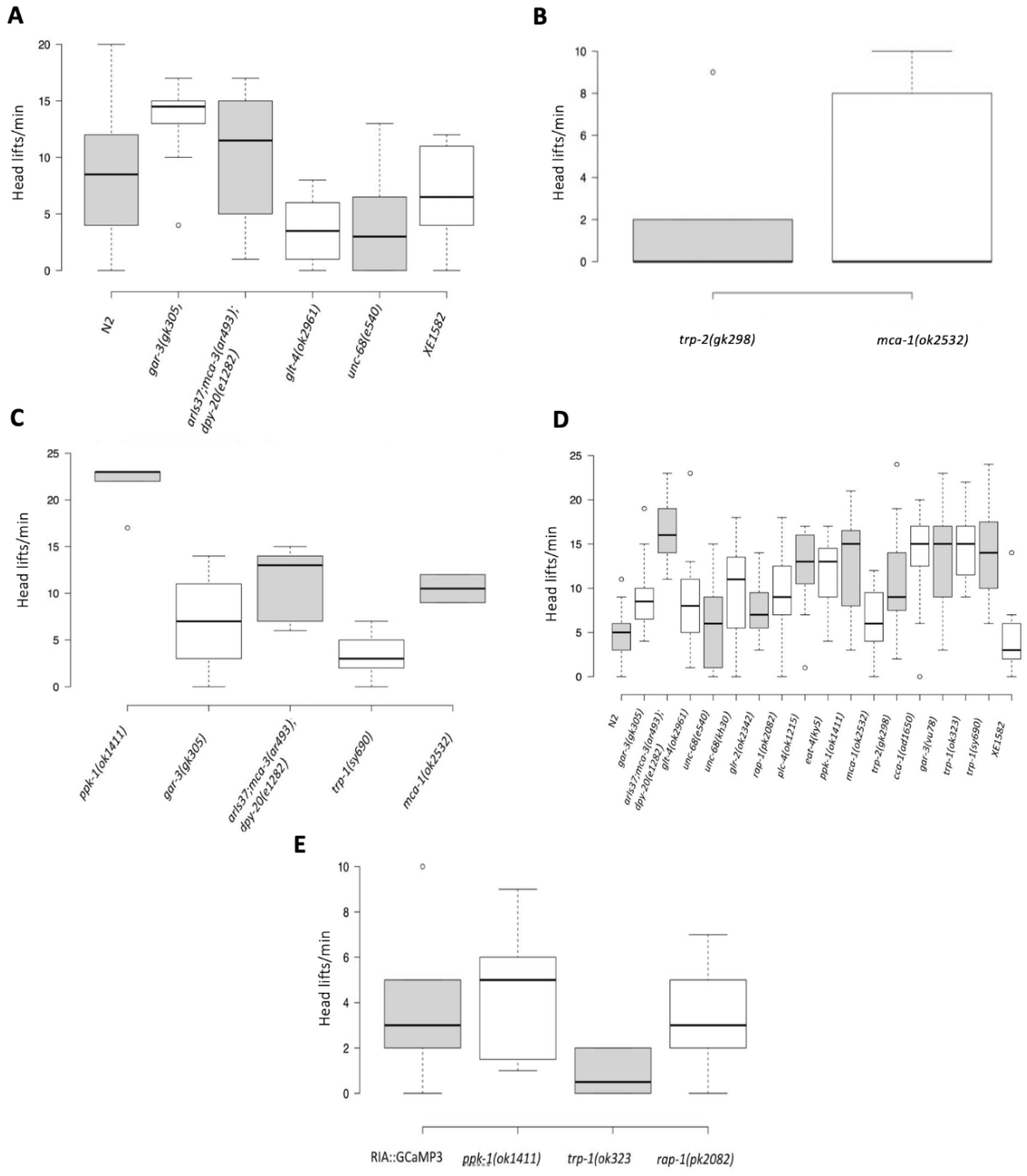
A
Head lifts/min
N2
gar-3(gk305)
arls37;mca-3(ar493);
dpy-20(e1282)
glt-4(ok2961)
unc-68(e540)
XE1582
B
Head lifts/min
trp-2(gk298)
mca-1(ok2532)
C
Head lifts/min
ppk-1(ok1411)
gar-3(gk305)
arls37;mca-3(ar493);
dpy-20(e1282)
trp-1(sy690)
mca-1(ok2532)
D
Head lifts/min
N2
gar-3(gk305)
arls37;mca-3(ar493);
dpy-20(e1282)
glt-4(ok2961)
unc-68(e540)
unc-68(kh30)
glr-3(ok2342)
rap-1(pk2082)
plc-4(ok1215)
eat-4(ky5)
ppk-1(ok1411)
mca-1(ok2532)
trp-2(gk398)
ccs-1(od1650)
gar-3(vu78)
trp-1(ok323)
trp-1(sy690)
XE1582
E
Head lifts/min
RIA::GCaMP3
ppk-1(ok1411)
trp-1(ok323
rap-1(pk2082)

**Figure 3.10 Dismissed head lifting assays conditions because of their degree of variance.** ***A,B,C,*** Different assays conditions were tested ranging from non-seeded plates (NSP) where 1- worms were picked, put on NSP, left for one hour and a half and then head lifts were scored ***A*** 2- Picked, washed in NGM buffer with 50mM salt during 20 minutes (rinse in same buffer at 10 minutes), put on NSP plates, wait 5 ***B*** or 20 ***C*** minutes and then head lifts were score. ***D,E,*** Assays were also tried on seeded plates (SP) where 1- worms were picked, put on SP, left for an hour and a half and then head lifts were counted ***D*** or 2– worms were picked blindly from experimenter by a colleague, left for an hour and a half on the new seeded plate and head lifts were score ***E***. All these conditions showed a great amount of variance and it was decided to not use any of them for future studies to be able to draw conclusions.

| gene | family gene | coding protein | strains |
|---|---|---|---|
| sel-12 | Suppresor/Enhancer of Lin-12 | ortholog of presenilin - transmembrane protein | AN87-GS1894-PS3818-RB1672-MMH120 |
| spe-4 | defective SPErmatogenesis | ortholog of presilin family - transmembrane protein | BA714 |
| unc-7 | UNCooridnated | encodes for innexin required for gap junction formation | CB5 |
| unc-9 | UNCooridnated | encodes for innexin required for gap junction formation | CB101 |
| unc-36 | UNCooridnated | encodes alpha2/delta subunit voltage gated calcium channel | CB251 |
| unc-68 | UNCooridnated | encodes a ryanodine receptor ortholog | CB540-HK30-TR2170-TR2171 |
| daf-16 | abnormal DAuer Formation | encodes FOXO homolog | CF1038 |
| ggr-2 | Ligand-Gated ion Channel | encodes a predicted member of the GABA/ glycine receptor family of ligand-gated chloride channels | CX12708 |
| mcu-1 | Mitochondrial Calcium Uniporter | predicted to be part of mitochondrial transmembrane calcium exchange system | CZ19982 |
| eat-16 | EATing: abnormal pharyngeal pumping | encodes for a protein from the family of regulator of G protein signaling | DA702 |
| avr-15 | altered AVeRmectin sensitivity | encodes for two glutamate-gated chloride channel | DA1051-DA1302-DA1316-DA1370 |

| | | | |
|---|---|---|---|
| avr-14 | altered AVeRmectin sensitivity | encodes for an alpha type unit of glutamate-gated chloride channel | DA1371-DA1384-DA1302- DA1316 |
| glc-1 | Glutamate-gated ChLoride channel | encodes for an alpha type unit of glutamate-gated chloride channel | DA1370-DA1384 |
| ser-1 | SERotonin/octopamine receptor family | encodes for putative ortholog of mammalian 5-HT2 metabotropic serotonin receptor | DA1814 |
| mgl-2 | Metabotropic GLutamate receptor family | encodes a Group I metabotropic glutamate receptor | DA2250 |
| mgl-1 | Metabotropic GLutamate receptor family | encodes a Group II metabotropic glutamate receptor | DA2250 |
| hop-1 | Homolog Of Presenilin | encodes one of The C. elegans presenilins | GS2447 |
| cup-5 | Coelomocyte UPtake-defective | encodes an ortholog of the human mucopilin1 gene | GS2477 |
| mca-3 | Membrane Calcium ATPase | encodes for a plasma membrane calcium ATPase PMCA | GS2527-MMH121 |
| cca-1 | Calcium Channel, Alpha subunit | encodes a calcium channel alpha subunit | JD21 |
| gar-3 | G-protein-linked Acetylcholine Receptor | encodes a G protein-linked muscarinic acetylcholine receptor | JD217-VC657-MMH116-MMH117 |
| exp-1 | EXPulsion defective (defecation) | encodes an excitatory, cation-selective GABA receptor | JT6 |

| | | | |
|---|---|---|---|
| glr-1 | GLutamate Receptor family (AMPA) | encodes an AMPA-type ionotropic glutamate receptor | KP4 |
| ric-7 | Resistance to Inhibitors of Cholinesterase | | KP2048-VC271-MMH113 |
| dop-2 | DOPamine receptor | homologous human gene dopamine receptor D2 | LX702 |
| eat-4 | EATing: abnormal pharyngeal pumping | encodes an ortholog of the mammalian BNPI vesicular glutamate transporter | MT6308 |
| lgc-55 | Ligand-Gated ion Channel | encodes an amine-gated chloride channel | MT14680 |
| gpa-14 | G Protein, Alpha subunit | encodes a member of the G protein alpha subunit family of heteromeric GTPases | NL788 |
| him-5 | High Incidence of Males (increased X chromosome loss) | | PS3818 |
| casy-1 | CAlSYntenin/Alcadein homolog | encodes a type I transmembrane protein calsyntenin/alcadein ortholog | RB888 |
| acr-16 | AcetylCholine Receptor | encodes an alpha-7-like homomer-forming subunit of nAChR superfamily | RB918 |
| rig-4 | neuRonal IGCAM | | RB1137 |
| acr-15 | AcetylCholine Receptor | homolog of an alpha type nicotinic acetylcholine receptor subunit | RB1172 |
| plc-4 | PhosphoLipase C | encodes a phospholipase C delta homolog | RB1173 |
| npr-1 | NeuroPeptide Receptor family | encodes a predicted G protein-coupled neuropeptide | RB1330 |

| | | | |
|---|---|---|---|
| | | receptor | |
| tax-6 | abnormal CHEmotaxis | encodes an ortholog of calcineurin A | RB1667 |
| ser-2 | SERotonin/octopamine receptor family | encodes 4 tyramine 7-transmembrane domain receptors (GPCRs) | RB1690 |
| glr-2 | GLutamate Receptor family (AMPA) | encodes an AMPA (non NMDA)-type ionotropic glutamate receptor subunit | RB1808 |
| ins-3 | INSulin related | encodes one of several insulin-related peptides | RB1915 |
| flp-7 | FMRF-Like Peptide | encodes an MVRFamide-containing peptide | RB1990 |
| glt-4 | GLutamate Transporter family | encodes an ortholog of glutamate/aspartate and neutral amino acid transporters | RB2185 |
| ins-4 | INSulin related | encodes an insulin-like peptide | RB2544 |
| trp-1 | TRP (transient receptor potential) channel family | encodes a transient receptor potential (TRP) channel | TQ225,-VC160 |
| rap-1 | RAP homolog (vertebrate Rap GTPase family) | encodes a member of the Ras superfamily of small GTPases | TZ181 |
| end-1 | ENDoderm determining | encodes a GATA-type transcription factor | VC271 |
| glc-2 | Glutamate-gated ChLoride channel | encodes the beta subunit of a glutamate-gated chloride channel | VC350, VC722 |

| | | | |
|---|---|---|---|
| trp-2 | TRP (transient receptor potential) channel family | encodes a transient receptor potential (TRP) channel | VC602 |
| ppk-1 | PIP Kinase | encodes a putative phosphatidylinositol-4-phosphate 5' kinase PPK | VC963 |
| rig-6 | neuRonal IGCAM | encodes a protein with Ig and fibronectin type III domains ortholog contactins | VC1125 |
| magi-1 | MAGI (Membrane Associated Guanylate kinase Inverted) homolog | encodes a multi PDZ-domain containing tight junction-associated protein | VC1408 |
| acc-2 | Acetylcholine-gated Chloride Channel | | VC1757 |
| cnx-1 | CalNeXin | encodes the *C. elegans* ortholog of calnexin, type I Ca2+ binding integral membrane protein of the ER | VC1801 |
| mca-1 | Membrane Calcium ATPase | encodes one of the PMCA | VC2000 |
| nmr-2 | NMDA class glutamate Receptor | encodes an ionotropic glutamate receptor (iGluR) subunit | VC2623 |
| gcy-2 | Guanylyl CYclase | encodes a receptor-type, transmembrane guanylyl cyclase | VC3024 |
| nmr-1 | NMDA class glutamate Receptor | encodes an NMDA-type ionotropic glutamate receptor subunit | VM487 |

**Table 3.1 List of genes and associated strains used for this study and the head lifting assay.** All strains were outcrossed against N2 strain (wild type) at least 3 times. Coding protein information was extracted from wormbase search (WormBase website, http://www.wormbase.org, release WS286, date 2022). See Material and Methods 2.1 for genotype information of the different strains.

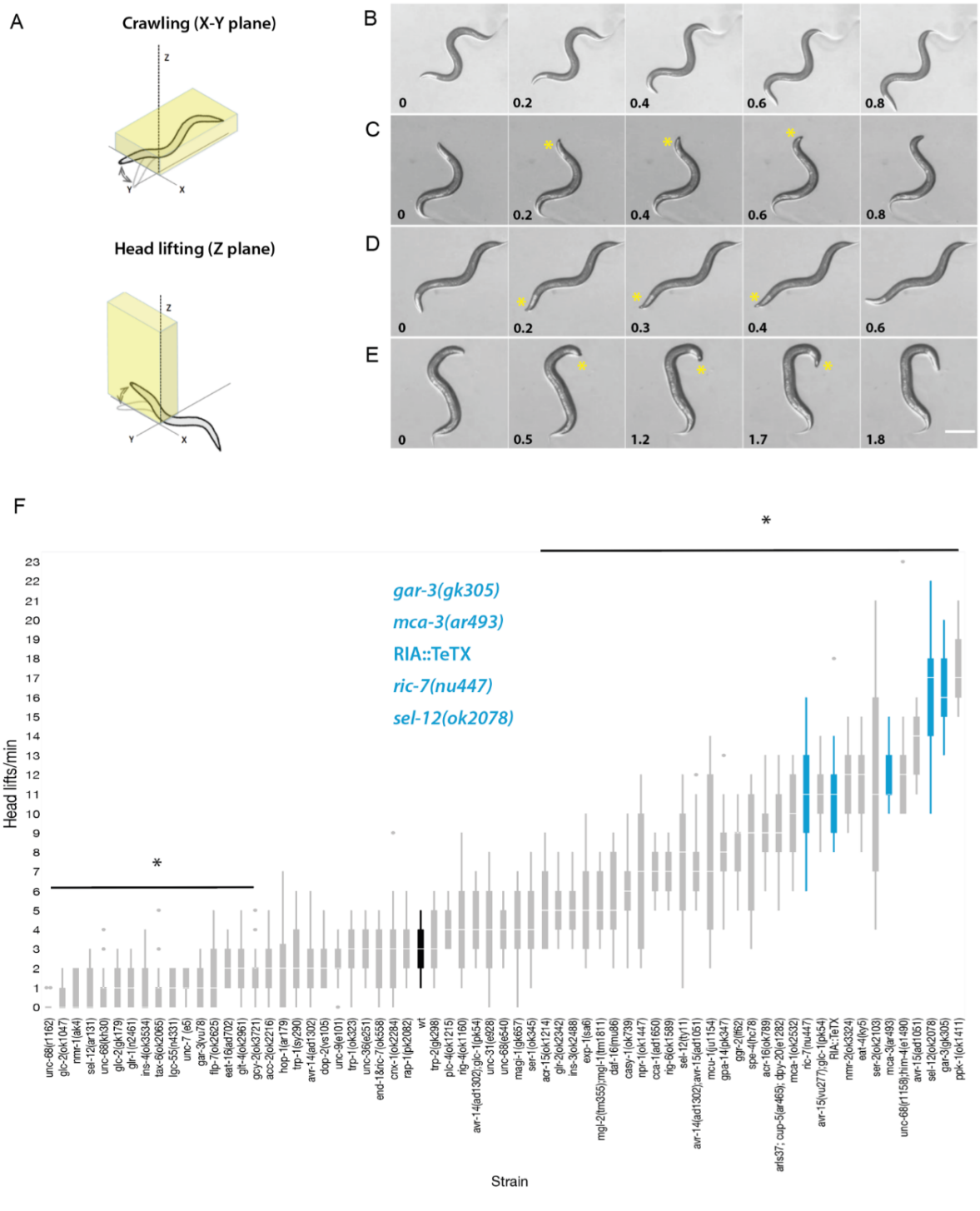
A
Crawling (X-Y plane)
Z
Y
X
Head lifting (Z plane)
Z
Y
X
B
0
0.2
0.4
0.6
0.8
C
0
0.2
0.4
0.6
0.8
D
0
0.2
0.3
0.4
0.6
E
0
0.5
1.2
1.7
1.8
F
Head lifts/min
Strain
gar-3(gk305)
mca-3(ar493)
RIA::TeTX
ric-7(nu447)
sel-12(ok2078)
*
*

**Figure 3.11 Head lifting phenotype as a correlate to identify genes implicated in RIA dynamics.** ***A****,* Schematic of head lifting phenotype when worms lift their head off the surface in the z (left-right) plane. ***B****,****C****,****D****,****E****,* Control (*N2*) worm showing no head lifting compared to sample worms showing light (type 1) ***C***, medium (type 2) ***D*** and heavy (type 3) ***E*** head lifting phenotype through time. Yellow asterisk shows head position and head lift occurrence. Last captured frame before head lifts starts is T=0. Time is in seconds. ***F****,* Selected head lifting assay for mutants of genes involved in neuronal calcium dynamics or G-protein signaling and glutamate receptors. Experiment was done as single-blind from the experimenter to reduce potential bias. Retained candidates are labeled in blue. Black is wild-type. * Student t-test vs wild-type *p value* < 0.001. n ≥ 15 for each strain.

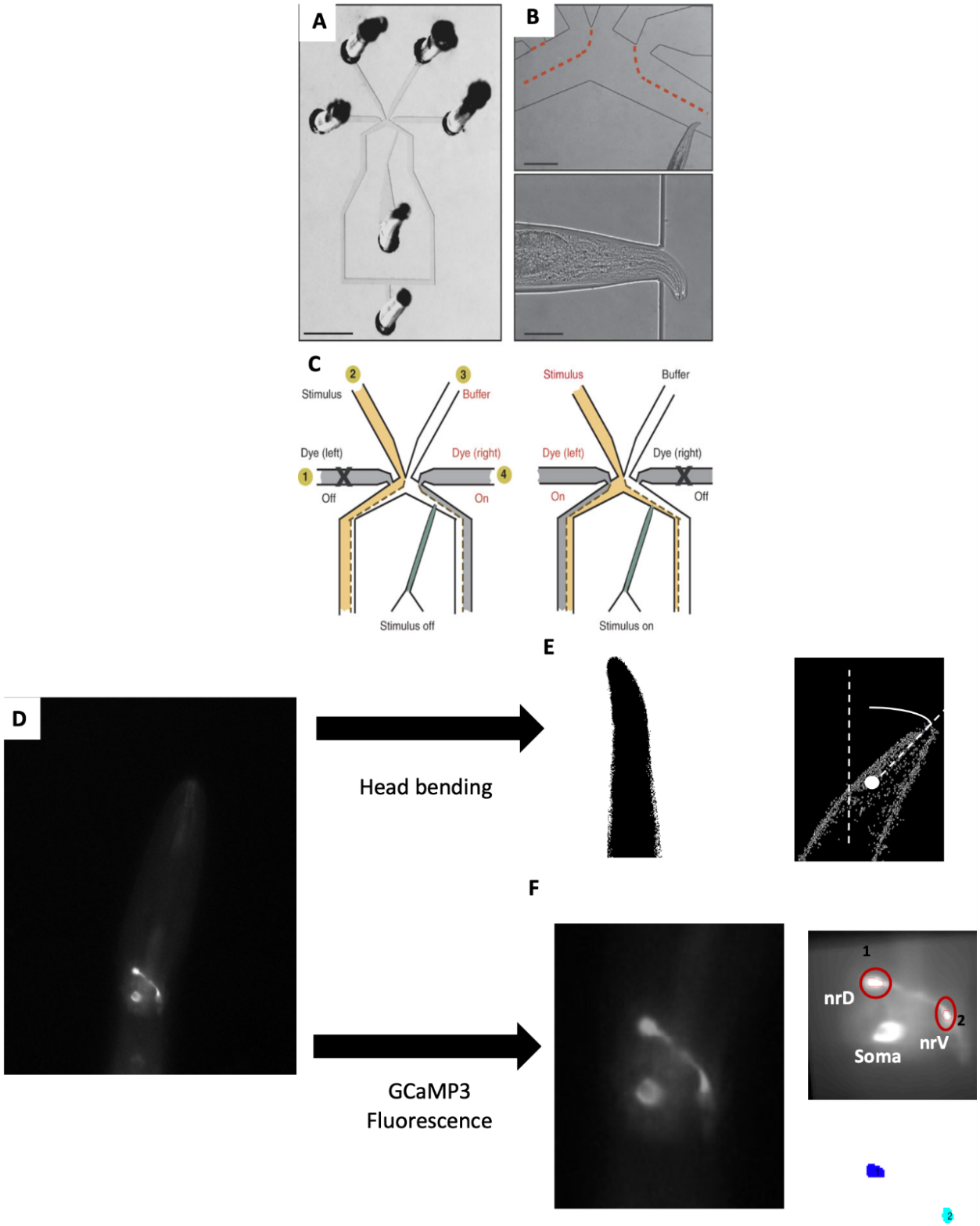
A
B
C
Stimulus
Buffer
Dye (left)
Dye (right)
Off
On
Stimulus off
Stimulus on
D
Head bending
E
F
GCaMP3
Fluorescence
nrD
nrV
Soma
1
2

**Figure 3.12 Calcium imaging procedure and analysis using Matlab.** ***A,B,C,*** Picture of the calcium imaging PDMS chip used for imaging calcium response in neurons ***A*** as well as head movement ***B*** following buffer or stimulus stream ***C*** when switching valves ON/OFF. ***D,E,F,*** Sample acquisition in chip of *Pglr-3*::GCamP3 strain showing RIA interneuron ***D*** and Fiji software processing for tracking head movement ***E*** as well as calcium signal intensity ***F*** in RIA compartments. Matlab processing with FluoroSNNAP code shown. Each time is analyzed according to the angle difference between the defined line (arbitrarily chosen) and the average of pixels from the tip of the head to determine head movement **(E-right panel)** and defined ROI fluorescence intensities at each time is also analyzed **(F-right panel)** to get a movement and fluorescence intensity pattern for further data analysis. Adapted in parts from (Chronis et al. 2007).

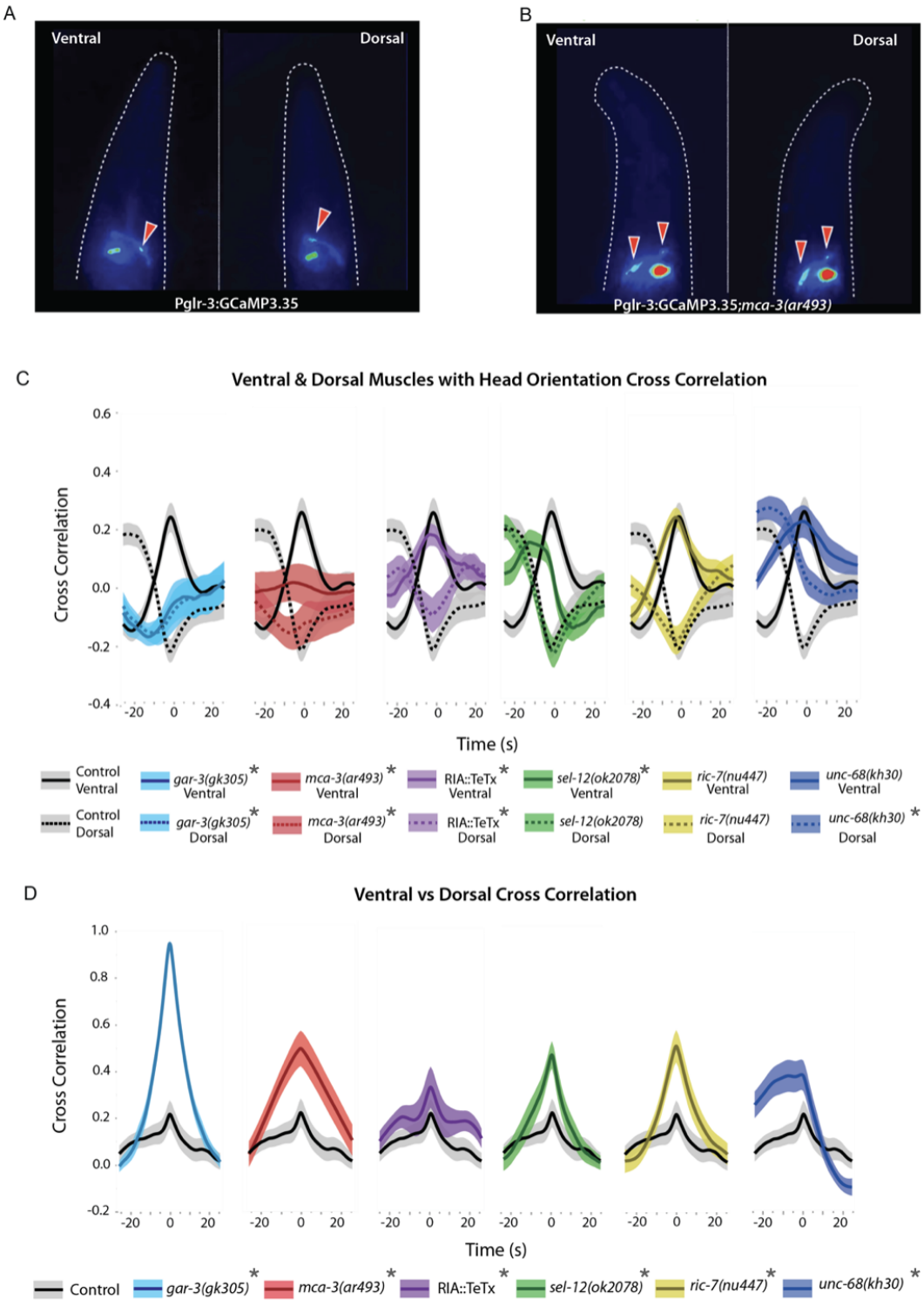
A
Ventral
Dorsal
Pglr-3:GCaMP3.35
B
Ventral
Dorsal
Pglr-3:GCaMP3.35;mca-3(ar493)
C
Ventral & Dorsal Muscles with Head Orientation Cross Correlation
Cross Correlation
Time (s)
Control Ventral
gar-3(gk305)* Ventral
mca-3(ar493)* Ventral
RIA::TeTx* Ventral
sel-12(ok2078)* Ventral
ric-7(nu447) Ventral
unc-68(kh30) Ventral
Control Dorsal
gar-3(gk305)* Dorsal
mca-3(ar493)* Dorsal
RIA::TeTx* Dorsal
sel-12(ok2078) Dorsal
ric-7(nu447) Dorsal
unc-68(kh30)* Dorsal
D
Ventral vs Dorsal Cross Correlation
Cross Correlation
Time (s)
Control
gar-3(gk305)*
mca-3(ar493)*
RIA::TeTx*
sel-12(ok2078)*
ric-7(nu447)*
unc-68(kh30)*

**Figure 3.13 Top head lifters impact motor calcium dynamics in RIA.** ***A,B,*** Sample acquisition in calcium imaging chip of *Pglr-3*::GCamP3 ***A*** showing RIA interneuron motor compartments (arrowheads) in sync with head movement and sample acquisition of *Pglr-3*::GCamP3; *mca-3(ar493*) ***B*** showing sustained activity in both compartments (dashed line outlines head). ***C,*** Cross correlation of compartmentalized activity of motor compartments with head movement in wild-type animals (black). No significant difference in *ric-7(nu447*) background and on the dorsal side in *sel-12(ok2078)* and *unc-68(kh30)* background. All other backgrounds significantly downgrade this response (*T test *p* values < $10^{-18}$ ). ***D,*** Compartmentalized activity in either nrV or nrD is represented in cross-correlation form, when one compartment has calcium activity, the other activity is downgraded in wild type. Due to the punctual activity of the loop in response to sensory cues, a slight positive correlation can be observed in wild type. In *gar-3(gk305), mca-3(ar493), ric-7(nu447), sel-12(ok2078)* and *unc-68(kh30)* backgrounds**,** this synchronous activity between nrV and nrD is significantly increased and the compartmentalized activity is downgraded (*T test *p* value < $10^{-20}$). FluoroSNNAP code used in Matlab for analysis, plotted in JMP Pro. Bold line is the mean of all individual trials. n ≥ 15

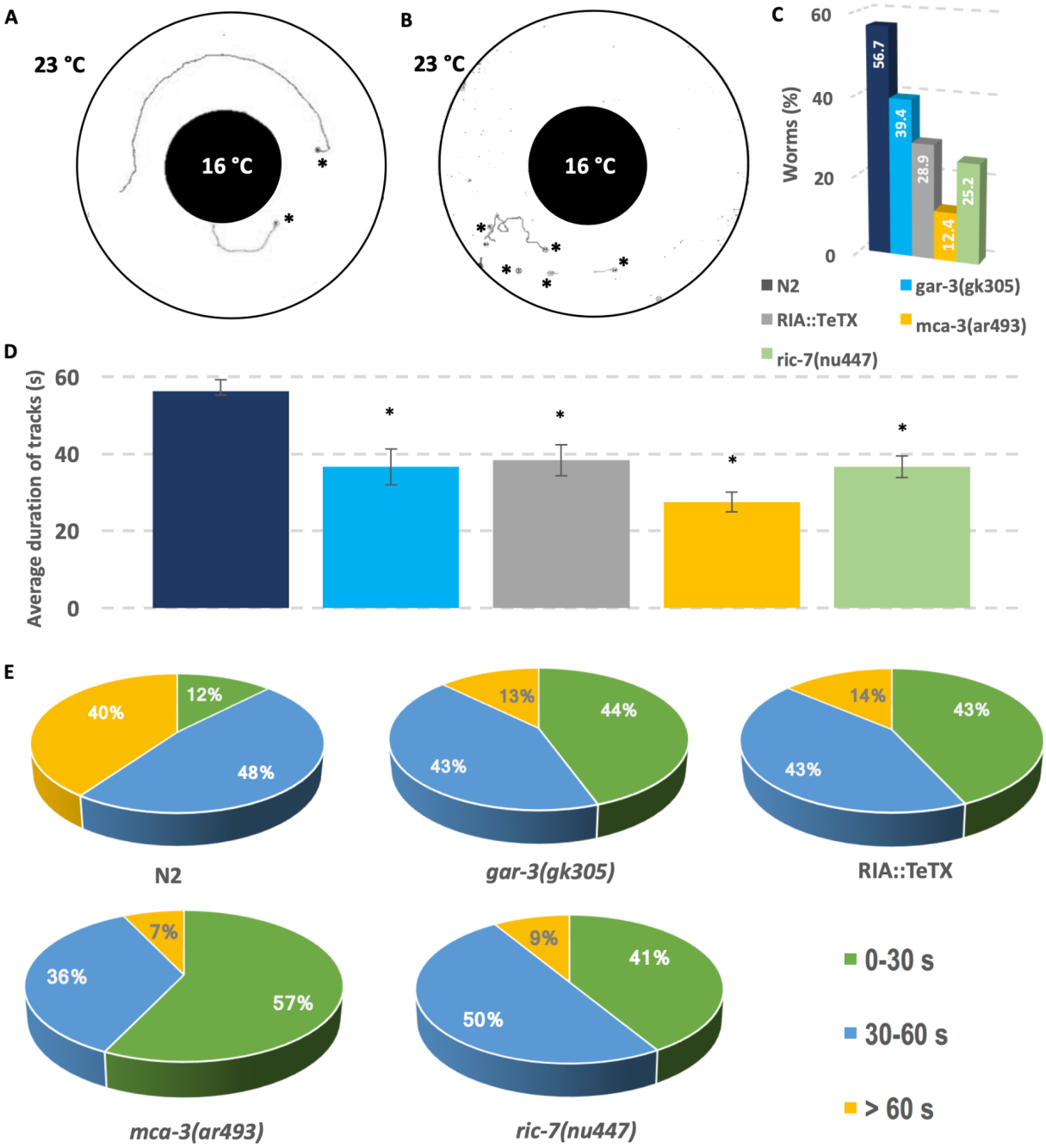
A
23 °C
16 °C
B
23 °C
16 °C
C
Worms (%)
60
40
20
0
56.7
39.4
28.9
12.4
25.2
N2
gar-3(gk305)
RIA::TeTX
mca-3(ar493)
ric-7(nu447)
D
Average duration of tracks (s)
60
40
20
0
E
12%
40%
48%
N2
13%
44%
43%
gar-3(gk305)
14%
43%
43%
RIA::TeTX
7%
36%
57%
mca-3(ar493)
9%
41%
50%
ric-7(nu447)
0-30 s
30-60 s
> 60 s

**Figure 3.14 Isothermal tracking is weakened in candidate strains.** ***A,B,*** Schematics of sample individual forward tracks as rendered after image processing in Fiji (Schindelin et al. 2012) using Particle Tracker (Sbalzarini and Koumoutsakos 2005; Chenouard et al. 2014) for wild type ***A*** and RIA::TeTX ***B***, asterisks show worms. Glacial acetic acid vial is put in the middle of a chemotaxis agar plate to create gradients ranging from 16°C in the middle (under the vial) and 23°C on the outside borders. Once the gradient has been established for 15 minutes, worms are placed on the plate after being washed with NGM buffer and behavior is recorded for 20 minutes. ***C,D,E,*** Percentage of total worms per strain that tracked isotherms during the assay was assessed ***C*** and duration of each track is then assessed by eye and average duration for every strain is plotted ***D***. Percentage of worms in each time category (0-30s, 30-60s or more than 60s) is also defined ***E***. It is possible to see that isothermal tracking behavior is impaired in all strains where RIA function is impaired and the percentage of worms that track isotherms significantly reduced. This suggests that RIA plays an important role in active sensing and that it is modulated by some of its molecular components as well as his own input (through *gar-3*) and output (RIA::TeTX). * significantly different from *wild type; p* value (t test) ≤ 0.01. n ≥ 105 for each strain.

# CHAPTER 4

## DISCUSSION

### 4.1 RIA loop as a new integrator of sensory cues for active sensing

The uniqueness of RIA in regard to its positioning in the nerve ring of *C. elegans* and the fact that it gets motor feedback as well as sensory cues, makes it a perfect candidate to study active sensing at the single-neuron level. In this thesis we shed light to new links between RIA function and head orientation at the molecular level in *C. elegans*. Indeed, it had been shown previously that in response to odor and temperature cues RIA is involved in steering (Mori and Ohshima 1995; Liu et al. 2018a). The latter is considered as an active sensing process and head movements play an important role in *C. elegans* active locomotion. Here, we have added another layer of the RIA function by showing that the loop region of the RIA integrates sensory stimuli and leads to head withdrawal in response to asymmetrically presented stimuli, in a head-orientation-dependent manner. This was observed through calcium imaging data which showed that the loop is active only when the head is bent mostly ventrally or dorsally (Ouellette et al. 2018). Interestingly, it was demonstrated that *C. elegans* display more curved and deeper head bends in one direction if neurotransmitter release is suppressed asymmetrically from RIA (acting as if an attractive odor was presented on one side) (Liu et al. 2018a). In this project, we described a complementary behavior which displays a head withdrawal paired with a reduced head bending when attractive odor is removed (this odor removal is considered to be a repulsive stimulus). Both behaviors have a role to play in steering. Moreover, we also showed that there is a posture-dependent gating mechanism for incoming sensory cues. This gating mechanism functions such that RIA selectively responds to the stimuli the worm encounters as it bends its head and not when the stimuli is mostly symmetric. This

showed that head movements regulate not only the RIA outputs, as we have shown previously, but also sensory responses. The signal that directs the response of the loop and the sensory calcium ($sCa^{2+}$) events is still unknown, but appears to be posture-dependent. Further studies are needed to look into upstream neurons signaling to the loop and finding which one/which circuit could be responsible for this gating mechanism.

### 4.2 RIA motor compartments as a feedback regulator

Other findings from this work showed that the calcium ($mCa^{2+}$) events from the motor compartments act as a switch to lead to asymmetric outputs from the nrV and nrD (Ouellette et al. 2018). Those $mCa^{2+}$ events decrease the time it takes for the response to peak in the contralateral compartment of head withdrawal (Ouellette et al. 2018). To dig more into this, and truly understand this proposed gate-and-switch mechanism, analyzing the synaptic release from RIA as well as how the postsynaptic neurons respond is essential. In order to address this, future studies should include the expression of a glutamate sensor specifically in RIA such as iGluSnFR (Marvin et al. 2013) or SynaptopHluorin (Burrone et al. 2006), in order to track RIA neurotransmitter release through head bending sensory events (Figure 3.1 A-G). Adding such a sensor to a GCaMP strain would also make it possible to track calcium levels and how $Ca^{2+}$ dynamics correlate with synaptic release in RIA. This would greatly help the global understanding of how RIA functions at the circuit level.

### 4.3 Unraveling potential motor neuron pathways involved in *C. elegans* head movements

As mentioned previously, we hypothesized that the RIA circuit could act in similar fashion as mammalian cholinergic signaling, wherein reafferent stimulation occurs with sensory gating in phase with the olfactory behavior and whisking (Rothermel et al. 2014; Eggermann et al. 2014). However, the head withdrawal we observed occurred on a rapid timescale and cannot be explained solely by the inhibition of the ipsilateral motor neurons. Rather, head withdrawal likely depends on the activation of contralateral motor neurons as well as muscle contraction. RIA receives feedback from SMDV only on the nrV and input from SMDD is received onto nrD, however both compartment outputs go to either head motor neurons (SMDD and SMDV) (Results Figure 3.6 A). As such, there may be target-specific differences in $mCa^{2+}$ signaling. To delve further into this, it would be essential to identify the receptors involved in this process at the head motor neuron level, as well as directly assessing the effect of RIA input on these motor neurons.

### 4.4 Potential new calcium dependent pathway to transmit information through the RIA

In a second aim, we also showed that when RIA function is impaired, muscle activity at the head level is defective and worms are unable to maintain a correct gait. This disruption leads to a novel phenotype we named “head lifting”, where the head of the animal moves off the surface in the left-right plane instead of the usual ventral-dorsal undulations. This phenotype allowed us to conduct a successful candidate screen and identify genes involved in the RIA circuit dynamics. Several genes were retained from

the screen, and were subsequently submitted to calcium imaging to assess their impact at the RIA level. Interestingly, the genes of interest standing out from the screening assay as heavy headlifters had been previously implicated in calcium dynamics.

Compared to the other candidate genes, *mca-3* had the most striking phenotype (only type 3 head lifts) and encodes a PMCA as mentioned previously. PMCAs have been well studied in vertebrates, where they were found to spatially regulate calcium in dendrites as well as maintaining the time course of neuron excitability (Scheuss et al. 2006; Garrity et al. 2010). This may point to a role of MCA-3 in regulating calcium dynamics at the RIA level. Further studies could address the degree of homology between RIA compartments and dendritic compartments in the way calcium is spatially controlled in both to better understand this mechanism and assess whether similar dynamics are at play.

Two other candidates, *ric-7* and *sel-12*, show a potential link to calcium dynamics as they are both implicated in mitochondrial function and mitochondria are required for correct calcium buffering and dynamics (Sarasija et al. 2018; Rawson et al. 2014). It was stated earlier that *ric-7* is a nematode only gene involved in the correct placement of mitochondria along axons. Moreover, *sel-12* is part of the PSEN family of genes which mediate calcium release from the ER to the mitochondria, and plays a role in maintaining the mitochondrial structure and function (Sarasija and Norman 2015; Sarasija et al. 2018). Evidence continues to mount supporting the importance of calcium trafficking between the ER and mitochondria, and a link between this type of calcium transport and certain neurodegenerative diseases is strongly suggested (Hirabayashi et al. 2017; Gómez-Suaga et al. 2018; Lau et al. 2018; Stoica et al. 2014). As such, *sel-12*

may play an important role in maintaining RIA function by regulating the interplay between the ER and mitochondria, in regards specifically to calcium dynamics. Mitochondria continue to be a subject of study, and increasingly so in relation to calcium dynamics. Mitochondria undergo calcium uptake through two processes: (1) calcium internalization by voltage-dependent anion channels (VDAC), which permit transport across the outer mitochondrial membrane (OMM) (Rapizzi et al. 2002; Báthori et al. 2006; Tan and Colombini 2007), and (2) a $Ca^{2+}$ uniporter (MCU) which permits transport across the inner mitochondrial membrane (IMM) (Oxenoid et al. 2016; Tsai et al. 2017). Interestingly, transport through MCU has recently been linked to synaptic release, as mitochondrial calcium uptake appears to play a role in clearing calcium from the presynaptic compartment of glutamatergic neurons (Kwon et al. 2016). Knowing all of this, a potential link between mitochondria and calcium in RIA motor compartments that involves *ric-7* and *sel-12* wouldn't be farfetched.

In addition to *mca-3, ric-7* and *sel-12*, the candidate gene *gar-3* was also of particular interest to us as we knew this gene to be expressed in the nrV and nrD from previous studies, and that *gar-3* encodes a GPCR known to be involved in RIA dynamics (Hendricks et al. 2012; Hendricks and Zhang 2013). Notably, *gar-3* is known to encode a muscarinic receptor orthologous to mammalian M1, M3 and M5 muscarinic receptor subtypes (Hwang et al. 1999). Such receptors are known to interact with type q G-proteins, which triggers the phospholipase C pathway (PLC); a signaling pathway that increases intracellular calcium levels through IP3, and subsequently activates protein kinase C (PKC) through DAG (Ishii and Kurachi 2006). More specifically, in *C. elegans*, it has been shown that GAR-3 interacts with EGL-30, which is an ortholog of a

mammalian Gq protein (Chan et al. 2012), and that GAR-3 regulates calcium-dependent processes during pharyngeal muscle contraction in *C. elegans* (Steger and Avery 2004). Taking into account the localisation of GAR-3 in the RIA (Hendricks et al. 2012), this adds another potential player to the calcium dynamics of RIA at the motor compartments level, where the interneuron receives feedback from the SMDs.

Finally, mutants for *unc-68* clearly display alternated RIA dynamics while being a low head lifter. It has been shown that *unc-68* codes for a ryanodine receptor that is expressed in muscles (Maryon et al. 1996; Forrester 2018). Moreover, ryanodine receptors release calcium into the cytoplasm upon activation from the endoplasmic or sarcoplasmic reticulum (Fill and Copello 2002). Therefore, the observed results could be due to a change inside the RIA itself or to muscles sending different corollary inputs to RIA, making its function look different.

To address all of those hypotheses and dig deeper into the fine tuning of the RIA circuit in regard to those genes, the logical next step is to express those candidate genes specifically in RIA and perform cell specific rescues to link them undeniably to RIA function. As such, during the course of this project, different approaches were tried but none led to stable transgenic lines expressing the genes in the RIA interneuron. All constructs were done using the Gateway system and the following extrachromosomal arrays injections did not render results (Figure 4.2 A-B). A new approach was designed based on the work of (Silva-García et al. 2019) to use CRISPR/Cas9 to insert single copies of the constructs directly into RIA using the SKI LODGE system (Figure 4.3 A). As such, a cassette with a chosen promoter (in our case, *pglr-3* for specific expression

in the RIA) is inserted in a stable chromosomal region and a part of that cassette is then interchangeable for any gene or probe to be expressed in the desired tissue/neuron/cell type as driven by the promoter that was picked. The whole background work to establish that system has been put in place (Figure 4.3 B). Moving forward, it will be possible to test and hopefully use it to continue the study of the role of those genes in regard to the RIA circuit.

### 4.5 Another way to transmit signals in the RIA?

Neuronal calcium acts as the main second messenger in neurons, and plays a key role in the release of neurotransmitters. Indeed, throughout scientific literature it is broadly documented that the release of neurotransmitters through the exocytosis of synaptic vesicles at the neuromuscular junction is initiated by an increase in calcium concentration within the presynaptic region (Jahn and Südhof 1994; Katz and Miledi 1967). Moreover, the increased concentration of intracellular calcium at the presynaptic region is induced by the opening of voltage-activated calcium channels, which are triggered by action potentials that depolarise the membrane (Bargmann 1998). However, it is broadly known in neurobiology that the *C. elegans* neuronal system is mainly isopotential and that no sodium-dependent action potentials have been detected in the nematode (Goodman et al. 1998). Interestingly, an all-or-none calcium-dependent action potential firing has recently been shown in the *C. elegans* sensory neuron AWA (Liu et al. 2018b), and was very recently suggested to also occur in the AVL and DVB motor neurons (Jiang et al. 2022). This suggests that *C. elegans* may be capable of employing a hybrid approach, seeing as neuronal responses appear to vary depending on the type of neuron. Taking into account the fact that we have shown that the RIA acts

as a gate-and-switch to correctly respond to sensory cues, as well as extensive involvement of the candidate genes in calcium regulation, perhaps future study may address whether action potentials occur in the RIA circuit as a means to deliver accurate input to muscles. Notably, local calcium events have already been observed in the RIA (Hendricks et al. 2012). In addition, the loop has been shown to responds to repulsive stimuli most strongly when the head is mostly bent on one side or the other, which triggers a whole axon calcium response that leads to the correct behavior when paired with the motor compartments' own calcium response (Ouellette et al. 2018). As such, maybe a certain level of intracellular calcium must be achieved in order to drive the appropriate behavior. This possible explanation is supported by the fact that several candidate genes are known to be involved in calcium dynamics at the level of the mitochondria or endoplasmic reticulum (ER),as well as encode calcium pumps (PMCA), all of which could regulate the firing and the transmission of action potentials through interactions with intracellular calcium.

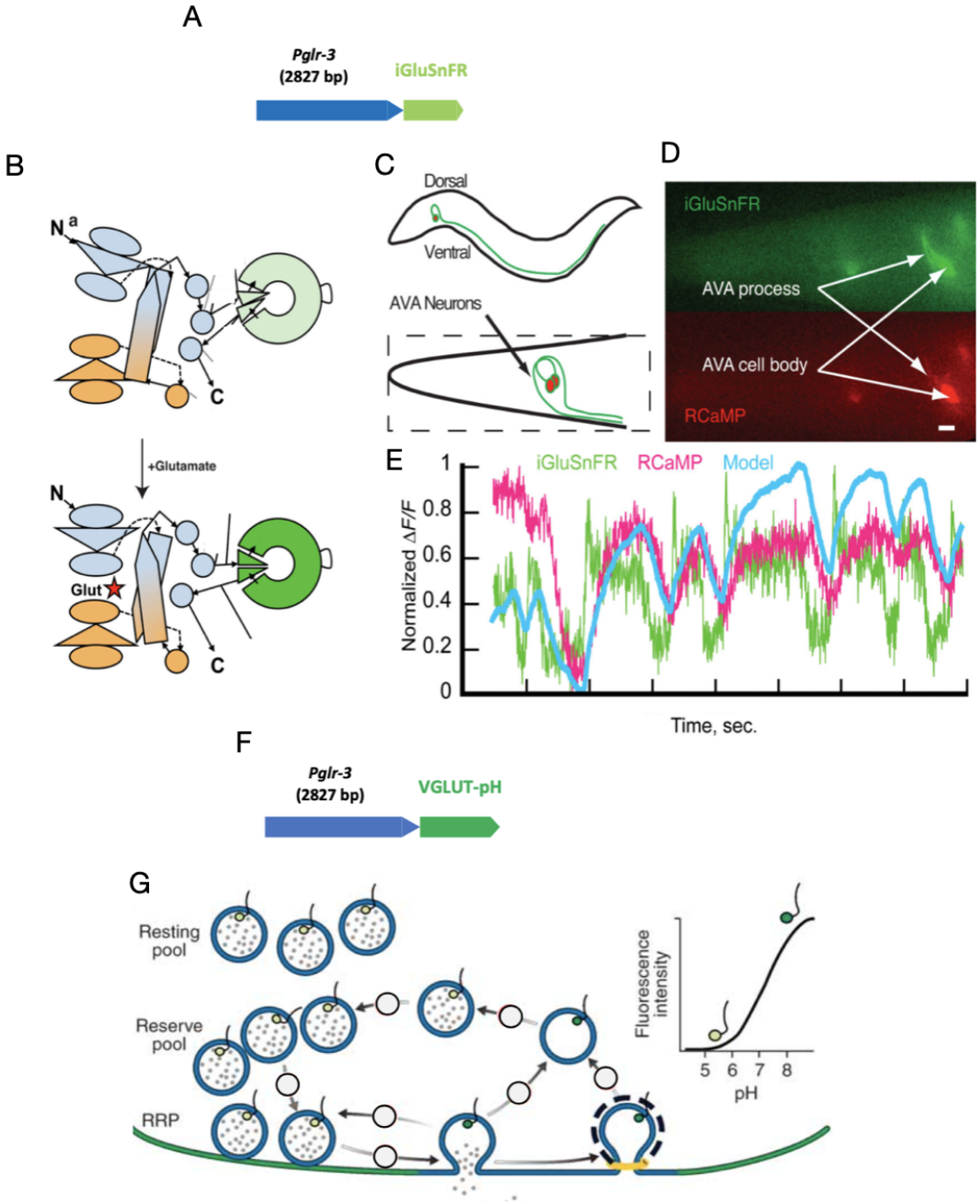
A
Pglr-3
(2827 bp)
iGluSnFR
B
N
a
C
+Glutamate
N
Glut
C
C
Dorsal
Ventral
AVA Neurons
D
iGluSnFR
AVA process
AVA cell body
RCaMP
E
iGluSnFR
RCaMP
Model
Normalized ΔF/F
1
0.8
0.6
0.4
0.2
0
Time, sec.
F
Pglr-3
(2827 bp)
VGLUT-pH
G
Resting
pool
Reserve
pool
RRP
Fluorescence
intensity
5
6
7
8
pH

**Figure 4.1 iGluSnFR and SynaptopHluorin fluorescent probes to visualize synaptic output.** (A) Schematic of RIA specific construct to be injected to produce stable transgenic line to visualize glutamate dynamics using iGluSnFR (B) Schematic of iGluSnFR structure and change of conformation when binding glutamate, that triggers bright fluorescence (C) AVA glutamatergic neurons and the stable expression of iGluSnFR as well as RCaMP to track calcium (D-E). (F) Schematic of RIA specific construct of synaptopHlorin to be injected to visualize synaptic output. SynaptopHlorin rely on the fact that synaptic vesicles have acidic pH when at rest (low fluorescence) and content becomes more basic when it fuses the membrane so the fluorescence, which is pH dependent in this probe, peaks when content is released (G). Both probes give the possibility to see both glutamate (output) release and calcium dynamics simultaneously with the use of different fluorescence colors tags. Adapted in parts from (Marvin et al. 2013; Burrone et al. 2006).

A

| Constructs | Stable lines | Expressing in RIA |
|---|---|---|
| pglr-3::mca-3::mneongreen::let-858 3'UTR | 3 (out of 4) | NO |
| pglr-3::ric-7::mneongreen::let-858 3'UTR | 5 (out of 6) | NO |
| pglr-3::sel-12::mneongreen::let-858 3'UTR | 5 (out of 7) | NO |
| pglr-3::VGLUT-pH::let-858 3' UTR | 3 (out of 4) | NO |
| pglr-3::cGal::let-858 3' UTR | 2 (out of 4) | NO |

B

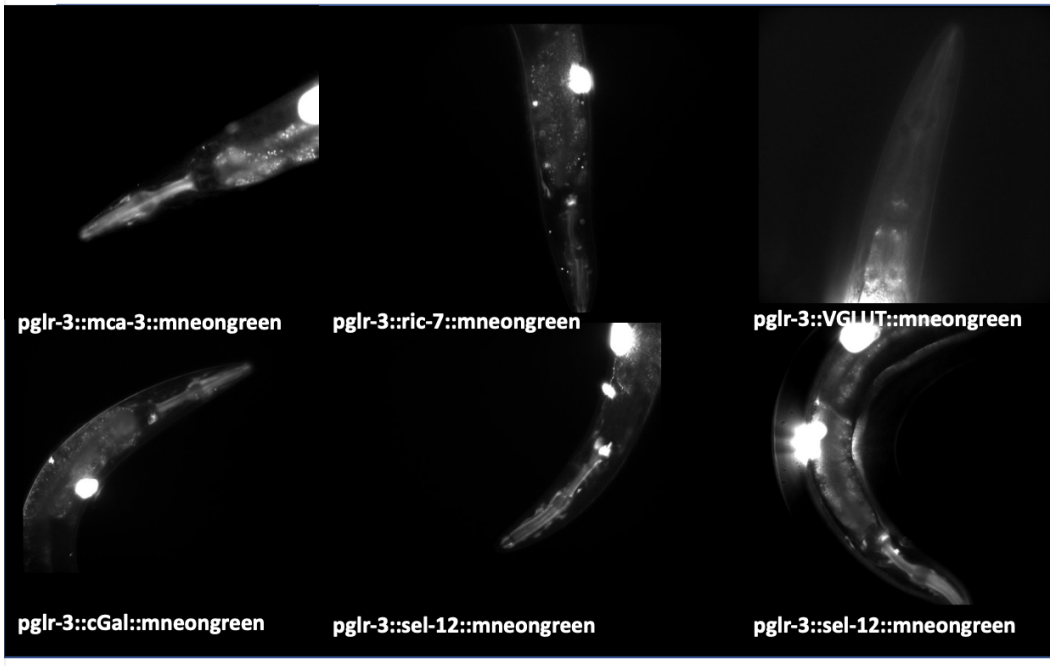

**Figure 4.2. Transgenic lines (non) expression** (A) Table of all constructs made and injected with associated number of lines obtained and their (non) expression in the RIA (B) Sample acquisitions of transgenic lines showing expression of the co-injection marker in coelomocytes but no specific expression of the desired genes driven in the RIA.

A

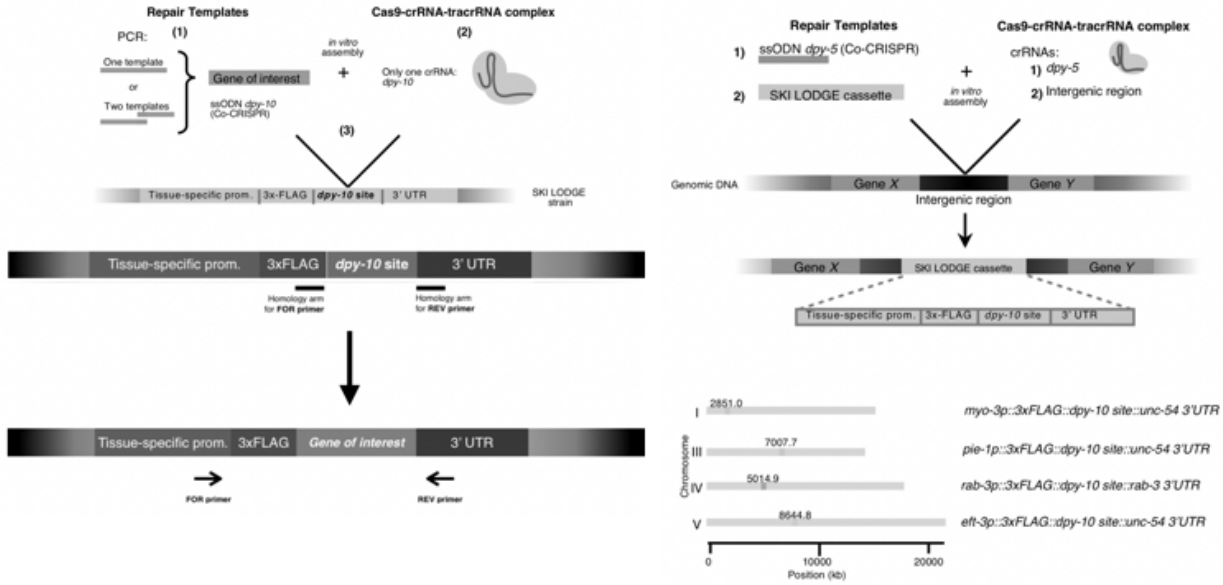
Repair Templates
Cas9-crRNA-tracrRNA complex
PCR:
(1)
(2)
One template
or
Two templates
Gene of interest
ssODN dpy-10 (Co-CRISPR)
in vitro assembly
+
Only one crRNA: dpy-10
(3)
Tissue-specific prom.
3x-FLAG
dpy-10 site
3' UTR
SKI LODGE strain
Tissue-specific prom.
3xFLAG
dpy-10 site
3' UTR
Homology arm for FOR primer
Homology arm for REV primer
Tissue-specific prom.
3xFLAG
Gene of interest
3' UTR
FOR primer
REV primer
Repair Templates
Cas9-crRNA-tracrRNA complex
1) ssODN dpy-5 (Co-CRISPR)
2) SKI LODGE cassette
+
in vitro assembly
crRNAs:
1) dpy-5
2) Intergenic region
Genomic DNA
Gene X
Gene Y
Intergenic region
Gene X
SKI LODGE cassette
Gene Y
Tissue-specific prom.
3x-FLAG
dpy-10 site
3' UTR
Chromosome
I
III
IV
V
2851.0
7007.7
5014.9
8644.8
0
10000
20000
Position (kb)
myo-3p::3xFLAG::dpy-10 site::unc-54 3'UTR
pie-1p::3xFLAG::dpy-10 site::unc-54 3'UTR
rab-3p::3xFLAG::dpy-10 site::rab-3 3'UTR
eft-3p::3xFLAG::dpy-10 site::unc-54 3'UTR

B

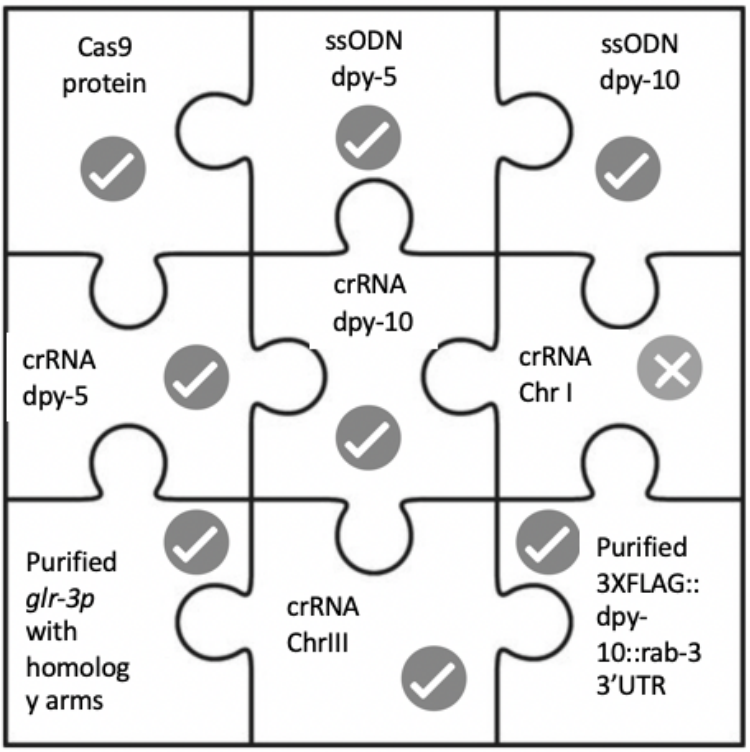
Cas9 protein
ssODN dpy-5
ssODN dpy-10
crRNA dpy-10
crRNA dpy-5
crRNA Chr I
Purified glr-3p with homolog y arms
crRNA ChrIII
Purified 3XFLAG:: dpy-10::rab-3 3'UTR

**Figure 4.3. New SKI LODGE strategy progress** (A) Schematic of the specifics of the SKI LODGE system adapted from (Silva-García et al. 2019) (B) Specifics of the components successfully purified and obtained through optimized protocols to lead to expression of SKI LODGE master strain following injection.

# CHAPTER 5

## CONCLUSION

Using the RIA circuit in *C. elegans* as a model to study active sensing at the single neuron level, we showed that, in this neuron that integrates both sensory and motor inputs, the sensory cues are gated through a specific compartment called the loop. This sensory gating is also dependent on head position and relies on the activated switch from its two motor compartments (nrV and nrD). We also demonstrated that using head lifting as a novel phenotype to screen for genes involved in RIA dynamics led to identifying good candidates that not only impair gait and head orientation but also specifically motor compartments calcium dynamics at the RIA level.

We have identified behavioral and physiological correlates of compromised RIA function to identify candidate mediators of mAChR function. We show that motor compartments of RIA impact muscle activity at the head level and, when function is disrupted, lead to an abnormal phenotype: head lifting. Using calcium imaging and cell-specific rescue in RIA, we characterize physiological and specific defects in candidate strains while assessing the relevant mechanisms of actions in RIA. While the screen put to light some top tier head lifters, some of those have a direct impact on all calcium dynamics in RIA as seen by performing calcium imaging. This phenotype can then be used paired with calcium imaging to determine which one plays a direct role in the RIA and which ones are involved in the broader downstream circuitry of it. These findings will be part of a paper we are submitting to introduce the new head lifting phenotype as a correlate to screen for molecular components involved in head orientation behavior in *C.elegans*.

Further cell specific studies are necessary to assess the localization of each of these genes and their specific activity in regard to RIA by performing rescue experiments. This is still being worked on right now and will be pursued by other members of the

laboratory based on the obtained component and the strategy that is well underway. All in all, this work led to shed light on active sensing at the single neuron level and allowed us to find and explore novel components of this process.

## REFERENCES


Ahissar E, Arieli A. 2001. Figuring space by time. *Neuron* **32**: 185–201. http://dx.doi.org/10.1016/s0896-6273(01)00466-4.

Ahissar E, Arieli A. 2012. Seeing via Miniature Eye Movements: A Dynamic Hypothesis for Vision. *Front Comput Neurosci* **6**: 89. http://dx.doi.org/10.3389/fncom.2012.00089.

Altun ZF, Hall DH. Nervous system, general description. *WormAtlas doi*.

Au WWL. 1993. The Sonar Signal Transmission System. In *The Sonar of Dolphins* (ed. W.W.L. Au), pp. 77–97, Springer New York, New York, NY https://doi.org/10.1007/978-1-4612-4356-4_5.

Babineau D, Lewis JE, Longtin A. 2007. Spatial acuity and prey detection in weakly electric fish. *PLoS Comput Biol* **3**: e38. http://dx.doi.org/10.1371/journal.pcbi.0030038.

Bajcsy R. 1988. Active perception. *Proc IEEE* **76**: 966–1005. http://dx.doi.org/10.1109/5.5968.

Bargmann CI. 1998. Neurobiology of the Caenorhabditis elegans genome. *Science* **282**: 2028–2033. http://dx.doi.org/10.1126/science.282.5396.2028.

Barry C, Hayman R, Burgess N, Jeffery KJ. 2007. Experience-dependent rescaling of entorhinal grids. *Nat Neurosci* **10**: 682–684. http://dx.doi.org/10.1038/nn1905.

Bartumeus F, da Luz MGE, Viswanathan GM, Catalan J. 2005. Animal search strategies: A quantitative random-walk analysis. *Ecology* **86**: 3078–3087. https://esajournals.onlinelibrary.wiley.com/doi/abs/10.1890/04-1806.

Báthori G, Csordás G, Garcia-Perez C, Davies E, Hajnóczky G. 2006. Ca2 -dependent Control of the Permeability Properties of the Mitochondrial Outer Membrane and Voltage-dependent Anion-selective Channel (VDAC). *Journal of Biological Chemistry* **281**: 17347–17358. http://dx.doi.org/10.1074/jbc.m600906200.

Benoit-Bird KJ, Au WWL. 2009. Phonation behavior of cooperatively foraging spinner dolphins. *J Acoust Soc Am* **125**: 539–546. http://dx.doi.org/10.1121/1.2967477.

Berg HC. 1975. Bacterial behaviour. *Nature* **254**: 389–392. http://dx.doi.org/10.1038/254389a0.

Berg RW, Kleinfeld D. 2003. Rhythmic whisking by rat: retraction as well as protraction of the vibrissae is under active muscular control. *J Neurophysiol* **89**: 104–117. http://dx.doi.org/10.1152/jn.00600.2002.

Brecht M, Naumann R, Anjum F, Wolfe J, Munz M, Mende C, Roth-Alpermann C. 2011. The neurobiology of Etruscan shrew active touch. *Philosophical Transactions of the Royal Society B: Biological Sciences* **366**: 3026–3036. http://dx.doi.org/10.1098/rstb.2011.0160.

Brecht M, Preilowski B, Merzenich MM. 1997. Functional architecture of the mystacial vibrissae. *Behav Brain Res* **84**: 81–97. http://dx.doi.org/10.1016/s0166-4328(97)83328-1.

Breimann L, Preusser F, Preibisch S. 2019. Light-microscopy methods in C. elegans research. *Current Opinion in Systems Biology* **13**: 82–92. https://www.sciencedirect.com/science/article/pii/S2452310018300842.

Brenner S. 1974. The genetics of Caenorhabditis elegans. *Genetics* **77**: 71–94. https://www.ncbi.nlm.nih.gov/pubmed/4366476.

Broadley KJ, Kelly DR. 2001. Muscarinic Receptor Agonists and Antagonists. *Molecules* **6**: 142–193. https://www.mdpi.com/5812 (Accessed December 14, 2022).

Brooks JX, Cullen KE. 2019. Predictive Sensing: The Role of Motor Signals in Sensory Processing. *Biol Psychiatry Cogn Neurosci Neuroimaging* **4**: 842–850. http://dx.doi.org/10.1016/j.bpsc.2019.06.003.

Burrone J, Li Z, Murthy VN. 2006. Studying vesicle cycling in presynaptic terminals using the genetically encoded probe synaptopHluorin. *Nat Protoc* **1**: 2970–2978. http://dx.doi.org/10.1038/nprot.2006.449.

Butler WN, Smith KS, van der Meer MAA, Taube JS. 2017. The Head-Direction Signal Plays a Functional Role as a Neural Compass during Navigation. *Curr Biol* **27**: 2406. http://dx.doi.org/10.1016/j.cub.2017.07.032.

Carafoli E, Santella L, Branca D, Brini M. 2001. Generation, control, and processing of cellular calcium signals. *Crit Rev Biochem Mol Biol* **36**: 107–260. http://dx.doi.org/10.1080/20014091074183.

Catania KC. 2011. The sense of touch in the star-nosed mole: from mechanoreceptors to the brain. *Philos Trans R Soc Lond B Biol Sci* **366**: 3016–3025. http://dx.doi.org/10.1098/rstb.2011.0128.

Chalasani SH, Chronis N, Tsunozaki M, Gray JM, Ramot D, Goodman MB, Bargmann CI. 2007. Dissecting a circuit for olfactory behaviour in Caenorhabditis elegans. *Nature* **450**: 63–70. http://dx.doi.org/10.1038/nature06292.

Chan JP, Hu Z, Sieburth D. 2012. Recruitment of sphingosine kinase to presynaptic terminals by a conserved muscarinic signaling pathway promotes neurotransmitter release. *Genes Dev* **26**: 1070–1085. http://dx.doi.org/10.1101/gad.188003.112.

Chenouard N, Smal I, de Chaumont F, Maška M, Sbalzarini IF, Gong Y, Cardinale J,

Carthel C, Coraluppi S, Winter M, et al. 2014. Objective comparison of particle tracking methods. *Nat Methods* **11**: 281–289. http://dx.doi.org/10.1038/nmeth.2808.

Chronis N, Zimmer M, Bargmann CI. 2007. Microfluidics for in vivo imaging of neuronal and behavioral activity in Caenorhabditis elegans. *Nat Methods* **4**: 727–731. http://dx.doi.org/10.1038/nmeth1075.

Cook SJ, Jarrell TA, Brittin CA, Wang Y, Bloniarz AE, Yakovlev MA, Nguyen KCQ, Tang LT-H, Bayer EA, Duerr JS, et al. 2019. Whole-animal connectomes of both Caenorhabditis elegans sexes. *Nature* **571**: 63–71. http://dx.doi.org/10.1038/s41586-019-1352-7.

Crapse TB, Sommer MA. 2008. Corollary discharge across the animal kingdom. *Nature Reviews Neuroscience* **9**: 587–600. http://dx.doi.org/10.1038/nrn2457.

de Brito OM, Scorrano L. 2010. An intimate liaison: spatial organization of the endoplasmic reticulum–mitochondria relationship. *EMBO J* **29**: 2715–2723. http://emboj.embopress.org/content/29/16/2715.abstract (Accessed May 24, 2019).

de Brito OM, Scorrano L. 2008. Mitofusin 2 tethers endoplasmic reticulum to mitochondria. *Nature* **456**: 605–610. http://dx.doi.org/10.1038/nature07534.

Derdikman D, Whitlock JR, Tsao A, Fyhn M, Hafting T, Moser M-B, Moser EI. 2009. Fragmentation of grid cell maps in a multicompartment environment. *Nat Neurosci* **12**: 1325–1332. http://dx.doi.org/10.1038/nn.2396.

Di Leva F, Domi T, Fedrizzi L, Lim D, Carafoli E. 2008. The plasma membrane Ca2+ ATPase of animal cells: structure, function and regulation. *Arch Biochem Biophys* **476**: 65–74. http://dx.doi.org/10.1016/j.abb.2008.02.026.

D'Souza RD, Vijayaraghavan S. 2014. Paying attention to smell: cholinergic signaling in the olfactory bulb. *Front Synaptic Neurosci* **6**: 21. http://dx.doi.org/10.3389/fnsyn.2014.00021.

Eggermann E, Kremer Y, Crochet S, Petersen CCH. 2014. Cholinergic signals in mouse barrel cortex during active whisker sensing. *Cell Rep* **9**: 1654–1660. http://dx.doi.org/10.1016/j.celrep.2014.11.005.

Emlen ST. 1967. Migratory Orientation in the Indigo Bunting, Passerina cyanea: Part I: Evidence for Use of Celestial Cues. *The Auk* **84**: 309–342. http://dx.doi.org/10.2307/4083084.

Faumont S, Lindsay TH, Lockery SR. 2012. Neuronal microcircuits for decision making in C. elegans. *Curr Opin Neurobiol* **22**: 580–591. http://dx.doi.org/10.1016/j.conb.2012.05.005.

Felder CC. 1995. Muscarinic acetylcholine receptors: signal transduction through multiple effectors. *FASEB J* **9**: 619–625.

https://www.ncbi.nlm.nih.gov/pubmed/7768353.

Fenton AA, Kao H-Y, Neymotin SA, Olypher A, Vayntrub Y, Lytton WW, Ludvig N. 2008. Unmasking the CA1 Ensemble Place Code by Exposures to Small and Large Environments: More Place Cells and Multiple, Irregularly Arranged, and Expanded Place Fields in the Larger Space. *Journal of Neuroscience* **28**: 11250–11262. http://dx.doi.org/10.1523/jneurosci.2862-08.2008.

Fill M, Copello JA. 2002. Ryanodine receptor calcium release channels. *Physiol Rev* **82**: 893–922. http://dx.doi.org/10.1152/physrev.00013.2002.

Forrester FM. 2018. The Role of Modified UNC-68 in Age-related Caenorhabditis elegans Muscle Function Loss. Columbia University https://academiccommons.columbia.edu/doi/10.7916/D8TB2KCN.

Garrity PA, Goodman MB, Samuel AD, Sengupta P. 2010. Running hot and cold: behavioral strategies, neural circuits, and the molecular machinery for thermotaxis in C. elegans and Drosophila. *Genes Dev* **24**: 2365–2382. http://dx.doi.org/10.1101/gad.1953710.

Glazener. Homing instinct of white-tailed deer. *Tex Game and Fish*.

Gómez-Suaga P, Bravo-San Pedro JM, González-Polo RA, Fuentes JM, Niso-Santano M. 2018. ER--mitochondria signaling in Parkinson's disease. *Cell Death Dis* **9**: 337. https://www.nature.com/articles/s41419-017-0079-3.

Goodman MB, Hall DH, Avery L, Lockery SR. 1998. Active currents regulate sensitivity and dynamic range in C. elegans neurons. *Neuron* **20**: 763–772. https://www.ncbi.nlm.nih.gov/pubmed/9581767.

Greenwood PM, Lin M-K, Sundararajan R, Fryxell KJ, Parasuraman R. 2009. Synergistic effects of genetic variation in nicotinic and muscarinic receptors on visual attention but not working memory. *Proc Natl Acad Sci U S A* **106**: 3633–3638. http://dx.doi.org/10.1073/pnas.0807891106.

Guić-Robles E, Valdivieso C, Guajardo G. 1989. Rats can learn a roughness discrimination using only their vibrissal system. *Behav Brain Res* **31**: 285–289. http://dx.doi.org/10.1016/0166-4328(89)90011-9.

Hafting T, Fyhn M, Molden S, Moser M-B, Moser EI. 2005. Microstructure of a spatial map in the entorhinal cortex. *Nature* **436**: 801–806. http://dx.doi.org/10.1038/nature03721.

Ha NM, Tran SH, Shim Y-H, Kang K. 2022. Caenorhabditis elegans as a powerful tool in natural product bioactivity research. *Applied Biological Chemistry* **65**: 1–18. https://applbiolchem.springeropen.com/articles/10.1186/s13765-022-00685-y (Accessed December 15, 2022).

Hao Y, Hu Z, Sieburth D, Kaplan JM. 2012. RIC-7 Promotes Neuropeptide Secretion. *PLoS Genetics* **8**: e1002464. http://dx.doi.org/10.1371/journal.pgen.1002464.

Harris JA, Petersen RS, Diamond ME. 1999. Distribution of tactile learning and its neural basis. *Proc Natl Acad Sci U S A* **96**: 7587–7591. http://dx.doi.org/10.1073/pnas.96.13.7587.

Hart, Anne C. 2006. Behavior (July 3, 2006), WormBook, ed. The C. elegans Research Community, WormBook, doi/10.1895/wormbook. 1.87. 1.

Hart AC, Sims S, Kaplan JM. 1995. Synaptic code for sensory modalities revealed by C. elegans GLR-1 glutamate receptor. *Nature* **378**: 82–85. http://dx.doi.org/10.1038/378082a0.

Heimendahl M von, von Heimendahl M, Itskov PM, Arabzadeh E, Diamond ME. 2007. Neuronal Activity in Rat Barrel Cortex Underlying Texture Discrimination. *PLoS Biology* **5**: e305. http://dx.doi.org/10.1371/journal.pbio.0050305.

Hendricks M, Ha H, Maffey N, Zhang Y. 2012. Compartmentalized calcium dynamics in a C. elegans interneuron encode head movement. *Nature* **487**: 99–103. http://dx.doi.org/10.1038/nature11081.

Hendricks M, Zhang Y. 2013. Complex RIA calcium dynamics and its function in navigational behavior. *Worm* **2**: e25546. http://dx.doi.org/10.4161/worm.25546.

Henshaw RE, Stephenson RO. 1974. Homing in the Gray Wolf (Canis lupus). *J Mammal* **55**: 234–237. http://www.jstor.org/stable/1379281.

Hill DN, Bermejo R, Zeigler HP, Kleinfeld D. 2008. Biomechanics of the vibrissa motor plant in rat: rhythmic whisking consists of triphasic neuromuscular activity. *J Neurosci* **28**: 3438–3455. http://dx.doi.org/10.1523/JNEUROSCI.5008-07.2008.

Hills TT, Todd PM, Lazer D, David Redish A, Couzin ID. 2015. Exploration versus exploitation in space, mind, and society. *Trends in Cognitive Sciences* **19**: 46–54. http://dx.doi.org/10.1016/j.tics.2014.10.004.

Hirabayashi Y, Kwon S-K, Paek H, Pernice WM, Paul MA, Lee J, Erfani P, Raczkowski A, Petrey DS, Pon LA, et al. 2017. ER-mitochondria tethering by PDZD8 regulates Ca2+ dynamics in mammalian neurons. *Science* **358**: 623–630. http://dx.doi.org/10.1126/science.aan6009.

Hwang JM, Chang DJ, Kim US, Lee YS, Park YS, Kaang BK, Cho NJ. 1999. Cloning and functional characterization of a Caenorhabditis elegans muscarinic acetylcholine receptor. *Receptors Channels* **6**: 415–424. https://www.ncbi.nlm.nih.gov/pubmed/10635059.

Iino Y, Yoshida K. 2009. Parallel use of two behavioral mechanisms for chemotaxis in Caenorhabditis elegans. *J Neurosci* **29**: 5370–5380.

http://dx.doi.org/10.1523/JNEUROSCI.3633-08.2009.

Ishii M, Kurachi Y. 2006. Muscarinic acetylcholine receptors. *Curr Pharm Des* **12**: 3573–3581. http://dx.doi.org/10.2174/138161206778522056.

Jahn R, Südhof TC. 1994. Synaptic vesicles and exocytosis. *Annu Rev Neurosci* **17**: 219–246. http://dx.doi.org/10.1146/annurev.ne.17.030194.001251.

Jiang J, Su Y, Zhang R, Li H, Tao L, Liu Q. 2022. C. elegans enteric motor neurons fire synchronized action potentials underlying the defecation motor program. *Nat Commun* **13**: 2783. http://dx.doi.org/10.1038/s41467-022-30452-y.

Jones G. 2021. Sensory biology: Tree mice use echolocation. *Curr Biol* **31**: R1074–R1076. http://dx.doi.org/10.1016/j.cub.2021.07.074.

Kato S, Xu Y, Cho CE, Abbott LF, Bargmann CI. 2014. Temporal responses of C. elegans chemosensory neurons are preserved in behavioral dynamics. *Neuron* **81**: 616–628. http://dx.doi.org/10.1016/j.neuron.2013.11.020.

Katz B, Miledi R. 1967. Ionic requirements of synaptic transmitter release. *Nature* **215**: 651. http://dx.doi.org/10.1038/215651a0.

Kepecs A, Uchida N, Mainen ZF. 2006. The sniff as a unit of olfactory processing. *Chem Senses* **31**: 167–179. http://dx.doi.org/10.1093/chemse/bjj016.

König P, Luksch H. 1998. Active sensing--closing multiple loops. *Z Naturforsch C* **53**: 542–549. http://dx.doi.org/10.1515/znc-1998-7-808.

Kwon S-K, Sando R 3rd, Lewis TL, Hirabayashi Y, Maximov A, Polleux F. 2016. LKB1 Regulates Mitochondria-Dependent Presynaptic Calcium Clearance and Neurotransmitter Release Properties at Excitatory Synapses along Cortical Axons. *PLoS Biol* **14**: e1002516. http://dx.doi.org/10.1371/journal.pbio.1002516.

Lau DHW, Hartopp N, Welsh NJ, Mueller S, Glennon EB, Mórotz GM, Annibali A, Gomez-Suaga P, Stoica R, Paillusson S, et al. 2018. Disruption of ER-mitochondria signalling in fronto-temporal dementia and related amyotrophic lateral sclerosis. *Cell Death Dis* **9**: 327. http://dx.doi.org/10.1038/s41419-017-0022-7.

Lever C, Burton S, Jeewajee A, O'Keefe J, Burgess N. 2009. Boundary vector cells in the subiculum of the hippocampal formation. *J Neurosci* **29**: 9771–9777. http://dx.doi.org/10.1523/JNEUROSCI.1319-09.2009.

Liu H, Yang W, Wu T, Duan F, Soucy E, Jin X, Zhang Y. 2018a. Cholinergic Sensorimotor Integration Regulates Olfactory Steering. *Neuron* **97**: 390–405.e3. http://dx.doi.org/10.1016/j.neuron.2017.12.003.

Liu Q, Kidd PB, Dobosiewicz M, Bargmann CI. 2018b. C. elegans AWA Olfactory Neurons Fire Calcium-Mediated All-or-None Action Potentials. *Cell* **175**: 57–70.e17.

http://dx.doi.org/10.1016/j.cell.2018.08.018.

Liu S, Shao Z, Puche A, Wachowiak M, Rothermel M, Shipley MT. 2015. Muscarinic receptors modulate dendrodendritic inhibitory synapses to sculpt glomerular output. *J Neurosci* **35**: 5680–5692. http://dx.doi.org/10.1523/JNEUROSCI.4953-14.2015.

Lohmann KJ, Lohmann CMF, Endres CS. 2008. The sensory ecology of ocean navigation. *J Exp Biol* **211**: 1719–1728. http://dx.doi.org/10.1242/jeb.015792.

Luo L, Clark DA, Biron D, Mahadevan L, Samuel ADT. 2006. Sensorimotor control during isothermal tracking in Caenorhabditis elegans. *J Exp Biol* **209**: 4652–4662. http://dx.doi.org/10.1242/jeb.02590.

Luo L, Cook N, Venkatachalam V, Martinez-Velazquez LA, Zhang X, Calvo AC, Hawk J, MacInnis BL, Frank M, Ng JHR, et al. 2014. Bidirectional thermotaxis in Caenorhabditis elegans is mediated by distinct sensorimotor strategies driven by the AFD thermosensory neurons. *Proc Natl Acad Sci U S A* **111**: 2776–2781. http://dx.doi.org/10.1073/pnas.1315205111.

Marvin JS, Borghuis BG, Tian L, Cichon J, Harnett MT, Akerboom J, Gordus A, Renninger SL, Chen T-W, Bargmann CI, et al. 2013. An optimized fluorescent probe for visualizing glutamate neurotransmission. *Nat Methods* **10**: 162–170. http://dx.doi.org/10.1038/nmeth.2333.

Maryon EB, Coronado R, Anderson P. 1996. unc-68 encodes a ryanodine receptor involved in regulating C. elegans body-wall muscle contraction. *J Cell Biol* **134**: 885–893. http://dx.doi.org/10.1083/jcb.134.4.885.

McCormick KE, Gaertner BE, Sottile M, Phillips PC, Lockery SR. 2011. Microfluidic devices for analysis of spatial orientation behaviors in semi-restrained Caenorhabditis elegans. *PLoS One* **6**: e25710. http://dx.doi.org/10.1371/journal.pone.0025710.

Milius S. 2004. Thoroughly Modern Migrants. *Sci News* **165**: 408. https://onlinelibrary.wiley.com/doi/abs/10.2307/4015111.

Mori I, Ohshima Y. 1995. Neural regulation of thermotaxis in Caenorhabditis elegans. *Nature* **376**: 344–348. http://dx.doi.org/10.1038/376344a0.

Muller RU, Bostock E, Taube JS, Kubie JL. 1994. On the directional firing properties of hippocampal place cells. *J Neurosci* **14**: 7235–7251. https://www.ncbi.nlm.nih.gov/pubmed/7996172.

O'Keefe J, Nadel L. 1979. The cognitive map as a hippocampus. *Behavioral and Brain Sciences* **2**: 520–533. http://dx.doi.org/10.1017/s0140525x00064256.

Ouellette M-H, Desrochers MJ, Gheta I, Ramos R, Hendricks M. 2018. A Gate-and-Switch Model for Head Orientation Behaviors in Caenorhabditis elegans.

*eNeuro* **5**. http://dx.doi.org/10.1523/ENEURO.0121-18.2018.

Oxenoid K, Dong Y, Cao C, Cui T, Sancak Y, Markhard AL, Grabarek Z, Kong L, Liu Z, Ouyang B, et al. 2016. Architecture of the mitochondrial calcium uniporter. *Nature* **533**: 269–273. http://dx.doi.org/10.1038/nature17656.

Peyrache A, Lacroix MM, Petersen PC, Buzsáki G. 2015. Internally organized mechanisms of the head direction sense. *Nat Neurosci* **18**: 569–575. http://dx.doi.org/10.1038/nn.3968.

Peyrache A, Schieferstein N, Buzsáki G. 2017. Transformation of the head-direction signal into a spatial code. *Nat Commun* **8**: 1752. http://dx.doi.org/10.1038/s41467-017-01908-3.

Phil MAHRBH, Harvey MA, Bermejo R, Phil H. 2001. Discriminative whisking in the head-fixed rat: optoelectronic monitoring during tactile detection and discrimination tasks. *Somatosensory & Motor Research* **18**: 211–222. http://dx.doi.org/10.1080/01421590120072204.

Picciotto MR, Higley MJ, Mineur YS. 2012. Acetylcholine as a neuromodulator: cholinergic signaling shapes nervous system function and behavior. *Neuron* **76**: 116–129. http://dx.doi.org/10.1016/j.neuron.2012.08.036.

Pierce-Shimomura JT, Morse TM, Lockery SR. 1999. The fundamental role of pirouettes in Caenorhabditis elegans chemotaxis. *J Neurosci* **19**: 9557–9569. https://www.ncbi.nlm.nih.gov/pubmed/10531458.

Porter J, Craven B, Khan RM, Chang S-J, Kang I, Judkewitz B, Volpe J, Settles G, Sobel N. 2007. Mechanisms of scent-tracking in humans. *Nat Neurosci* **10**: 27–29. http://dx.doi.org/10.1038/nn1819.

Prigg T, Goldreich D, Carvell GE, Simons DJ. 2002. Texture discrimination and unit recordings in the rat whisker/barrel system. *Physiol Behav* **77**: 671–675. http://dx.doi.org/10.1016/s0031-9384(02)00917-4.

Putman NF, Jenkins ES, Michielsens CGJ, Noakes DLG. 2014. Geomagnetic imprinting predicts spatio-temporal variation in homing migration of pink and sockeye salmon. *J R Soc Interface* **11**. http://dx.doi.org/10.1098/rsif.2014.0542.

Ranade S, Hangya B, Kepecs A. 2013. Multiple modes of phase locking between sniffing and whisking during active exploration. *J Neurosci* **33**: 8250–8256. http://dx.doi.org/10.1523/JNEUROSCI.3874-12.2013.

Rapizzi E, Pinton P, Szabadkai G, Wieckowski MR, Vandecasteele G, Baird G, Tuft RA, Fogarty KE, Rizzuto R. 2002. Recombinant expression of the voltage-dependent anion channel enhances the transfer of Ca2+ microdomains to mitochondria. *J Cell Biol* **159**: 613–624. http://dx.doi.org/10.1083/jcb.200205091.

Rawson RL, Yam L, Weimer RM, Bend EG, Hartwieg E, Horvitz HR, Clark SG, Jorgensen EM. 2014. Axons degenerate in the absence of mitochondria in C. elegans. *Curr Biol* **24**: 760–765. http://dx.doi.org/10.1016/j.cub.2014.02.025.

Role LW, Berg DK. 1996. Nicotinic receptors in the development and modulation of CNS synapses. *Neuron* **16**: 1077–1085. https://www.ncbi.nlm.nih.gov/pubmed/8663984.

Rothermel M, Carey RM, Puche A, Shipley MT, Wachowiak M. 2014. Cholinergic inputs from Basal forebrain add an excitatory bias to odor coding in the olfactory bulb. *J Neurosci* **34**: 4654–4664. http://dx.doi.org/10.1523/JNEUROSCI.5026-13.2014.

San-Miguel A, Lu H. 24AD. September 2013. Microfluidics as a tool for C. elegans research. *Worm-Book https://doi org/10 1895/wormbook* **1**.

Sarasija S, Laboy JT, Ashkavand Z, Bonner J, Tang Y, Norman KR. 2018. Presenilin mutations deregulate mitochondrial Ca2 homeostasis and metabolic activity causing neurodegeneration in Caenorhabditis elegans. *eLife* **7**. http://dx.doi.org/10.7554/elife.33052.

Sarasija S, Norman KR. 2015. A γ-Secretase Independent Role for Presenilin in Calcium Homeostasis Impacts Mitochondrial Function and Morphology in Caenorhabditis elegans. *Genetics* **201**: 1453–1466. http://dx.doi.org/10.1534/genetics.115.182808.

Sauer EGF. 1958. CELESTIAL NAVIGATION BY BIRDS. *Sci Am* **199**: 42–47. http://www.jstor.org/stable/24941079.

Sauman I, Briscoe AD, Zhu H, Shi D, Froy O, Stalleicken J, Yuan Q, Casselman A, Reppert SM. 2005. Connecting the navigational clock to sun compass input in monarch butterfly brain. *Neuron* **46**: 457–467. http://dx.doi.org/10.1016/j.neuron.2005.03.014.

Savelli F, Yoganarasimha D, Knierim JJ. 2008. Influence of boundary removal on the spatial representations of the medial entorhinal cortex. *Hippocampus* **18**: 1270–1282. http://dx.doi.org/10.1002/hipo.20511.

Sbalzarini IF, Koumoutsakos P. 2005. Feature point tracking and trajectory analysis for video imaging in cell biology. *Journal of Structural Biology* **151**: 182–195. http://dx.doi.org/10.1016/j.jsb.2005.06.002.

Scheuss V, Yasuda R, Sobczyk A, Svoboda K. 2006. Nonlinear [Ca2 ] Signaling in Dendrites and Spines Caused by Activity-Dependent Depression of Ca2 Extrusion. *Journal of Neuroscience* **26**: 8183–8194. http://dx.doi.org/10.1523/jneurosci.1962-06.2006.

Schiavo GG, Benfenati F, Poulain B, Rossetto O, de Laureto PP, DasGupta BR, Montecucco C. 1992. Tetanus and botulinum-B neurotoxins block neurotransmitter release by proteolytic cleavage of synaptobrevin. *Nature* **359**: 832–835.

http://dx.doi.org/10.1038/359832a0.

Schindelin J, Arganda-Carreras I, Frise E, Kaynig V, Longair M, Pietzsch T, Preibisch S, Rueden C, Saalfeld S, Schmid B, et al. 2012. Fiji: an open-source platform for biological-image analysis. *Nature Methods* **9**: 676–682. http://dx.doi.org/10.1038/nmeth.2019.

Schütz C, Dürr V. 2011. Active tactile exploration for adaptive locomotion in the stick insect. *Philos Trans R Soc Lond B Biol Sci* **366**: 2996–3005. http://dx.doi.org/10.1098/rstb.2011.0126.

Silva-García CG, Lanjuin A, Heintz C, Dutta S, Clark NM, Mair WB. 2019. Single-Copy Knock-In Loci for Defined Gene Expression in Caenorhabditis elegans. *G3: Genes, Genomes, Genetics* g3–400314. https://www.g3journal.org/content/early/2019/05/07/g3.119.400314.abstract.

Smear M, Shusterman R, O'Connor R, Bozza T, Rinberg D. 2011. Perception of sniff phase in mouse olfaction. *Nature* **479**: 397–400. http://dx.doi.org/10.1038/nature10521.

Solstad T, Boccara CN, Kropff E, Moser M-B, Moser EI. 2008. Representation of geometric borders in the entorhinal cortex. *Science* **322**: 1865–1868. http://dx.doi.org/10.1126/science.1166466.

Stamper SA, Roth E, Cowan NJ, Fortune ES. 2012. Active sensing *via* movement shapes spatiotemporal patterns of sensory feedback. *Journal of Experimental Biology* **215**: 1567–1574. http://dx.doi.org/10.1242/jeb.068007.

Steger KA, Avery L. 2004. The GAR-3 muscarinic receptor cooperates with calcium signals to regulate muscle contraction in the Caenorhabditis elegans pharynx. *Genetics* **167**: 633–643. http://dx.doi.org/10.1534/genetics.103.020230.

Stiernagle T. 2006. Maintenance of C. elegans. *WormBook*. http://dx.doi.org/10.1895/wormbook.1.101.1.

Stoica R, De Vos KJ, Paillusson S, Mueller S, Sancho RM, Lau K-F, Vizcay-Barrena G, Lin W-L, Xu Y-F, Lewis J, et al. 2014. ER–mitochondria associations are regulated by the VAPB–PTPIP51 interaction and are disrupted by ALS/FTD-associated TDP-43. *Nature Communications* **5**. http://dx.doi.org/10.1038/ncomms4996.

Straka H, Simmers J, Chagnaud BP. 2018. A New Perspective on Predictive Motor Signaling. *Current Biology* **28**: R232–R243. http://dx.doi.org/10.1016/j.cub.2018.01.033.

Tan W, Colombini M. 2007. VDAC closure increases calcium ion flux. *Biochimica et Biophysica Acta (BBA) - Biomembranes* **1768**: 2510–2515. http://dx.doi.org/10.1016/j.bbamem.2007.06.002.

Taube JS. 2007. The Head Direction Signal: Origins and Sensory-Motor Integration. *Annual Review of Neuroscience* **30**: 181–207. http://dx.doi.org/10.1146/annurev.neuro.29.051605.112854.

Thomas JA, Moss CF, Vater M. 2004. *Echolocation in Bats and Dolphins*. University of Chicago Press https://play.google.com/store/books/details?id=qjemeaVFBTUC.

Tian L, Hires SA, Mao T, Huber D, Chiappe ME, Chalasani SH, Petreanu L, Akerboom J, McKinney SA, Schreiter ER, et al. 2009. Imaging neural activity in worms, flies and mice with improved GCaMP calcium indicators. *Nat Methods* **6**: 875–881. http://dx.doi.org/10.1038/nmeth.1398.

Tiwari P, Dwivedi S, Singh MP, Mishra R, Chandy A. 2013. Basic and modern concepts on cholinergic receptor: A review. *Asian Pacific Journal of Tropical Disease* **3**: 413–420. https://www.sciencedirect.com/science/article/pii/S2222180813600948.

Tsai C-W, Wu Y, Pao P-C, Phillips CB, Williams C, Miller C, Ranaghan M, Tsai M-F. 2017. Proteolytic control of the mitochondrial calcium uniporter complex. *Proc Natl Acad Sci U S A* **114**: 4388–4393. http://dx.doi.org/10.1073/pnas.1702938114.

Ulanovsky N, Moss CF. 2008. What the bat's voice tells the bat's brain. *Proc Natl Acad Sci U S A* **105**: 8491–8498. http://dx.doi.org/10.1073/pnas.0703550105.

Umanskaya A, Andersson D, Xie W, Reiken S, Marks AR. 2014. C. elegans as a model to study ryanodine receptor function in aging. *Biophys J* **106**: 111a. https://www.cell.com/biophysj/pdf/S0006-3495(13)01912-7.pdf.

Verfuß UK, Miller LA, Pilz PKD, Schnitzler H-U. 2009. Echolocation by two foraging harbour porpoises (*Phocoena phocoena*). *Journal of Experimental Biology* **212**: 823–834. http://dx.doi.org/10.1242/jeb.022137.

Wachowiak M. 2011. All in a Sniff: Olfaction as a Model for Active Sensing. *Neuron* **71**: 962–973. https://www.sciencedirect.com/science/article/pii/S0896627311007859.

Wakabayashi T, Sakata K, Togashi T, Itoi H, Shinohe S, Watanabe M, Shingai R. 2015. Navigational choice between reversal and curve during acidic pH avoidance behavior in Caenorhabditis elegans. *BMC Neurosci* **16**: 79. http://dx.doi.org/10.1186/s12868-015-0220-0.

Watts BD, Smith FM, Hines C, Duval L, Hamilton DJ, Keyes T, Paquet J, Pirie-Dominix L, Rausch J, Truitt B, et al. 2021. The annual cycle for whimbrel populations using the Western Atlantic Flyway. *PLoS One* **16**: e0260339. http://dx.doi.org/10.1371/journal.pone.0260339.

White JG, Southgate E, Thomson JN, Brenner S. 1986. The Structure of the Nervous System of the Nematode Caenorhabditis elegans. *Philosophical Transactions of the Royal Society B: Biological Sciences* **314**: 1–340. http://dx.doi.org/10.1098/rstb.1986.0056.

Wiltschko R, Wiltschko W. 2003. Mechanisms of Orientation and Navigation in Migratory Birds. *Avian Migration* 433–456. http://dx.doi.org/10.1007/978-3-662-05957-9_31.

Winter SS, Taube JS. 2014. Head Direction Cells: From Generation to Integration. *Space,Time and Memory in the Hippocampal Formation* 83–106. http://dx.doi.org/10.1007/978-3-7091-1292-2_4.

Zhao T, Hao Y, Kaplan JM. 2018. Axonal Mitochondria Modulate Neuropeptide Secretion Through the Hypoxic Stress Response in Caenorhabditis elegans. *Genetics* **210**: 275–285. http://dx.doi.org/10.1534/genetics.118.301014.

Zuo Y, Perkon I, Diamond ME. 2011. Whisking and whisker kinematics during a texture classification task. *Philos Trans R Soc Lond B Biol Sci* **366**: 3058–3069. http://dx.doi.org/10.1098/rstb.2011.0161.